THE APPLICATION OF EPS GEOFOAM IN MITIGATING THE APPROACH PROBLEMS IN INTEGRAL ABUTMENT BRIDGES

Ahmed Al-qarawi
MSc. Engineering

This thesis is submitted as a fulfilment for the degree of

Master of Engineering (Honours)

School of Computing Engineering and Mathematics

Western Sydney University

March 2016

This thesis is dedicated to,

My wife, Nesmah Abdullah, My kids, Leen and Ali

and

My beloved Mother

Declaration

Date: March 2016

Author: Ahmed Swadi Mohammed Al-qarawi

Title: THE APPLICATION OF EPS GEOFOAM IN MITIGATING APPROACH PROBLEMS IN INTEGRAL ABUTMENT BRIDGES

Degree: Master of Engineering (Honours)

I certify that the work presented in this thesis is, to the best of my knowledge and belief, original, except as acknowledged in the text, and the material has not been submitted, either in full or in part, for a degree at this or any other institution.

I certify that I have complied with the rules, requirements, procedures and policy relating to my higher degree research award of Western Sydney University.

Author's signature

Abstract

The traditional construction procedure of bridges involves the use of expansion joints to allow for unrestricted superstructure movements against the temperature induced deformations. However, expansion joints have been demonstrated to be vulnerable to deterioration as a result of various environmental and operational factors. Therefore, they pose an intractable challenge to the engineers represented by the costly and frequent maintenance works they require. In that regard, the Integral Abutment Bridge (IAB) system presents an attractive alternative to overcome such problems. In addition to the advantages achieved by eliminating the expansion joints, the IABs have desirable structural performance and offer simple and rapid construction procedures.

The IABs as yet have their unique problems that ensue from the regular expansions and contractions in the superstructure. The structural system of IABs relies on the abutments movements to accommodate such changes in the dimensions of the bridge. The repetitive abutment movements, against and away from the retained soil, result in two principle detrimental effects in bridge approaches. These effects involve long term build-up of the lateral earth pressure and settlement in the approach soil. In consequence to these effects, the abutments will experience an escalated soil pressure that may exceed the design values and possibly damage the abutment. Moreover, the developed settlement at the bridge approaches will lead to safety and riding quality issues for the bridge users.

The aforementioned problems in IABs have drastically reduced the advantages of IABs and restrict their use to limited conditions. For instance, in Australia the use of IABs is only permitted for bridges with a total length not exceeding 70m. Hence, a practical remedy measure that alleviates the approach problems in IABs to allowable states will maximize the potential benefits of this system and allows for utilizing it in a wider range of design context. The existing remedy measures, represented by the run-on concrete slabs and using heavily compacted backfill at bridge approaches are as yet inefficient and do not provide an effective solution for the approach problems in IABs. As a rational measure, using a low stiffness fill material between the abutments and the retained soil can absorb the energy imposed by the abutment movements and consequently minimize its effects on the approach soil. Thus, the

expanded polystyrene geofoam (EPS) is deemed to present an excellent choice over the other fill materials due to its unique characteristics. The EPS is a very light material, highly compressible and energy absorbing. It also offers a cost effective choice with easy and rapid installation.

The present thesis aims to extend an insight into the soil-structure interaction behaviour in the IAB with particular emphasis to the soil settlement and the lateral pressure issues at bridge approaches. It then investigates the effectiveness of the EPS geofoam in mitigating these effects. Physical modelling together with numerical analyses have been utilized to perform these investigations.

A finite element model, first, developed using ABAQUS/standard software and used to simulate, in prototype dimensions, a wide-base embedded abutment experiencing cyclic movements as would be anticipated to occur in IABs. The model was validated using centrifuge test results from previous literature and employed to perform a parametric study on the dominant factors affecting the soil-abutment interaction behaviour. An experimental program then carried out to investigate the influence of the mode of wall movement, rotation or translation, and the effectiveness of the EPS geofoam inclusion using a physical model of a small wall retaining loose sand on one side. The experimental test results of the small wall were used to validate a finite element model that incorporated an EPS geofoam inclusion. The EPS behaviour was simulated using a hyper-foam constitutive model and calibrated using the laboratory test results.

Following which, finite element modelling was applied to investigate the impact of using EPS geofoam inclusion in prototype dimensions on the soil settlement and lateral earth pressures in IABs. Different geometrical arrangements for the EPS inclusion have been investigated and conclusions about the optimum EPS arrangements have been given.

Finally, the research conclusions and recommendations for future studies in regard to the soil-structure interaction behaviour in IABs and the possible remedy measures using the EPS geofoam are presented.

Acknowledgments

First, I would like to extend my sincere gratitude and appreciation to my principal supervisor, Professor Chin Leo, for his invaluable and continuous support throughout the research period. His constant attention and guidance have been of great help in publishing the outcomes of this research in addition to the successful completion of the thesis. I am deeply grateful to him for every effort and advice he provided toward the completion of my degree.

I also extend my gratitude to my co-supervisor, Associate Professor Samanthika Liyanapathirana, for her assistance and attention throughout every stage in my research period.

I would like to acknowledge Western Sydney University, the School of Computing, Engineering and Mathematics (SCEM) for providing the necessary laboratory facilities and the wok environment. I would like to thank Dr Sanka Ekanayake and Mr Thomas Ring for their assistance and help in my research work.

I would also like to gratefully thank my lovely wife for her great support, efforts and interest she has provided throughout my study.

Table of Contents

List of Figures

List of Tables

List of Symbols

Latin

d	Horizontal wall displacement
E	Elasticity modulus
E_{cc}	Small strain stiffness of compacted soil
E_o	Small-strain modulus
E_p	Operational stiffness of soil
g	Gravity
H	Height of the retained soil
K^*	The critical coefficient of lateral earth pressure according to the UK BA42/96 specification
K_a	Active coefficient of lateral earth pressure
K_o	At-rest coefficient of lateral earth pressure
K_p	Passive coefficient of lateral earth pressure
N	Number of wall movement cycles
n	Scale factor between centrifuge and prototype dimensions
P_a	Active soil pressure
P_p	Passive soil pressure
u_1	Displacement in *x* direction
u_2	Displacement in *z* direction
z	Depth from soil surface

Greek

γ	Unit weight of the retained soil
$\emptyset$	Friction angle of the soil
δ	Angle of friction between the soil and the wall

ε	Total strain
ε_o	Immediate strain
ε_t	Time dependant strain in EPS
μ	Poisson ration
Ψ	Dilation angle of soil
θ	The inclination angle of the interface planar between the EPS and the soil
σ_h	Horizontal stress
σ_v	Vertical stress
ε_v	Volumetric strain
Δx	Deformation in *x* direction
Δz	Deformation in *z* direction

Abbreviations

AASHTO	American Association of State Highway and Transportation Officials
CPE8R	Eight-node quadratic element with reduced integration
EPS	Expanded Polystyrene
FE	Finite Element
FHWA	American Federal Highway Association
IABs	Integral Abutment Bridges
LVDT	Linear variable differential transformer

Chapter One

Introduction

1.1 Background

Bridges are conventionally designed and constructed with expansion joints in the deck to accommodate the potential movements in the longitudinal direction of the bridge. These movements are caused by various factors such as the expansion and contraction due to the fluctuations in the ambient temperatures, post-construction shrinkage, creep and the long term settlement of the bridge approaches. The expansion joints are usually exposed to severe loading conditions due to the aforementioned deck movements as well as the continuous traffic loading. As a result, they require regular maintenance throughout the lifetime of the bridge, which is costly and inconvenient for the bridge users. Expansion joints have therefore always been a source of construction and maintenance inconvenience to bridge engineers. Consequently, the concept of joint-less or integral abutment bridges (IABs) has been proposed as a remedy. In a typical IAB, the bridge deck is physically and structurally free of joints and is rigidly connected to the abutments as a single structural unit.

The first use of the integral abutment bridges was recorded in 1938 in the United States and since then they have been widely utilized around the world. Nowadays, IABs represent the standard choice of bridge construction in many countries such as US and the United Kingdom. The IAB system provides an excellent alternative to overcome the expansion joint issues in addition to achieving substantial savings in the construction and maintenance costs.

In spite of the various advantages of the IAB system, it is not without some inherent problems of its own, which largely limit its use. The problems in the IABs are due to the complicated soil-structure interaction behaviour unique to this type of bridges. The expansion and contraction of the bridge deck in response to the variations in the ambient temperatures will be reflected on the abutments in cycles of passive/active movements due to the absence of expansion joints (Figure 1.1(a)). Although the amplitude of such movements is very small and only ranges within few tens of millimetres, it could result in significant structural and geotechnical problems in the

long term. This is because the cyclic movements of the abutment will result in settlement in the approach soil and an increase in the lateral earth pressures acting on the abutment wall. The settlement usually produces a trough at bridge approach (Figure 1.1(b)), which poses rideability and safety issues to bridge users. Furthermore, the stress ratcheting effects developed under the densification of the approach soil will impose an escalated loading on the bridge structure which is not encountered in jointed or conventional bridges.

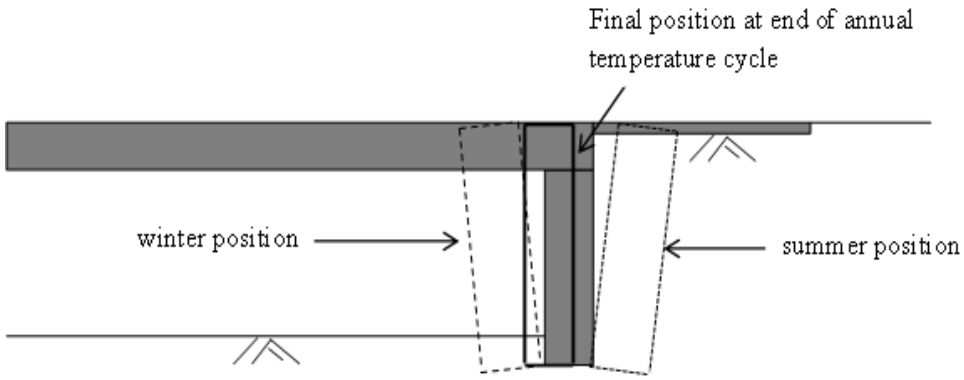

(a)

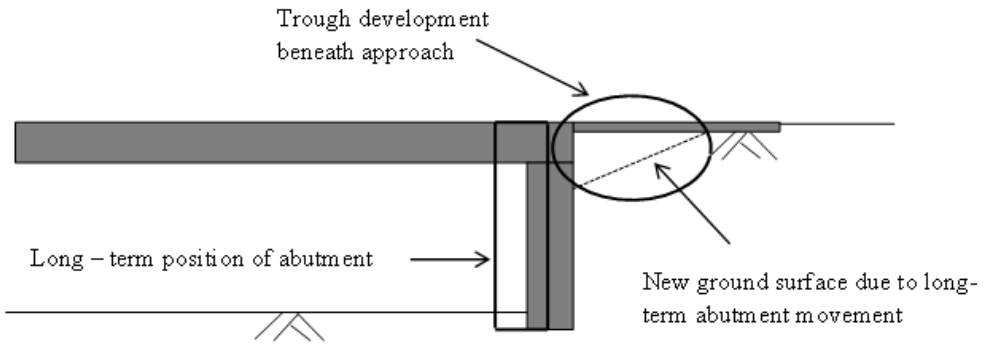

(b)

Figure 1.1 Abutment thermally induced movements and the subsequent effects on bridge approaches (Horvath, 2000)

The temperature induced effects and the subsequent approach settlement and lateral pressures in the IABs represent primary impediments that largely restrict the use of IABs to limited ranges of bridge length. Therefore, introducing a practical engineering solution to rectify or at least alleviate the effects of the approach issues

in IABs has been a principle concern of the geotechnical and structural engineers dealing with the integral abutment bridges. Such a solution will broaden the use of the IABs and maximize their engineering and economic advantages.

The current practices which are utilized to overcome the approach problems in IABs involve the use of concrete run-on slab at the bridge approaches to span the possible settlement. However, the use of run-on slab is arguable and engineers in some countries such as the UK do not recommend it as it complicates the approach maintenance works (Lock, 2002). In such cases, the engineers rely on regular approach patching and pavement overlying to rectify the settlement effects. Other available measure is to use well compacted backfill at the bridge approaches, which may minimise the soil settlement. However, it has been found that heavily compacted backfill result in significant escalation in the lateral earth pressure acting on the abutment wall due to the cyclic movements. Hence, current remedial measures have only a limited success in alleviating the problems produced by the abutment movements.

A logical approach to mitigate these problems entail inserting a compressible fill material between the abutment wall and the retained soil. The inclusion will then absorb the abutment movements with a minimal disturbance transferred to the adjacent soil. It is hypothesized that such a remedial measure will greatly attenuate the settlements and lateral earth pressure issues in IABs. Among many of the fill materials, the expanded polystyrene geofoam (EPS) provides an excellent choice for such a purpose (Horvath, 1997). The EPS is highly compressible and possesses high compression strength to weight ratio. It has an excellent record of success in a wide range of geotechnical applications such as a fill material for light weight embankments, compressible inclusion behind retaining structures and stabilisation of slopes, etc. Nevertheless, the potential use of EPS geofoam in rectifying the intractable approach problems in IABs has not been thoroughly investigated.

In this research, the application of the EPS as a compressible inclusion in the IAB approaches will be rigorously studied with a focus on producing a possible remedy for the soil settlement and the lateral pressure ratcheting issues. However, utilizing the EPS geofoam in such an application requires a proper understanding of the soil-abutment interaction behaviour in the IABs and an insight into the important factors

affecting such behaviour. This research will thus include a study of the primary factors influencing the abutment-soil behaviour and produce conclusions to improve the existing design approaches.

1.2 Research Impetus and Objectives

A considerable amount of research effort has been expended in the past to investigate the temperature effects on the IABs. The majority of these research studies were focused on predicting the lateral pressures and, to a lesser extent, the settlement of bridge approaches rather than developing a practical and effective remedial measure for these problems. Therefore, the existing design practice does not include detailed standard guidelines on the possible use of EPS geofoam in the approaches of the IABs.

The primary aim of this thesis is to investigate the predominant factors that govern the soil-wall interaction in IABs and develop the existing knowledge for the possible application of the EPS geofoam to mitigate the approach problems. The specific objectives of this study include:

- Perform a comprehensive review of the current literature that concerns the soil settlement and the lateral pressure ratcheting problems in IABs. This will also include reviewing the primary characteristics of the EPS geofoam and its applications. This literature review will summarize the existing relevant knowledge, identify the research gaps and eventually determine the outlines of this study.
- Develop a two-dimensional finite element model to simulate the effects of abutment movements on the retained soil and validate that model with reliable experimental data from the literature.
- Conduct a parametric study to investigate the influence of a number of important factors governing the soil-abutment interaction in an IAB using finite element modelling.
- Perform laboratory experiments on a small physical model to study the effects of the mode of wall movement on the soil settlement and the lateral pressures encountered in the IAB approaches.
- Investigate the potential influence of the EPS geofoam on the settlement and lateral pressure by using the physical model.

- Conduct experiments as required and calibrate a constitutive model to simulate the soil-wall interaction behaviour when an ESP inclusion is involved.
- Validate the finite element model with EPS geofoam inclusions using results from the physical model.
- Develop a two-dimensional finite element model to investigate the potential use of EPS inclusions in prototype dimensions for different geometric configurations of EPS.
- Produce a set of conclusions highlighting the primary factors that govern the wall-soil interaction and the potential use of EPS geofoam in attenuating the approach settlement and lateral pressure ratcheting in IABs.

1.3 Scope and Limitations

The scope of this study involves both theoretical and experimental investigations of the soil-structure interactions associated with the IABs as a result of the fluctuations in the ambient temperature. In particular, the study focuses on the approach problems, namely, the settlement of the approach soil and the escalation in the lateral earth pressures acting on the abutment under passive-active cyclic abutment movements. The utilization of the expanded polystyrene geofoam compressible inclusion to alleviate the approach problems in IABs is also included in the scope of this study.

However, It is worthwhile noting that the influence of long term creep and temperature effects on the EPS geofoam are considered beyond the scope of the study. Also, the densification in the soil due to the cyclic active-passive wall movements is not included in the constitutive model of soil. Due to the extensive scope of work needed to incorporate creep, temperature and densification effects, these will be left for a future study.

1.4 Structure of Thesis

- Chapter Two

  Chapter two involves a comprehensive review of the current literature dealing with the approach problems in integral abutment bridges. Particular focus is given to the effects of the temperature induced abutment movements and the

subsequent lateral pressure escalation and soil settlement. Then the existing measures utilized to tackle the approach problems are discussed. The general characteristics and applications of the EPS geofoam in the geotechnical engineering are also reviewed. Finally, the gaps in the current knowledge of the soil-structure interaction in IABs are identified.

- Chapter Three

  This chapter consists of numerical analyses for a concrete abutment with the retained soil experiencing cyclic movements. A plane strain finite element model is developed using the ABAQUS/Standard to simulate the wall. Validation of the finite element model using centrifuge test results is presented in this chapter. Also, a parametric study is conducted to investigate the influence of soil properties and the pattern of the temperature changes on the approach settlements and the lateral soil pressures.

- Chapter Four

  In this chapter, an experimental program is carried out on a physical model represented by a small wall retaining loose sand and subjected to passive/active movement cycles. During the tests, the settlement at the soil surface and lateral soil pressures acting on the wall are measured. This test program aims to investigate the effectiveness of EPS geofoam in mitigating the soil settlement and the lateral earth pressure issues. Also the wall-soil interaction behaviour under different modes of wall movements (rotation or translation) has been investigated.

- Chapter Five

  The effectiveness of EPS geofoam in alleviating the approach problems in IABs in prototype dimensions has been investigated in detail in this chapter using finite element simulation. A two-dimensional plane strain ABAQUS model has been developed and verified using the physical model test results described in chapter four. Two different arrangements of EPS inclusions are discussed based on the angle of the interface plane between the soil and the EPS wedge.

- Chapter Six

  In this chapter, the final conclusions derived from the work conducted in this study and the recommendations for future studies in regard to the use of EPS geofoam to overcome the approach problems in the IABs are presented.

1.5 Publications

The outcomes of this study have been summarized and submitted for publication as described below:

- Alqarawi, A., Leo, C. J., Liyanapathirana, D. S. and Ekanayake, S. D. (2015). Parametric study on the approach problem of an integral abutment bridge subjected to cyclic loading due to temperature changes. *Journal of Applied Mechanics and Materials* (Manuscript accepted)
- Alqarawi, A., Leo, C. J., Liyanapathirana, D. S. and Ekanayake, S. D. (2015). A study on the effects of abutment cyclic movements on the approach of integral abutment bridges. *Australian Geomechanics Journal.* (Manuscript accepted).
- Alqarawi, A., Leo, C. J., Liyanapathirana, D. S. and Ekanayake, S. D. (2016). The approach problem of an integral abutment bridge subjected to cyclic loading due to temperature changes. *19th Southeast Asian Geotechnical Conference and 2nd Association of Geotechnical Societies in Southeast Asia, Malaysia 2016*. (Manuscript accepted).
- Alqarawi, A., Leo, C. J., Liyanapathirana, D. S. and Ekanayake, S. D. (2016). The effects of mode of wall movement and the use of EPS geofoam on the approach problems in integral abutment bridges. (Manuscript in preparation for submission based on Chapters 4 and 5 of this thesis)

Chapter 2

Literature Review

2.1 Introduction

Bridges are commonly built with expansion joints to allow for the movements occurring within the deck of the bridge. These movements involve the expansions and contractions caused by the temperature changes, shrinkage and creep or the long term settlements of the sides of the bridge. Bridge expansion joints are normally exposed to severe loading conditions as a result of the continuous traffic loadings. Consequently, they deteriorate or lose their intended function quite rapidly and require regular maintenance throughout the lifetime of the bridge. A defective expansion joint can be a source of various problems to the bridge structure and bridge users. It may allow the salt-laden water to leak from the pavement surface into the bridge girders, bearings and the concrete substructure causing corrosion and deterioration of bridge substructure (Mistry, 2005). A survey on 200 bridges in the United Kingdom revealed that the expansion joints are the dominant source of costly and traffic-retarding maintenance works (Lock, 2002). Moreover, defective expansion joints can produce a serious hazard to bridge users due to the broken or loosen parts. Therefore, maintaining a bridge to a high level of performance and safety standard requires costly and frequent maintenance works.

Because of the potential construction and maintenance problems associated with the expansion joints, a new trend of bridge constructions has arisen. The new concept aims to construct a bridge system that is physically and structurally free of joints or bearings. This type of bridge systems are referred to as Integral Abutment or Joint-less bridges (IAB). Terms like “continuous bridges” and “rigid bridges” have also been used in literature to describe the IABs (Bayoglu, 2004). In a typical integral abutment bridge, the deck is continuously running along the bridge without joints and is rigidly connected to the bridge abutments as a single structural unit. Abutments, on the other hand, are used to retain the soil backfill on both sides of the bridge. Figure 2.1 shows a typical IAB system.

In this chapter, a comprehensive literature review has been conducted to outline the dominant problems encountered in IABs and in particular the interaction behaviour between the approach soil and bridge substructure. Since the current study investigates the application of the Expanded Polystyrene (EPS) geofoam to mitigate the potential approach problems in IABs, the behaviour of EPS will also be reviewed in this chapter.

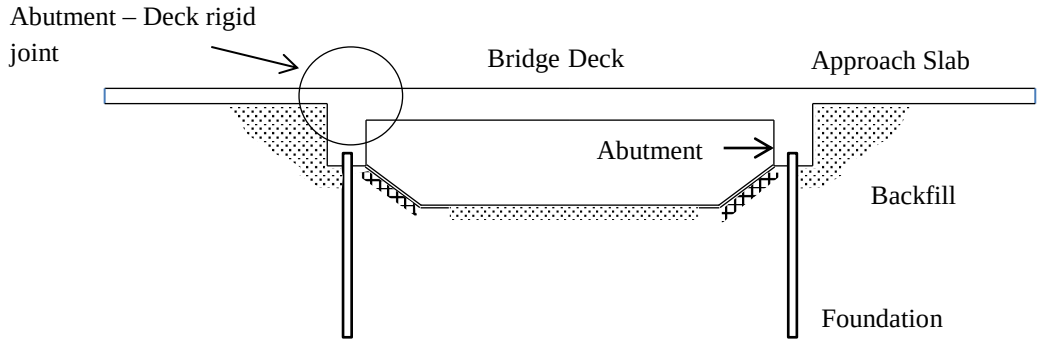

Fig. 2.1 Integral Abutment Bridge System

2.2 Integral Abutment Bridges (IABs)

Integral bridges have been used since 1938 in Ohio, United States (Burke, 2009). During the following decades, the concept of integral bridges has been progressively adopted in many countries around the world. In 1980, the American Federal Highway Association (FHWA) recommended to construct bridges with overall lengths of 90 m for steel bridges, 150 m for cast-in-place concrete bridges and 183 m for post-tensioned bridges as IABs (Hassiotis, 2005). In 1996 the British Highways Agency advised to use the integral bridge system for any bridge up to 60m length (Lock, 2002). In Japan, the construction of the first integral bridge was completed in 1996 while South Korea constructed its first integral bridge in 2002 (Burke, 2009). In Australia, IABs are receiving growing interest and considered as an option in recent projects. In the Peninsula Link Highway project in Victoria, eleven out of thirty bridges were constructed with IABs (Gibbens and McManus, 2011).

Currently, the IABs are the standard design option in most of the US states (Hassiotis, 2005). Although the IABs are still outnumbered compared to the conventional or jointed bridges, the overall trend of bridges construction seems to be moving toward IABs (Mistry, 2005).

2.3 Advantages of IAB system

Integral bridges are generally performing efficiently and last longer than traditional bridges with less maintenance works (Burke, 2009). The attributes of IABs are principally ensuing from eliminating of the expansion joints and bearings from the bridge deck. The advantages of IABs can be summarized as below,

- Minimise the construction cost and project time.
- Significant savings in the potential maintenance costs throughout the lifetime of the bridge.
- Ease of design and construction
- The structural continuity improves the bridge structural performance in terms of resisting seismic loads
- Eliminate the possible safety issues due to defective joints and alleviate riding quality issues.

2.4 Problems and Limitations of IABS

Although, the IAB system is likely to overcome the construction and maintenance difficulties caused by the expansion joints, other problems seem to be inherently associated with IABs. Temperature fluctuations that occur on both diurnal and seasonal basis will result in changes in the dimensions of the bridge. Bridge deck will expand or contract in response to the changes in the ambient temperature. Such changes in the bridge dimensions cannot be accommodated within the bridge deck due to the absence of the expansion joints. Therefore, the thermal induced deformations will be reflected on the bridge abutments in terms of rotational and translational movements, against and away from the retained approach soil, corresponding to the temperature changes. During the hot or summer seasons, the deck will expand and will push the abutments toward the retained soil, while in the winter seasons abutments will be displaced in the reverse direction towards the bridge deck. As the abutment is normally connected to the deck at the top end, the greatest magnitude of displacement typically occurs at the highest end of the abutment and decreased down towards the base (Horvath, 2000).

Temperature variation has critical effects in integral abutment bridges and their impacts can be as significant as the live loads (Thevaneyan et al., 2014). Therefore,

even when abutment displacement is relatively small and does not exceed a few tens of millimetres, it may constitute a source of significant long term structural and geotechnical problems.

An in-depth understanding of the effects imposed by the temperature induced cyclic movement of bridge abutments is still lacking. This is a result of the complex interaction mechanism between the retained soil and the bridge structure (Huntly and Valsangkar, 2013). However, according to the literature, there are two primary detrimental effects result from the abutment movements as discussed below.

2.4.1 Long term built–up of lateral earth pressures:

When a bridge deck expands under a temperature increase during the hot season, it will push the abutments against the retained soil which increases the lateral pressure imposed on the abutment by the backfill. In that case, earth pressures will certainly exceed the at–rest pressure (K_o) or the initial pressure of the abutment. In the reverse cycle, when the abutment is displaced towards the bridge deck as a result of bridge contraction, a wedge-shaped part of soil will slide into the gap induced behind the abutment. This part of soil will resist the abutment returning back to its initial position when temperature rises again. As such, the abutment will experience an extent of inward translational movement relative to its original position. The repetition of that scenario will lead to increased lateral pressure on abutments in an accelerated rate causing what is called *stress ratcheting* (Horvath, 2000; England et al., 2000). The build-up of lateral pressure under this phenomenon may take many years to occur, but it can produce a serious structural problem that may result in abutment failure.

2.4.2 Settlement of the bridge approach

The cyclic movement of the abutment towards and away from the retained soil and the associated increase in lateral pressure will result in soil densification and volume contraction of the retained backfill (Ng et al., 1998). Furthermore, soil slumping will also occur behind the abutment wall due to both the cyclic rotational and translational movements of the abutment. Eventually, the aforementioned impacts will collectively contribute to develop the classical soil trough at the bridge approaches. Figure 2.2 shows a typical soil trough developed at an IAB approach.

The size, pattern and depth of the soil trough depend on different factors such as the frequency and amplitude of the cyclic movement, depth and type of the abutment wall and the properties of the backfill (Cosgrove and Lehane, 2003). Some theoretical data proposes that the influence zone of settlement extends to a distance equals to 2*H*, whereas *H* represents the height of the abutment. However a finite element analysis performed by Arzoe et al. (1999) show that the influence zone may extend to a distance more than 3*H* from the face of the abutment.

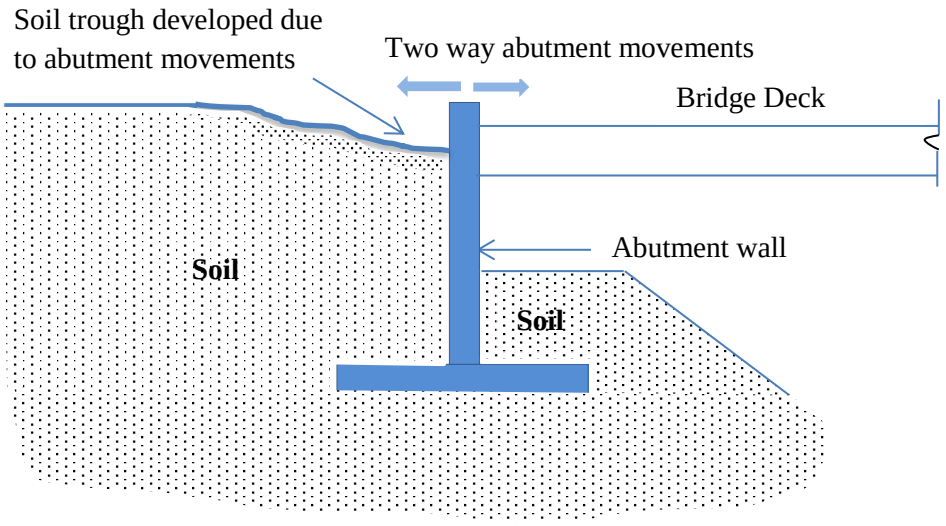

Fig. 2.2 Typical approach settlement in integral bridge due to abutment cyclic movements

The information available on the effects of abutment movements in IABs on the approach soil is still far from complete. Limited experimental tests have been conducted to investigate the settlements and lateral pressures at the approach soil that include centrifuge tests, (Springman et al., 1996; Ng. et al., 1998), small scale experiments at a normal gravity (England et al., 2000; Cosgrove and Lehane, 2003; Tatsuoka et al., 2009) in addition to field data collected from in-service IABs (Wolde-Tinsae, 1988; Hoppe and Gomez, 1996; Arzoy et al., 1999; Hoppe, 2005; Civjan et al., 2007; Barr et al., 2013; Huntley and Valsangkar, 2013).

2.5 An Overview of the Existing Theories

2.5.1 Lateral Earth Pressures

Lateral earth pressures behind bridge abutments were generally estimated using classical theories such as Coulomb and Rankine. They introduce methodologies for calculating the active and passive earth pressures taking into account a plane failure surface (Khodair, 2009). Rankine theory assumes a linear variation of stress at the interface with a frictionless wall and calculates the active and passive pressures using the following formulas,

$$P_a = \gamma z K_a \tag{2.1}$$

$$P_p = \gamma z K_p \tag{2.2}$$

where γ is the unit weight of the soil, z is the depth from the soil surface, K_a and K_p are the active and passive coefficients of lateral earth pressures respectively and are defined as,

$$K_a = \frac{1-sin\emptyset}{1+sin\emptyset} \tag{2.3}$$

$$K_p = \frac{1+sin\emptyset}{1-sin\emptyset} \tag{2.4}$$

In Coulomb theory, earth pressures behind a vertical wall retaining a backfill is calculated as follow,

$$K_a = \frac{cos^2\emptyset}{cos\delta\left[1+\{sin(\emptyset+\delta)sin\emptyset/cos\delta\}^{1/2}\right]^2} \tag{2.5}$$

$$K_p = \frac{cos^2\emptyset}{cos\delta\left[1-\{sin(\emptyset-\delta)sin\emptyset/cos\delta\}^{1/2}\right]^2} \tag{2.6}$$

where $\emptyset$ refers to the friction angle of the soil, δ is the angle of friction between the soil and the wall.

Despite that the IABs are widely utilized across the world, there is no standard or unified design approach that describes the magnitude and distribution of lateral earth pressure acting on the abutments (Arzoy et al., 1999; Huntly and Valsangkar, 2013). The current design guidelines are based on empirical approaches or past experiences from previously constructed structures. This may ensue from the lack of

understanding for the soil-structure interaction issues unique to this type of structures.

The US practice involves significant variations in the design guidelines and limitations of the integral bridges among different states. However, the recommendations of the American Association of State Highway and Transportation Officials (AASHTO) are generally adopted in many states in US (Bayoglu, 2004).

In Australia, the design of IABs is primarily based on the UK Design Manual for Roads and Bridges, BA42/96(2003) which is issued by the British Highways and Bridges Agency.

The UK Design Manual for Roads and Bridges, BA42/96 (2003) provides some guidelines to estimate the value and distribution of the lateral earth pressure acting on the abutment of integral bridges. Based on experimental data and field observations, the UK BA42/96 (2003) developed the following equations to calculate the lateral earth pressure coefficient (*K*).

For shallow abutment wall ($H \leq 3m$)

$$K^* = K_o + \left(\frac{d}{0.025H}\right)^{0.4} K_p \tag{2.7}$$

For Full height abutment ($H > 3m$) hinged at its bottom end

$$K^* = K_o + \left(\frac{d}{0.015H}\right)^{0.6} K_p \tag{2.8}$$

where K^* refers to the lateral earth pressure coefficient at the passive state, d is the horizontal wall displacement, H is the retained height of the soil, K_o represents the theoretical at-rest lateral earth pressure coefficient ($1 - sin\emptyset$) and K_P is the Coulomb passive coefficient of lateral pressure calculated at soil-abutment friction angle δ equal to half of the soil internal friction angle $\emptyset$.

Figures 2.3 and 2.4 show the distribution of the lateral earth pressures behind (a) frame abutment and (b) full height embedded wall as suggested by the UK BA42/96 (2003). It is apparent that the coefficient of lateral pressure is assumed to be constant at a value equal to K^* at the upper part of the abutment and decreases linearly toward K_o at the bottom of the wall.

England and Tsang (2005) modified the recommended equation of the UK Highways Agency (BA42/96, 2003) where the passive pressure coefficient K^* is calculated from Equation 9.

$$K^* = K_o + \left(\frac{d}{0.03H}\right)^{0.6} K_p \quad (2.9)$$

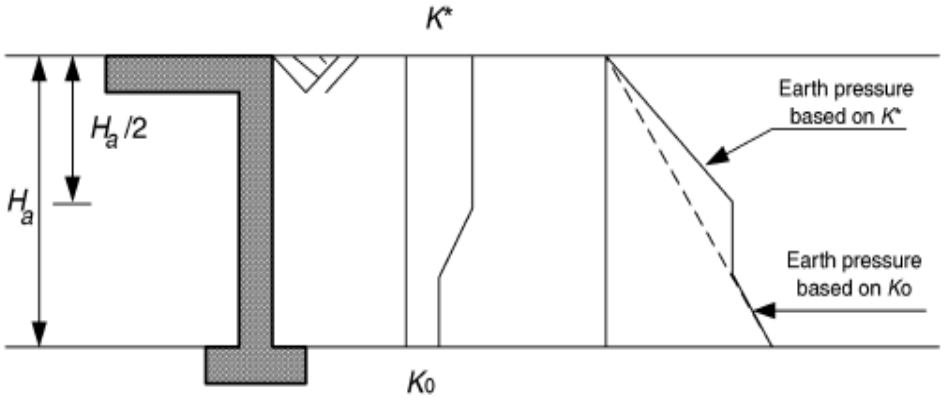

Fig. 2.3 Lateral earth pressure distribution behind frame abutment (BA42/96, 2003)

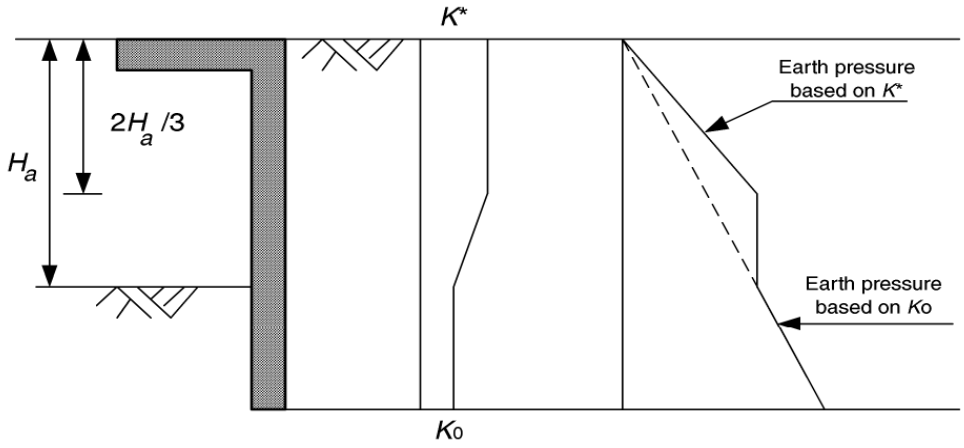

Fig. 2.4 Lateral pressure distribution behind full height embedded wall (BA42/96, 2003)

It is apparent that the recommendations given by the UK BA42/96 (2003), Equations 7 and 8, do not account for the number of abutment rotations required for the possible hardening and stiffness increase in the retained backfill. This approach does not take into account the findings of a number of researchers who observed an escalation in the lateral stresses with the number of movement cycles (Ng. et al., 1998; England et al., 2000; Horvath, 2000; Lehane, 2011).

Lehane (2011) reported centrifuge test results conducted at the University of Western Australia on a deep wall integral bridge. He reported that stresses behind abutment wall increase linearly with the logarithm of the number of cycles, *N*, up to 100 cycles. However, values of lateral stress asymptote between 100 and 1000 cycles. He also stated that the location of the maximum lateral pressure is observed at the upper half of the wall height.

According to Lehane (2011), the escalation in the lateral stresses is associated with an increase in the stiffness of the soil adjacent to the wall. He emphasised that the estimation of lateral stresses has to account for the actual or, as described by him, the "operational stiffness" of the soil E_p. Based on a backward analysis from test results, he found that, at a relatively small wall displacements, the operational stiffness (E_p) of the soil relates primarily to the small-strain modulus E_o and is independent to the initial soil density. Lehane (2011) suggested that the E_p can be assumed as 40% of the small-strain stiffness of the compacted backfill E_{oc}.

Lehane (2011) compared the lateral stresses computed using a simple elastic FE model that utilises the operational stiffness of the soil E_p with the recommendations given in the UK publication BA42/96(2003), i.e. Equations 7 and 8.

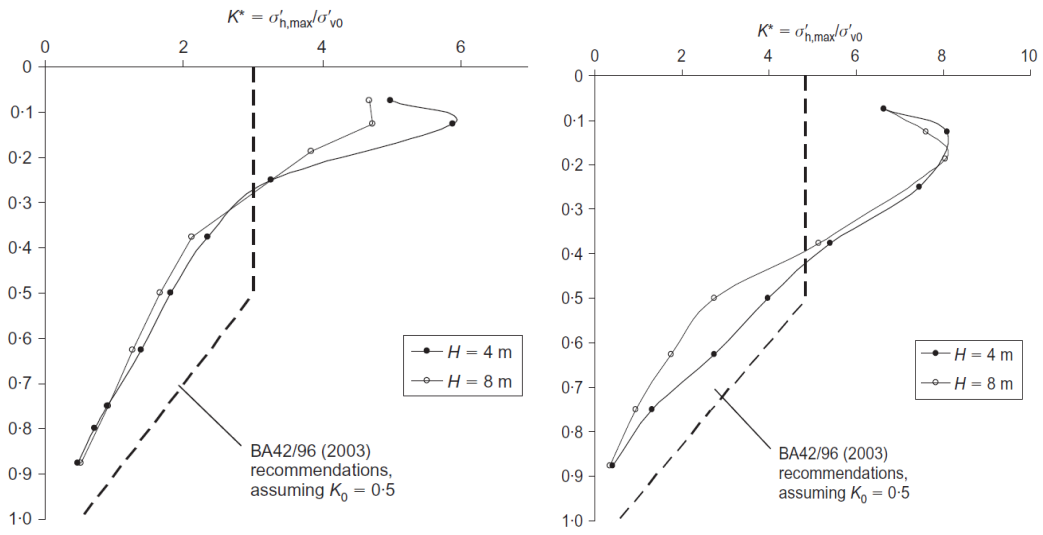

(a) (b)

Fig. 2.5 Comparison of the value of K^* as predicted by Lehane (2011) with those recommended in the UKBA42/96 (2003) at displacement amplitude equal to (a) 0.2% and (b) 0.5%

He found that the UK BA42/96(2002) recommendations underestimate the lateral earth pressure at the upper third of the abutment, as shown in Figure 2.5.

Broms and Ingelson (1971) measured the lateral earth pressures acting on the abutments in 150m and 110m integral bridges in Sweden. Based on the observed data, they propose that the lateral earth pressure behind an abutment experiencing cyclic movements varies linearly from zero at the top (at soil surface) to Rankine passive pressure at $1/3$ H then decreases linearly to Rankine active pressure at the bottom of the wall (H refers to the retained height of the abutment). This proposed envelope for lateral pressure accounts for the stresses developed due to the compaction of the backfill in addition to the rotational movements of the abutments. Sandford and Elgaaly (1974) modified this pressure envelope, as given in Figure 2.6, considering the pressure acting at the toe of the abutment equals to the at-rest pressure instead of the Rankine active pressure.

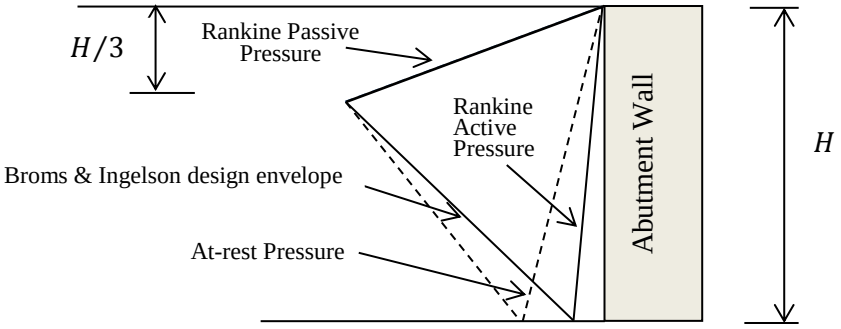

Fig. 2.6 Earth Pressure distribution behind Abutment (After Bayoglu, 2004)

Ng. et al. (1998) conducted centrifuge tests on loose and dense sand backfills subjected to range of cyclic perturbations. According to Ng. et al. (1998) the temperature effects in IABs result in rotational and translational movements in bridge abutments. It was found that the active movements of the wall lead to slippage of soil particles into the gap between the wall and soil which results in an increase in lateral earth pressure. They stated that the development of high lateral pressures is dependent to the amount of perturbation, number of cycles and the density of the soil. However, at a given magnitude of perturbation, the lateral earth pressure coefficient K increases with the number of cycles in a decreasing rate. The test results showed that, 50% to 70% of the total increase in the value of K after 100 cycles is actually occurring within the first 20 cycles.

Throughout the test, the value of K has always been exceeding the at-rest pressure coefficient K_o. After applying the annual perturbations ($\pm 30mm$) the maximum measured value of K exceeded the theoretical value of the passive earth pressure coefficient K_p. The critical values of lateral pressures observed in the test were all located closer to the surface of the soil than to the base of the wall.

England et al. (2000) conducted an experimental program on a small wall retaining a sandy soil. Rotational amplitudes (d/H) ranging from 0.13% to 0.9% were applied (d refers to the horizontal displacement of bridge deck at one side at the abutment top level and H represents the total height of the abutment). The test results reported by England et al. (2000) showed a rapid escalation in the lateral stresses from the initial K_o value during the first ten cycles. However, stresses thereafter were increasing at a slower rate. The maximum value of the lateral pressure coefficients K measured at a passive state, after 300 cycles of ±0.125% amplitude, was 2.6 and recorded at the upper third of the wall height. On the other hand, the active pressure was found to be insensitive to the increase in the number of cycles and varied in small range between 0.1 and 0.2.

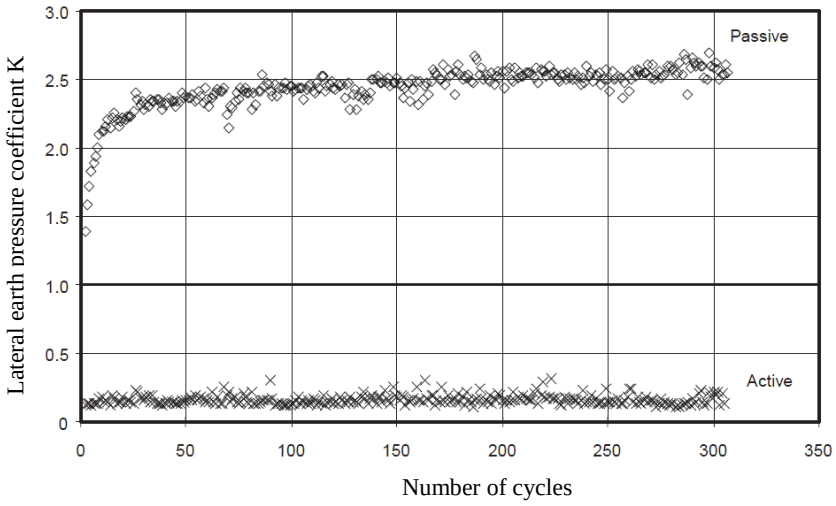

Fig. 2.7 Variation of the pressure coefficient K with the number of cycles (England et al., 2000).

Tatsuoka et al. (2009) conducted series of plane – strain tests on a 505mm high small wall retaining loose sand. Tests involved using hinge – supported wall, at its bottom end, which allows only rotational movement as well as embedded wall in which translation and rotation movements are fairly free. Horizontal amplitudes (d/H)

ranging between 0.2% and 0.6% were applied at the top of the wall (*d* refers to the horizontal displacement at the top of the wall and *H* represents the total height of the wall). Two styles of horizontal displacement involving "active-only" and "active/passive" were applied (active-only refers to the wall movement within a range between initial and active positions while active/passive refers to the wall movement within the range of passive - active positions).

After a number of loading cycles, escalations in the lateral stresses were apparent in both active and active/passive tests. Lateral pressure coefficient *K* became five times higher than the initial value K_o after 200 cycles of 0.2% active-only displacement as shown in Fig. 2.8.

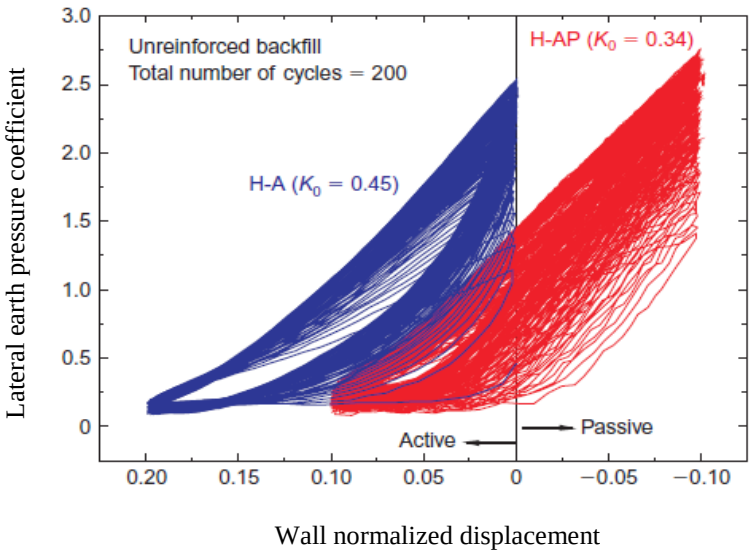

Fig. 2.8 Relationship between the lateral pressure coefficient, *K* and the horizontal wall displacement, in active and active/passive conditions (Tastsouka et al., 2009)

Huntley and Valsangkar (2013) reported field data collected, over three years, from 76m length two-span integral bridge in Brunswick, Canada. The bridge was instrumented during the construction with six load cells (three at each abutment) mounted at 0.25H, 0.5H and 0.75H (H refers to the abutment height). The abutments were also provided with deformation and tilt meters to detect any translation or rotation in the abutment. The results showed that the movements of the abutments, translation and rotation, are generally conforming to the temperature fluctuations. However, the abutments did not exhibit equal movements whereas the western abutment rotates slightly more than the eastern one. According to Huntly and

Valsangkar (2013) this variation may ensue from different exposure to the sun light or from some differences in degree of compaction of the approach backfill.

The field data indicate that lateral stresses acting on the abutments were correlating with the temperature changes and wall movements. Maximum lateral earth pressures were recorded during summer in each of the three years. The stresses at the western abutment recorded high values at the upper sensor compared to the mid and lower sensors, while in the eastern abutment stresses were almost constant throughout the height of the abutment. This highlights the influence of the movement mode on stress distribution, where the motion in the eastern abutment was predominantly translation with a very small amount of rotation.

Huntly and Valsnagkar (2013) compared the measured data with those calculated using different theoretical models. The comparison illustrated in Figure. 2.9 shows that none of the existing models suitably captures the behaviour of lateral earth pressure acting on the abutment. It is apparent that all the models are largely conservative in the lower part of the abutment while in the upper part, passive pressure was fully mobilised and exceeded most of the theoretical values.

Huntly and Valsangkar (2013) also stated that stress ratcheting trend has not been observed in the field data. However, it is evident that the period of observation reported by them is considerably short (three years) which consists of only three seasonal cycles ($N = 3$). Moreover, the movement envelopes of the abutments are relatively small (approximately ±7mm for the eastern abutment and ±9mm for the western abutment), which reflects a small displacement amplitudes. Therefore, stress ratcheting effects are unlikely to occur within these conditions.

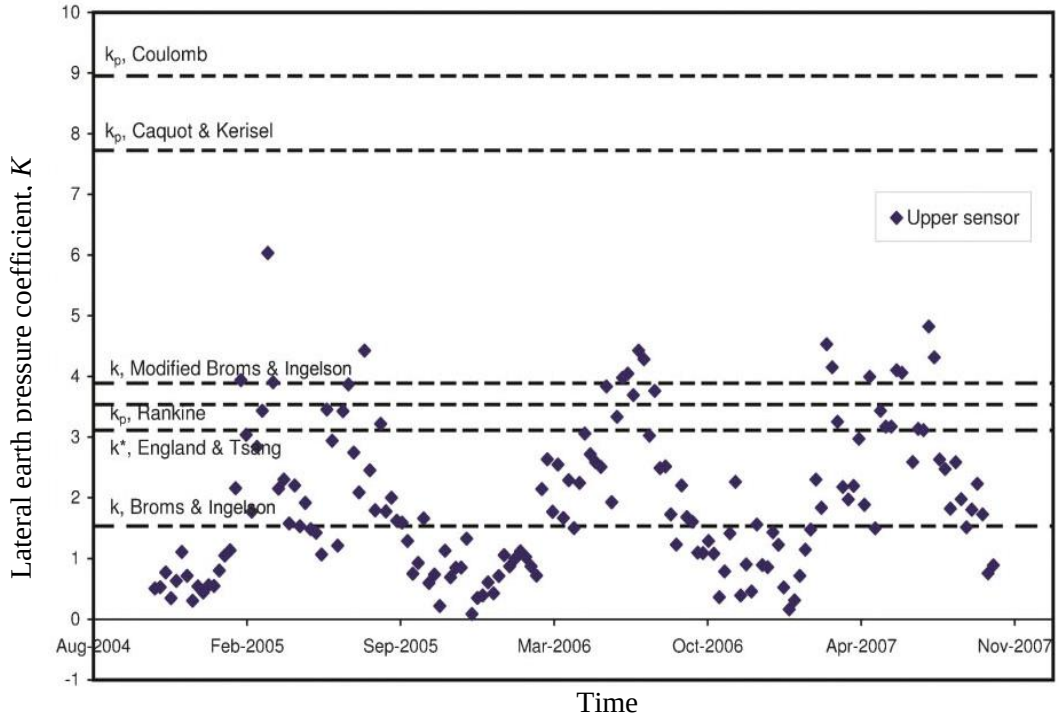

Fig. 2.9 (a)

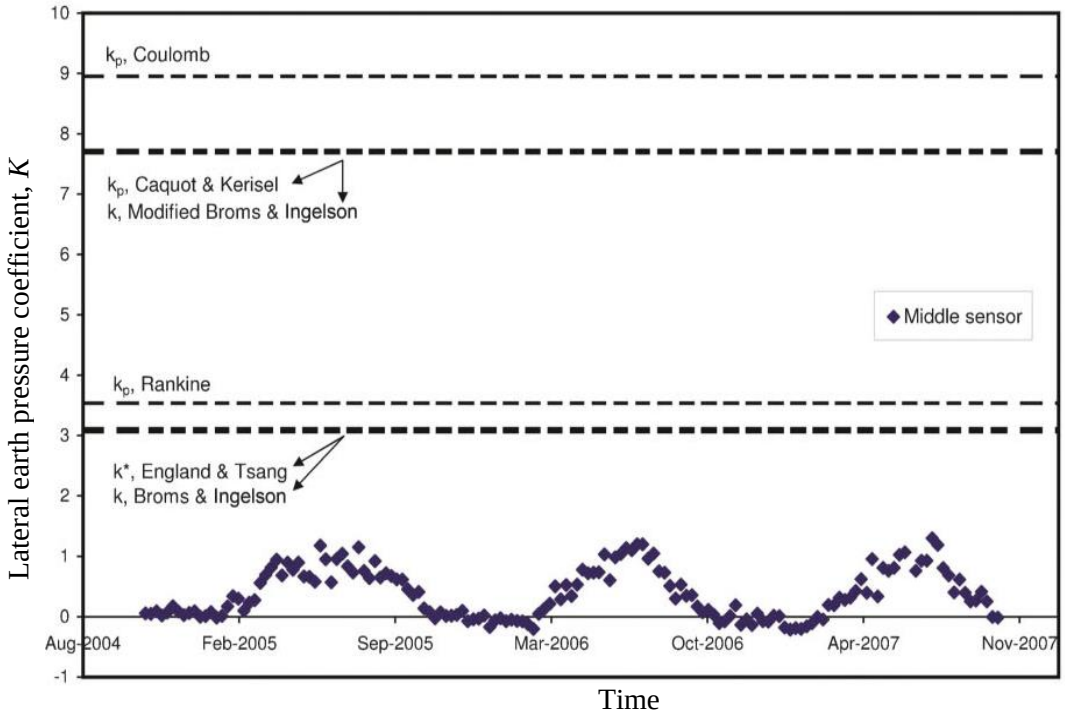

Figure 2.9 (b)

Figure 2.9 Measured earth pressures at (a) the upper and (b) middle sensors of the western abutment (Huntly and Valsangkar, 2013)

Hoppe and Gomez (1996) reported field data collected from 98m two-span semi integral bridge with 2.7m height concrete back wall in Virginia-USA. The bridge

was instrumented during the construction stage and data were recorded for two and half years. The collected data showed a daily variation in the lateral pressures acting on the back wall in conformance with the temperature changes. Full passive earth pressure was mobilised at the back of the wall and recorded at the upper pressure cell (at 1.3m from the top). The maximum weekly pressures acting on the wall for the period between January 1994 and January 1996 are presented in Figure 2.10. It is apparent that a slight escalation in the average values of maximum stresses occurs during this period. Abutments A and B showed similar behaviours in terms of lateral pressure development but with differences in the magnitudes. Maximum lateral stresses recorded in Abutments A and B were 175kPa and 200kPa respectively. According to Hoppe and Gomez (1996) such variation might be a result of different degree of compaction of soil in both approaches.

Based on a backward analysis from the field data, they observed that the computed internal shear angle and unit weight of the soil (35°, 18kN/m^3) are higher than initial values used in the design. This indicates densification effects occurred in the approach backfill.

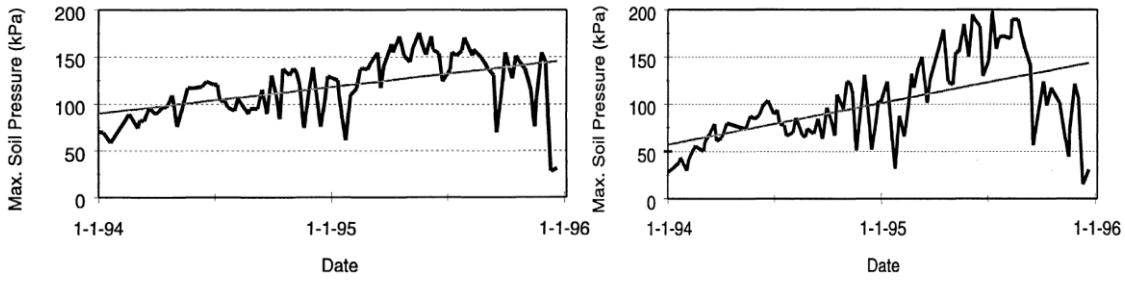

(a) (b)

Fig. 2.10 Maximum weekly soil pressures acting on (a) back-wall A and (b) back-wall B (Hoppe and Gomez, 1996)

It can be observed from the previous review, that predicting maximum lateral pressures in the IABs using various models depends primarily on the theoretical value of lateral earth pressure coefficient K_p.The existing design guidelines do not provide a conclusive information on the method of calculating K_p. Therefore, designers are usually free to choose the method to determine the value of K_p, which consequently reflect a difference in the design outcomes. Tan et al. (2015) compared the UK BA42/96 (2003) lateral earth pressure coefficient K^* computed based on Rankine and Coulomb theories, as shown in Figure. 2.11. It was found that at d/H

equals to 1%, the difference in the values of $K^*$was approximately 30% and 20% in Equations 7 and 9 respectively.

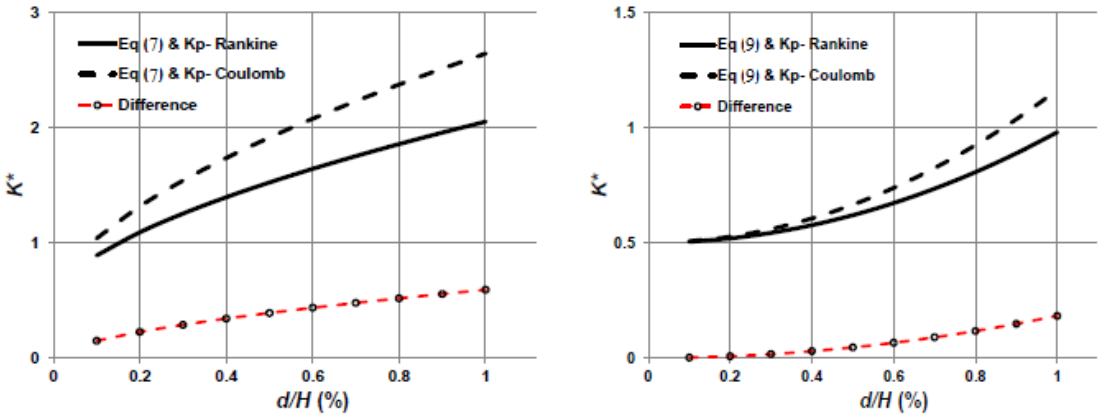

(a) (b)

Fig. 2.11 Variation in the Value of K^*computed based on (a) Equation 7 & (b) Equation 9 (After Tan et al., 2015)

2.5.2 Settlement of the Approach Soil

Settlement of the approach soil is a very common problem in the integral bridges. Both, the experimental tests as well as the field observations show that the retained backfill experiences an extent of settlement as a result of the movements of the abutments (Ng. et al., 1998; England at al., 2000; Cosgrove and Lehane, 2003; Tatsuka et al., 2009).

The centrifuge test results of Ng. et al. (1998) showed significant soil settlements in the proximity of the wall after 100 cycles of (±60mm) perturbations. According to Ng. et al. (1998), the combination of the rotational and translational movements of the wall results in densification and volume contraction in the adjacent soil. Dense and loose soils exhibited different settlement profiles, as illustrated in Figure. 2.12. A sink-like trough was observed in the dense backfill with a maximum settlement of 660mm. On the other hand, the loose soil produced a steady settlement increasing towards the abutment wall with maximum settlement reaching 700mm. The influence zone of settlement in loose soil was approximately two times greater than that in the dense soil.

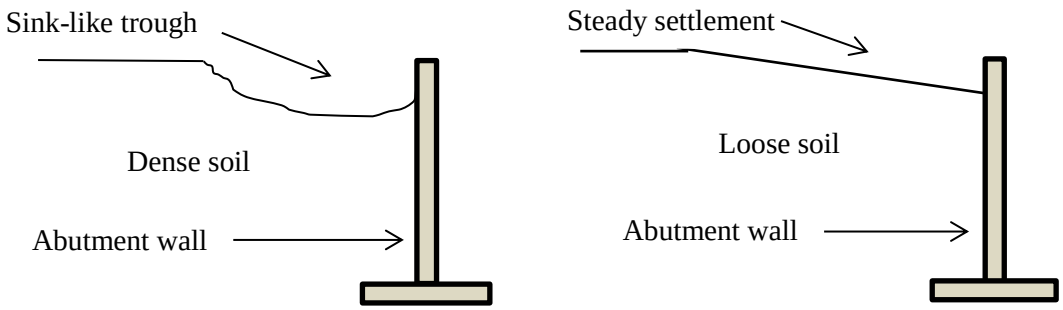

(a) (b)

Fig. 2.12 Typical Soil Settlement Profiles in (a) dense soil and (b) loose soil

Ng. et al. (1998) stated that the settlement depends primarily on the amplitude and the number of perturbation cycles. They also found that the magnitude of the shear strain developed at the end of 100 cycles of given amplitude is 3 – 20 times higher than the value under monotonic loading conditions with the same displacement amplitude.

The settlement results observed by England et al. (2000) showed a progressive increase in the maximum settlement of soil surface with the number of cycles but at a slightly reducing rate. Their results indicated that the settlement is sensitive to the amplitude of wall movement and, unlike the lateral stresses, did not approach a limiting value after 300 cycles, as it appears in Figure 2.13.

According to England et al. (2000), the settlement is a result of the densification effects in the backfill due to the wall movements against and away from the soil. Such effects are identified by the heave in the free surface of the soil at 350mm distance from the wall. The results reported by England et al. (2000) showed an active slip wedge of soil developed adjacent to the wall. It is apparent, from Figure 2.14, that the slip wedge was progressing with the number of cycles to reach an absolute settlement of approximately 40mm after 60 cycles of combined daily (0.042%) and annual (0.25%) perturbations.

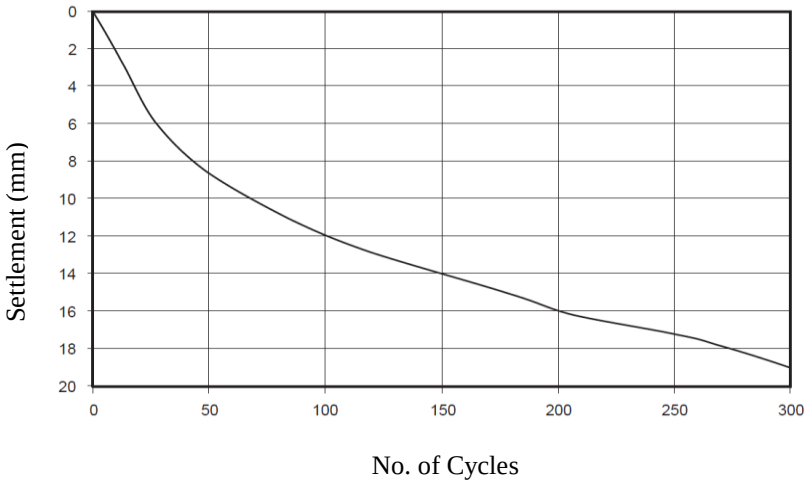

Fig. 2.13 Relationship between maximum settlement and the number of cycles (England et al., 2000)

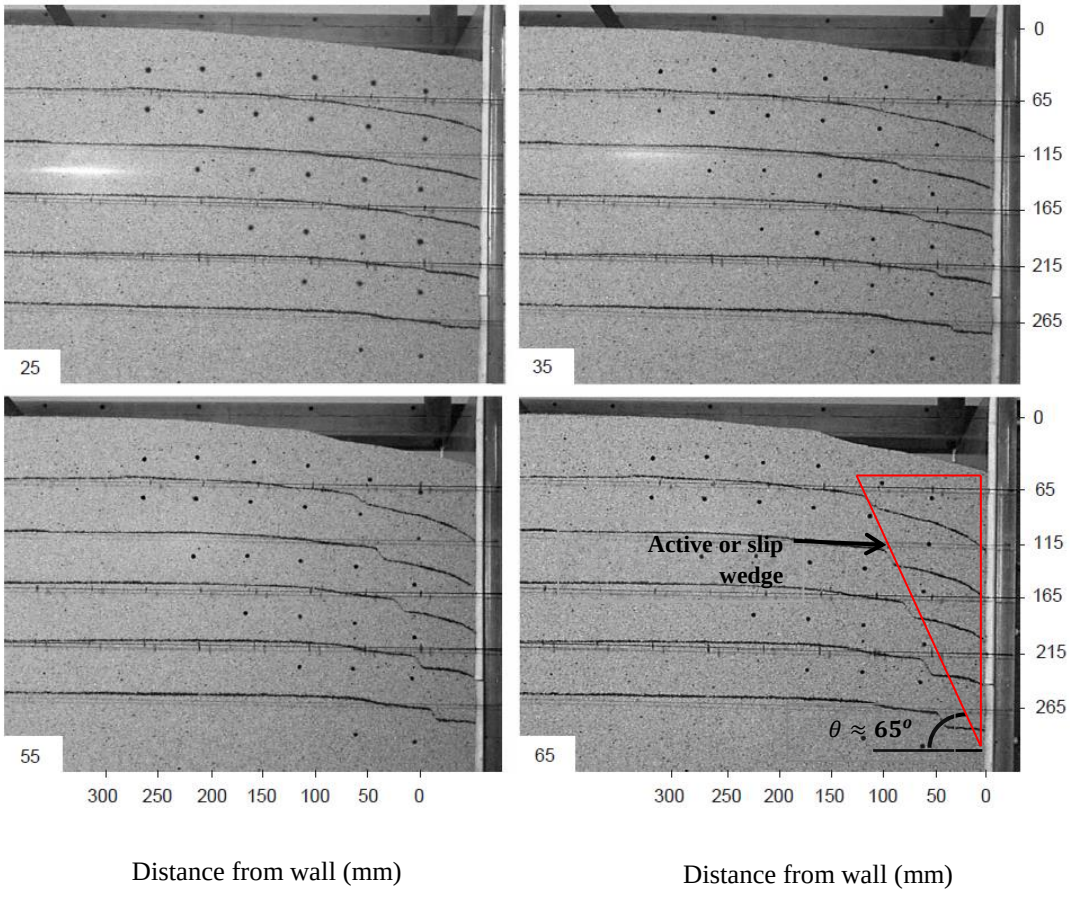

Fig. 2.14 Settlement of loose sand after 25, 35, 55 and 65 of combined daily and annual cycles (England et al., 2000)

Tatsuoka et al. (2009) reported similar conclusions as a result of testing loose sand retained by a 505mm high wall and subjected to cyclic displacements. The settlement

of the soil, in response to the wall movement, was gradually increasing with the number of cycles. Maximum settlement observed at 5cm from the wall after 50 cycles of displacement (*d*/H) equal to 0.2% was almost 0.7% of the wall height *H*.

Tatsuoka et al (2009) justifies that settlement in the soil surface by the dual – ratchet mechanism. A small active sliding occurs in the loosened soil adjacent to the wall, due to wall active movement, forming an active soil wedge. During the passive phase of wall movement, the active wedge is going to be compressed as part of a larger passive soil wedge. According to Tatsuoka et al. (2009) the deformation in the small active wedge will not be substantially recovered during the passive movement and will therefore be accumulated with further deformations in the subsequent active movements. On the other hand, the passive wedge, which is not completely affected by the active movement, experiences a repetitive compression which leads to densification and volumetric contraction. Therefore, the settlement is eventually a result of accumulated dual volumetric deformations in the active and passive wedges of the soil. The mechanism proposed by Tatsuoka et al. (2009) is illustrated in Figure. 2.15.

Cosgrove and Lehane (2003) conducted experiments on a 1m high loose backfill subjected to cyclic loading. The tests were intended to represent an abutment wall subjected to temperature induced cyclic loading. Two tests were conducted in which different numbers of cycles and loading amplitudes were applied as given in Table 2.1. They used an optical measurement system, in which a number of visual targets had been embedded in the soil, to capture the extent and direction of soil movements in response to the cyclic displacement of the wall.

Table 2.1 Tests details as described by Cosgrove and Lehane (2003)

Test	Displacement (d/*H*)%	Number of cycles (*N*)
1	0.63	120
2	0.23	500

According to Cosgrove and Lehane (2003), both tests showed significant settlements in the soil surface after 100 cycles of wall movement. They stated that settlement in the soil surface varies nonlinearly with the number of cycles. The absolute measured

settlements, after 100 cycles, were equal to 20% and 10% of the total wall height in test 1 and test 2 respectively.

Based on the movement vectors illustrated in Figures 2.16 (a) and 2.16 (b), a triangular small wedge of soil moves at inclined downward direction during wall active displacement while a reversal movement direction is observed during the passive wall displacement. As observed in Figure 2.9 (b) (during the passive phase of the cycle), the direction of movement is predominantly horizontal with a very small vertical component. That means the precedent inclined active motion was not equally reversed during the passive phase of the movement. This behaviour indicates the occurrence of unrecoverable vertical deformation in the active wedge. The subsequent cycles are also expected to behave similarly, perhaps with different deformation behaviour in the active soil wedge. The accumulation of such deformations is the likely primary reason contributing to settlements observed in the approach of IABs.

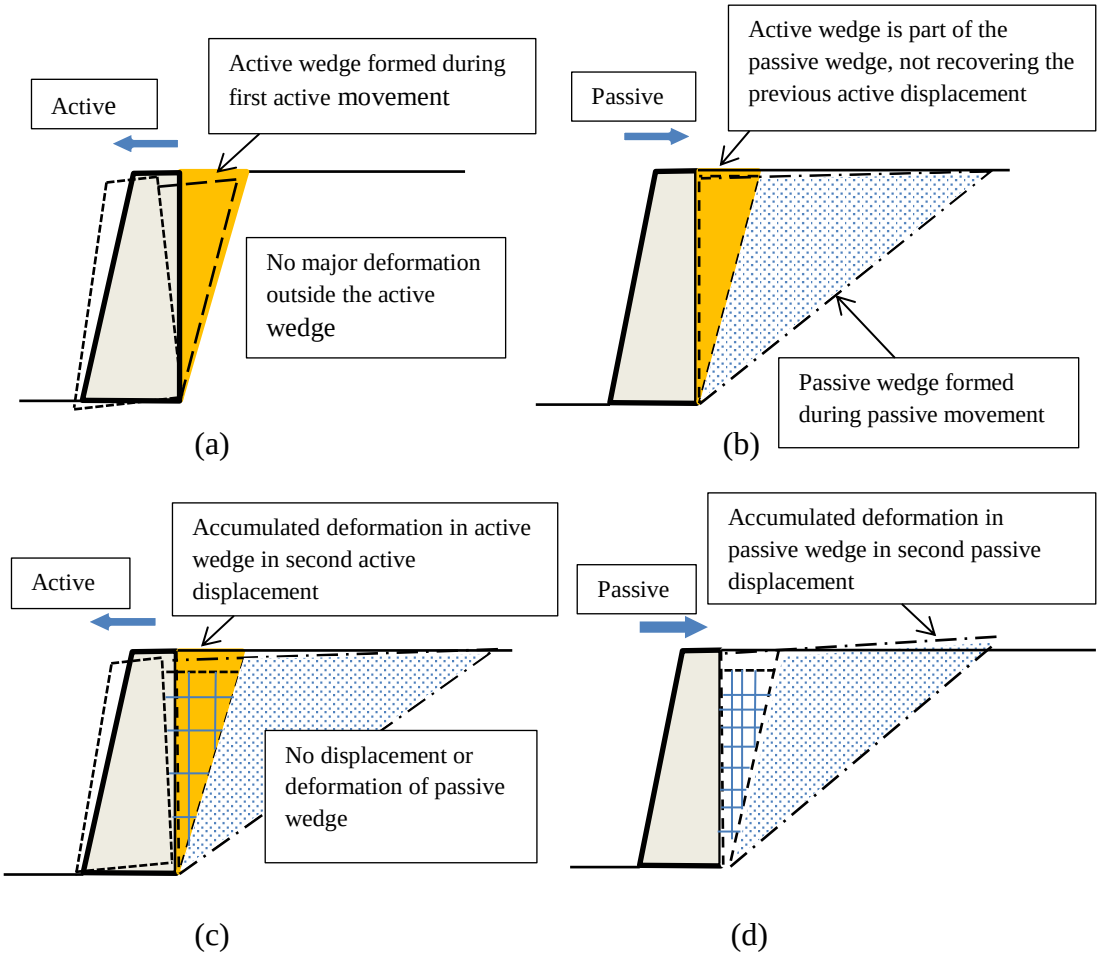

Fig. 2.15 Dual ratchet mechanism due to wall rotational movement (After Tatsuoka et al., 2009)

It is apparent from Figures 2.6 (c) and 2.6 (d) that the movement effects during the first cycle ($N = 1$) are very small or negligible at or beyond 500mm from the wall. That defines the boundaries of the *influence zone* in response to wall rotation. In contrast with the movement styles at $N = 50$, less extents of active and passive displacements are observed. That may justify the reduction in the settlement incremental rate after many cycles of wall movements. However, the *influence zone*, after 50 cycles, is extended to more than 600mm from the wall, which indicates more volume of soil is being affected by the wall movements.

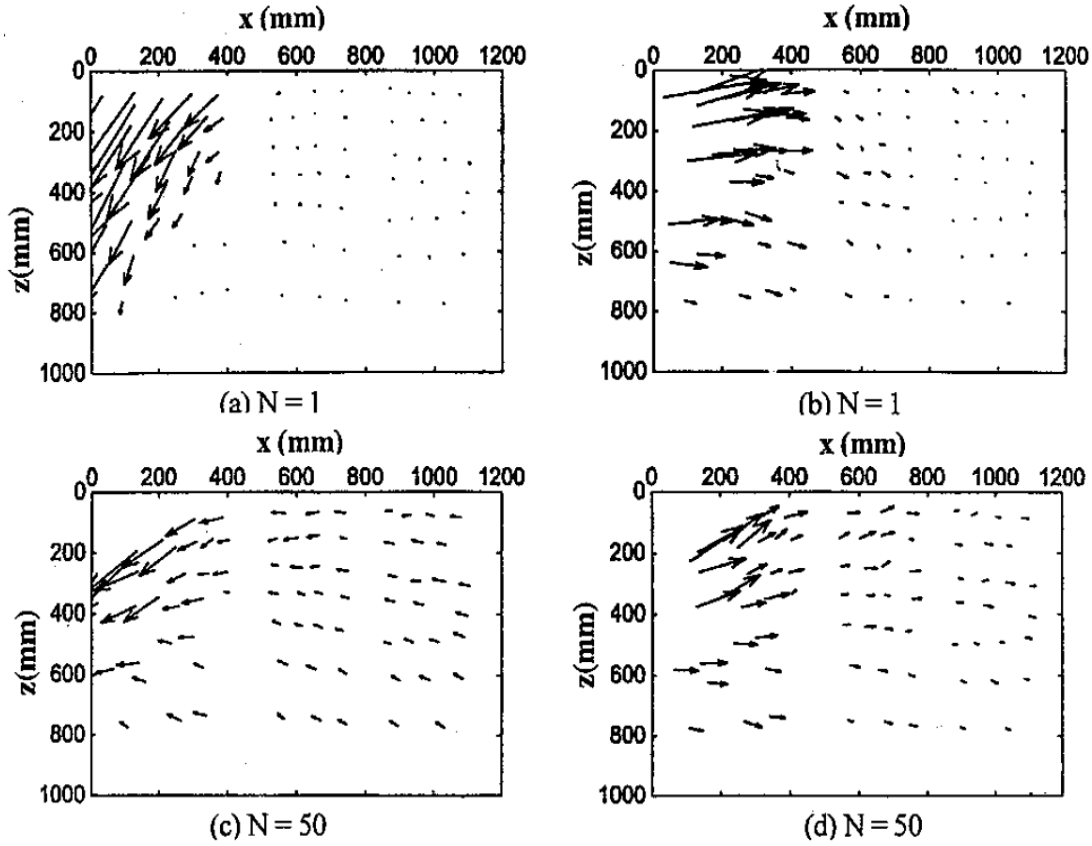

Fig. 2.16 Active and passive movement vectors (Cosgrove and Lehane, 2003)

2.6 Measures to Solve Approach Problems in IABs

The design guidelines of IABs vary widely from one country to another and therefore standard measures utilised to alleviate the approach problems in IABs are not clearly established. The use of run-on slab and well compacted soil in the vicinity of the abutment are the common suggestions to minimise the approach settlements (Horvath, 2000; Lock, 2002). Springman et al (1996) (cited in Lock, 2002) suggested that loose backfills should not be used in IAB approaches, irrespective of the use of

approach slabs. However, in the United Kingdom and in some of the US states, the use of the run-on slab is not advised as the settlement will occur whether or not approach slab is provided (Lock, 2002). Also, the presence of the run-on slab will complicate and increase the cost of the maintenance works for settled backfill as compared to soil overlay and pavement patching (Hoppe and Gomez, 1996). On the other hand the use of heavily compacted backfill was proven to increase the stiffness of the retained soil and consequently results in high lateral pressures on the bridge abutments (Hoppe, 2005).

Nam and Park (2014) reported some construction details and field observations data from the first IAB constructed in South Korea. In an attempt to minimize the lateral earth pressures on the abutment, 1.0m wide and 3.3m high *pressure relief zones* were provided at bridge approaches adjacent to the abutments. The zone was filled with coarse sub-base cohesion-less material type A-1-a (according to AASHTO classification system). The concept of using this material was to minimize the interlocking effects of backfill materials due to the horizontal movements of the abutments and consequently alleviate the passive earth pressures. However, the reported data represents only the first two years after the opening of the bridge (two annual cycles) during which the maximum recorded displacement amplitude were +8.8mm (passive) and -3.3mm (active). Both are relatively small amplitudes. Nevertheless, passive pressure was mobilised behind the wall and maximum recorded value of K_p reached approximately 4.4 (50% of Rankine passive pressure) during the summer of the second year. Such results show no evidence of avoiding higher lateral pressures after many cycles of abutment movements.

2.7 Expanded Polystyrene Geofoam (EPS)

The expanded polystyrene (EPS) geofoam is a polymeric material belonging to the family of the geosynthetic. The EPS possesses unique favourable characteristics among which its extremely low density. The EPS used in civil engineering applications has a density range from as low as 12kg/m^3(less than a hundredth of typical soil fill density)(Horvath, 1994). It also has favourable mechanical and thermal properties such as its compressive strength and thermal insulation characteristics (BASF, 2006). In addition to that, EPS is an environmentally friendly material and provides a cost effective choice for construction. These features have

collectively put the EPS geofoam as one of the best light-weight materials available. Therefore it has several geotechnical applications such as a light weight fill for embankments, a compressible inclusion for retaining structures, and a stabilization material for slopes, in addition to its potential use in integral abutment bridge systems.

2.7.1 Physical Properties

The EPS is a cellular rigid material formed of polyhedron expanded polystyrene particles. The expanded polystyrene particles are fused together during the manufacturing process forming an integrated cellular structure with air voids in between the particles. The polystyrene particles themselves are formed of vast number of air filled closed cells. Figure 2.17 shows the internal micro structure of an EPS specimen.

The density of EPS is an important factor that affects many of its physical and mechanical properties. During the manufacturing process, it is possible, to a certain extent, to control the density of EPS by controlling the quantity of moulded polystyrene beads. Therefore, EPS can be produced in variety of densities between 10kg/m³ and 50kg/m³. However, in most of the geotechnical applications, the density of EPS used is 20kg/m³ (Horvath, 1994).

In addition to its ultra-light weight, EPS is inherently non-biodegradable material and chemically inactive with soil or water (Horvath, 1994). It also doesn't offer a nutritive medium for undersoil organisms. These features made the EPS a durable geotechnical material.

(a) EPS specimen

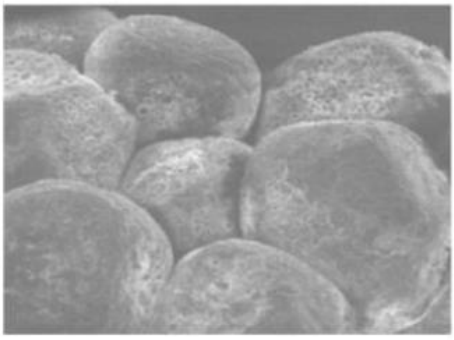

(b) EPS particles

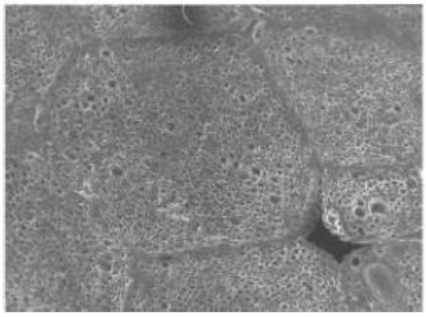

(c) EPS particles and cells

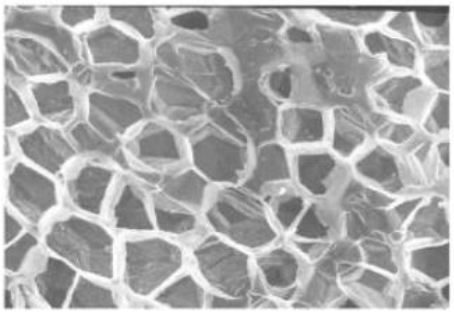

(d) Air filled closed cells

Fig. 2.17 Internal structure of EPS (Ossa and Romo, 2009)

2.7.2 Mechanical Properties of EPS

2.7.2.1 Stress-Strain Relationship

The stress-strain relationship of EPS in compression, like its other mechanical and physical properties, correlates to its density. Higher the density of EPS, the higher will be its compressive strength. Table 2.2 shows selected values of EPS densities with the corresponding compressive strength. Nevertheless, the stress-strain relationship of EPS is qualitatively similar irrespective of its density (Horvath, 1994).

Table 2.2 10% strain - compressive strength of EPS with different densities (Elraji 2000).

Density (kg/m^3)	12	15	18	22	29
Compressive strength at 10% strain (kPa)	35	69	90	104	173

In rapid compression tests, EPS is known to exhibit a linear elastic behaviour immediately after loading. That behaviour is represented by the initial straight part of the stress-strain diagram. Slope of that linear part is defined as the Elastic Modulus

or Young's Modulus of EPS. The value of the elastic modulus of EPS, as mentioned before, is affected by its density. Within this zone (the elastic zone) the micro cell walls tend to bend and buckle in an attempt to absorb the energy induced by the applied load. As a result, the elastic stiffness of the material will be decreased and its behaviour will transform into a plastic stiffness (*Ep*) (Ossa and Romo, 2009). It was found that the linear relationship between the applied stress and strain continues until the value of strain reaches to approximately between 1% - 1.5% (Horvath, 1994). For well conservative design considerations, researchers recommended to identify the elastic limit as the point where the developed strain is equal to 1% (Arellano and Stark, 2009). Therefore, the stress measured at 1% strain is referred as the elastic limit of the EPS.

Beyond the point of elastic limit the material starts to yield. During this phase, large amount of energy is dissipated by the continuous deformation of cell walls and hinges and through expelling cells encapsulated air (Ossa and Romo, 2009). The yield of EPS is found to occur over a range rather than a certain point at the stress-strain diagram. That zone of the stress-strain relationship ends up at approximately 10% strains. The stress measured at this point (strain equal to 10%) is generally referred as the compressive strength of EPS (Horvath, 1994).

Following the yield range, EPS exhibits a pure plastic strain-hardening behaviour. During this phase, the internal structure and particle geometry are continuously modified. The internal voids between particles are mostly vanished while the closed cell walls are completely collapsed. The change in the material internal structure continues until the polystyrene particles are totally damaged and reversed to their original nature as polystyrene beads. However, no clear mode of failure appears in the stress strain relationship of EPS.

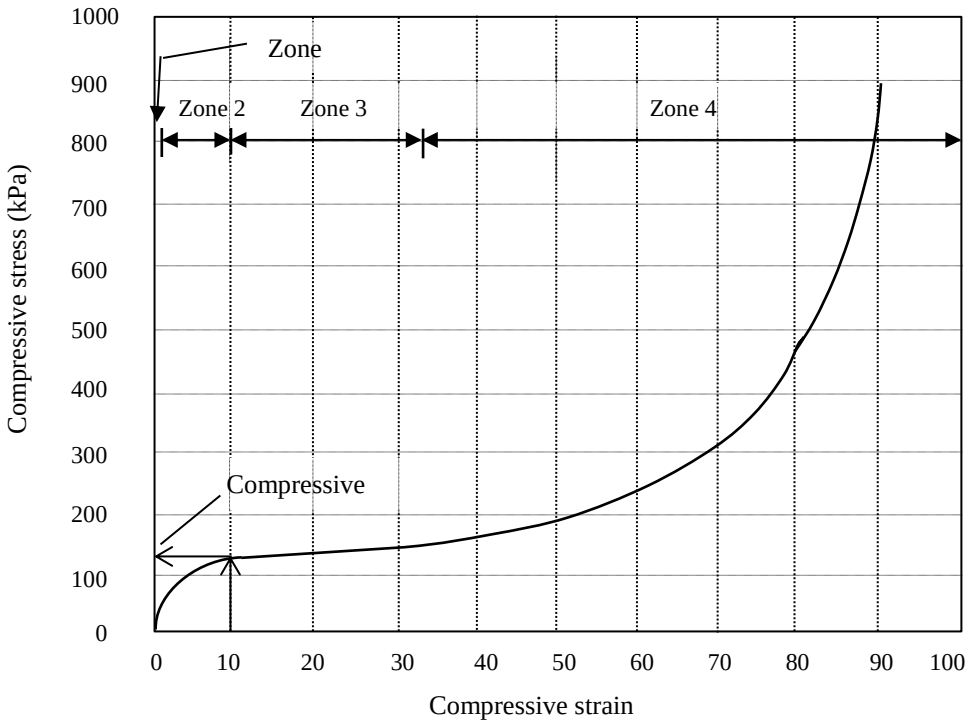

Fig. 2.18 EPS Stress-Strain relationship in rapid unconfined compression test (Arellano and Stark, 2009)

2.7.2.2 Time Dependant Behaviour

EPS is found to exhibit time dependent behaviour represented by the creep and stress relaxation when it is subjected to sustained loading conditions. Creep refers to the plastic deformation developed over a period of time under sustained load, while the stress relaxation is expressed as the reduction in stress with time under constant strain. Creep and relaxation are in fact reciprocal phenomena appearing in EPS behaviour due its visco-plastic characteristics.

In a typical axial compression test, an EPS specimen will deform elastically upon application of load. Shortly after and when specimen exceeds its elastic limit, it will enter into the plastic zone and some part of the developed strain will be irreversible. The total strain at this stage is the combination of elastic strain plus the creep or time dependent strains. The total strain can also be decomposed into immediate and time-dependent components as follows:

$$\varepsilon = \varepsilon_o + \varepsilon_t \tag{2.10}$$

where ε is the total strain developed after a certain time (t), ε_o is the immediate strain due the load application, which also represents the elastic component of the strain and ε_t is the creep or the time-dependant strain developed during the time (t)

The amount of creep in EPS is susceptible to the initial applied load and EPS density (Chun et al., 2004). Horvath (1994) stipulated that small or negligible amount of creep is observed in specimens subjected to an initial strain below 1%, but significant increase in the developed creep occurred when the specimen was initially strained by more than 1%. Accordingly a design criterion was suggested to limit the applied load on EPS blocks below the elastic limit to avoid excessive time dependent deformation (Arellano and Stark, 2009).

Elraji (2000) described the results of creep test for different EPS specimens with different initial loading levels. The result showed dramatic increase in creep when the initial loading was 70% of compressive strength, while the creep effects were limited when the initial stress levels were 30% and 50 % of its compressive strength

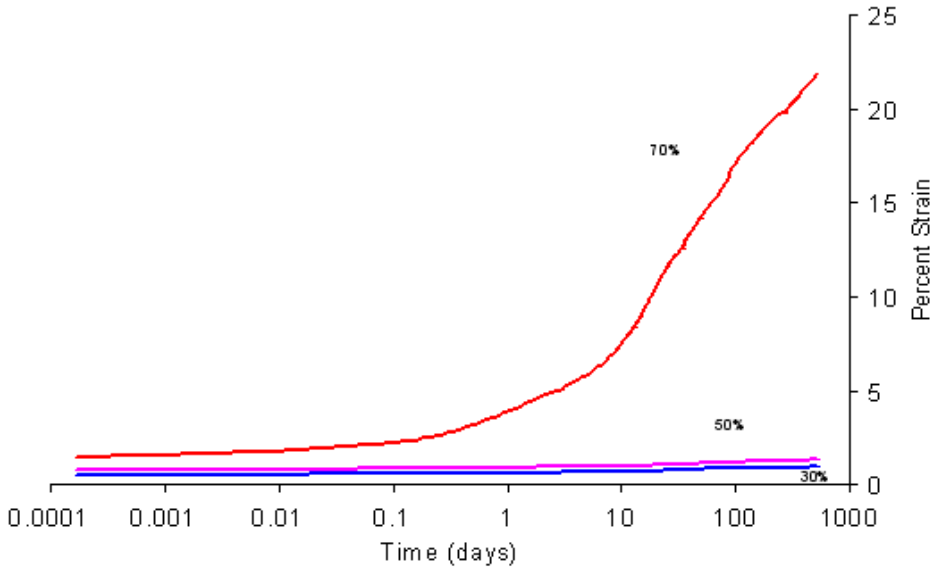

Figure 2.19 Time dependant behaviour of EPS at different stress levels (Elraji, 2000)

2.7.3 Applications of EPS in Mitigating Approach Problems in IABs

There is no evidence in literature indicating the use of EPS geofoam, as a design requirement, for the specific purpose of mitigating the approach problems in IABs. According to Barr et al. (2013), none of the European countries require the use of any type of inclusion behind the abutments in the IABs. However, a few US states

are using some sort of elastic materials as inclusions behind the abutments in IABs (Barr et al., 2013).

The inherent properties of the EPS make it a perfect alternative to the persistent lateral pressures and soil settlements in integral bridges. Hoppe (2005) reported field data collected, over five years, from an integral bridge on Jackson River in state of Virginia in the United States. The bridge was the first IAB in the US to include a compressible inclusion with a principle role aiming to mitigate the settlements and lateral pressure problems. The inclusion represented by 250mm thick board of elasticised polystyrene (EPS) placed between the retained backfill and the concrete back wall along the width of the bridge. The height of the EPS board was terminated at 0.76m from the top of the wall to allow for placing a pressure cell that measures the lateral pressures directly on the wall (without inclusion).

The 100m long and 16.6m wide three span integral bridge was instrumented during the construction stage and was opened for traffic in 1999. Three pressure cells were provided at each abutment mounted at 0.63m, 1.12m and 1.6m from top of the wall. The reported data include lateral soil pressure, acting on the abutment walls, and the settlement in the approach soil recorded during the period from 1999 until 2005.

Fig. 2.20 EPS inclusion in Jackson River Bridge, Virginia, US (Hoppe, 2005)

According to Hoppe (2005) lateral earth pressures were reduced significantly behind the EPS inclusion compared to the upper part of abutment (where there is no EPS inclusion). Maximum stress in the middle sensor was approximately 7% to 10% of the upper sensor. However, lateral pressure in the upper part of the abutment is certainly higher than that in the middle or the lower parts. Therefore for a fair comparison, pressures need to be measured at similar locations.

The settlement at the approach soil for the period between November 1999 and December 2004 was monitored. Limited surface settlement, approximately 20mm, observed at the end of that period. The bridge approaches were maintained only once with pavement patching since the opening of the bridge. Hoppe (2005) compared that maintenance works with those carried out in another integral bridge in the City of Rockingham County, which has approximately the same length. The latter suffered excessive settlement at the vicinity of abutment and approach pavement was repeatedly patched.

2.8 Gaps in the Current Knowledge

The integral abutment bridges are widely utilized around the world because of their structural merits and the substantial cost savings associated with the elimination of the expansion joints. However, the absence of the expansion joints also has negative impacts. The problems unique to this kind of bridges are primarily caused by its inability to accommodate the temperature induced deformations in the deck of the bridge. The cyclic movements of the bridge abutments and the associated lateral pressure escalation and soil settlements place a great limitation on the use of the IABs, especially in terms of the length of their span. Solving such problems will enable the use of IABs of greater span and maximize their potential benefits.

The information reported in literature regarding soil-structure interactions in IABs do not uniformly agree and seem to be dependent on the conditions under which they were obtained. As a result, the existing guidelines dealing with the approach problems in IABs vary widely and are largely conservative in most of the cases.

Moreover, the main focus of a majority of the existing researches is the soil-structure interaction behaviour in IABs under the temperature induced movement of bridge abutments. These were mostly carried out using different experimental and numerical

methods to investigate the lateral earth pressures and the approach settlements caused by abutment movements. In contrast, very limited efforts were devoted to study the possible remedies for such intractable problems. Therefore, effective and practical measures to adequately rectify the lateral pressures and approach settlements in the IABs are currently unavailable. The recommendations given in most of the existing design manuals are limited to using well compacted soil in the vicinity of the abutment to minimise the soil settlement. However, stiff soil is likely to cause the development of high lateral pressure on the abutments due to the latter's movement (Hoppe, 2005) and will also experience an amount of undesirable settlement. Using the run-on or approach concrete slab is still debatable as it does not prevent the development of the settlement. Moreover, run-on slab can only be effective when the settlement is relatively small (few millimetres) which is, however, not the case with a large percentage of IABs where a significant amount of settlement is developed. Therefore, the aforementioned measures tend to alleviate the symptoms to a degree but not solve the problem. Generally, the current practice in many countries in Europe as well as in the US recommends using a regular pavement overlaying and surface patching programme to overcome the approach settlement. Again, this measure does not provide an effective solution in addition to being costly and traffic retarding over the long term.

The data reported by Hoppe (2005) indicated that the EPS performs well in attenuating the lateral pressures and the settlements at the bridge approaches. According to him, the EPS inclusion was able to accommodate the movement of the abutment with minimum disturbance to the adjoining soil. However, the potential capability of the EPS to mitigate the approach problems in IABs has not been sufficiently investigated. In fact, the knowledge about the potential use of EPS in the IABs is very limited and insufficient to produce guidelines to help engineers overcome the lateral pressures and settlement problems.

The expanded polystyrene (EPS) geofoam has unique characteristics, including its extremely light weight. As a highly compressible material, the EPS can provide an effective inclusion to absorb the abutment movement with minimal effects on the adjoining soil. At the same time, its compressive strength is sufficient to bear the vertical load. Nevertheless, it has not been utilized in mitigating the approach problems in IABs extensively. This is because of the lack of available knowledge of

this application. This research intends to address the gaps in the knowledge and provide a more rigorous insight into the possible use of EPS as a compressible inclusion in IABs by studying the optimum arrangements of the EPS blocks, the interaction between soil and EPS and the actual behaviour of the EPS when used in IABs.

Chapter Three

Numerical Simulation of Abutment Wall Experiencing Cyclic Movement

3.1 Introduction

The field data collected from in-service IABs provide important information on the soil-structure interaction behaviour. However, collecting the field data requires a significantly long time and is limited to certain instrumented IABs. Moreover, the reported field data such as from Hoppe and Gomez (1996) and Huntly and Valsangkar (2013) showed an extent of variation in the behaviour of the IABs depending on the mode of abutment movements. It would appear that the mode of movement plays an important role in the subsequent settlement and lateral pressure escalation effects. Inherent differences were observed in IABs depending on various factors including the abutment type, properties of the backfill and the range of temperature change. Therefore, the field data are quite specific to the conditions of the structures where the data were collected, and cannot be easily extrapolated to other field cases with a different set of conditions.

On the other hand, the numerical analysis approach has been adopted by many researchers to investigate the behaviour of IABs (Ng. et al., 1998; Arzoy et al., 1999; Dicleli, 2000; Horvath, 2000; Kim and Laman, 2010; Bloodworth et al., 2012). It provides a flexible tool to study a wide range of cases in a shorter time. In this chapter, the approach problems in IABs represented by the settlement and lateral pressures escalation will be investigated using a finite element simulation. A finite element model was developed using the ABAQUS/Standard software and verified by the experimental centrifuge data reported by Ng. et al. (1998). The settlement and lateral earth pressure issues were addressed in the model and the influence of different parameters are discussed.

3.2 Building the Finite Element Model

The finite element (FE) model was developed, using the ABAQUS/Standard (ABAQUS, 2013), to simulate a concrete abutment wall retaining a soil backfill and subjected to cyclic movements as would be expected to occur in an IAB. The FE model has been verified using centrifuge test data (Ng. et al., 1998) in which the presence of a settlement trough and stress ratcheting were observed.

3.2.1 Determination of Scale Factors and Model Dimensions

The geotechnical centrifuge modelling is utilised to perform geotechnical tests on laboratory scale physical models. In the centrifuge test, the gravitational force is elevated, by spinning the model, to achieve stress levels equivalent to those in the actual prototype model in field. The dimensions in the centrifuge tests are largely downscaled compared to the corresponding dimensions of the prototype. Due consideration must be given to the centrifuge model dimensions and materials to enhance the similarity to the corresponding prototype.

The data reported by Ng. et al. (1998), involves a series of centrifuge tests conducted on a sandy soil. The retaining wall was subjected to a range of cyclic displacements under a gravitational acceleration of $60g$. Fig. 3.1 shows the experimental setup of the centrifuge model as given by Ng. et al. (1998).

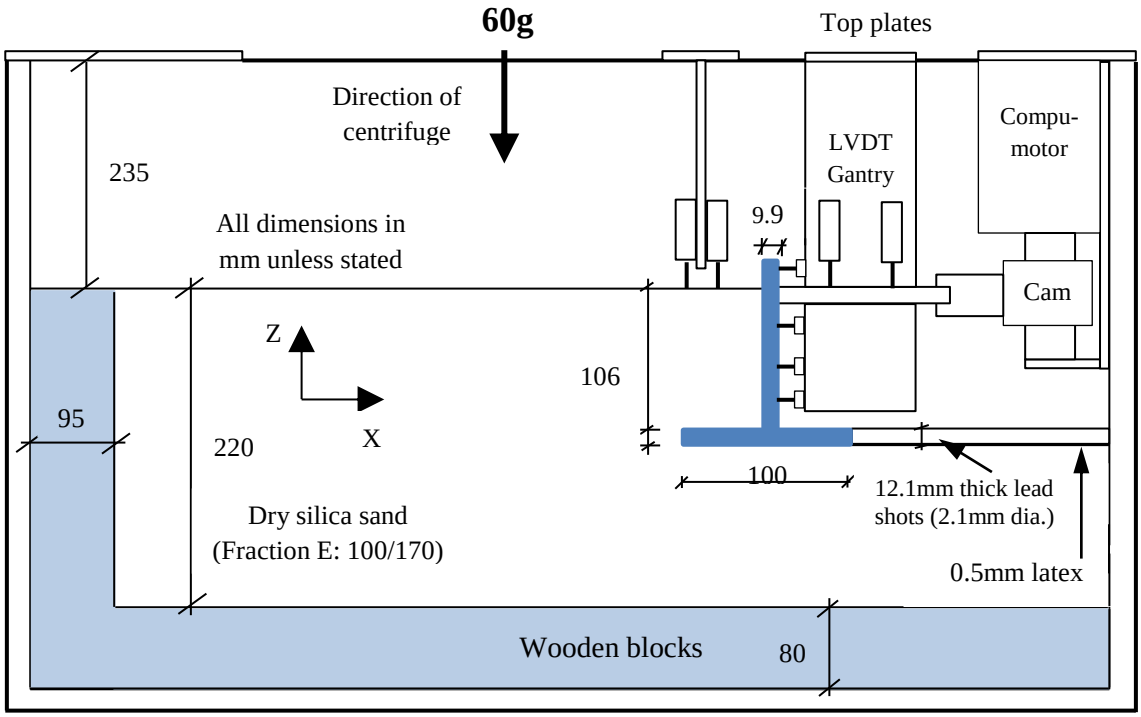

Figure 3.1 The experimental setup of the centrifuge test (Ng. et al., 1998)

For the purpose of validation, the geometry, material properties and the applied loads used in the finite element model are imposed identical to those prescribed in the centrifuge tests. The scaling factors have been determined on account of the centrifuge acceleration in order to produce identical self-weight stresses between the centrifuge model and the prototype. It is worthwhile noting that the scaling factors utilised in centrifuge modelling have been determined by considering the physical system of the bridge abutment under cyclic loading as a function of six variables,

$$f = (\sigma, \rho, g, u, x, t) \tag{3.1}$$

where, σ, ρ, g, u, x, t are stress, density, gravity, displacement, length and time respectively. Since equation (3.1) involves three physical dimensions (length, mass and time), then based on the Buckingham theorem of dimensional analysis, the number of equivalent dimensionless variables in (3.1) is given by $p = m - k = 6 - 3 = 3$ (m = number of physical variables and k = number of physical dimensions) (Butterfield, 1999). In the geotechnical centrifuge model, the following three dimensionless parameters have been invoked:

$$\pi_1 = \frac{\sigma}{\rho g u}, \pi_2 = \frac{u}{g t^2}, \pi_3 = \frac{u}{x} \tag{3.2}$$

so that the system represented by equation (3.1) can now be written in terms of the dimensionless parameters as,

$$f = (\pi_1, \pi_2, \pi_3) \tag{3.3}$$

In order to achieve similarity between the centrifuge and prototype models, the dimensionless parameters for both models have to be made equal, i.e.

$$\frac{\pi_1^m}{\pi_1^p} = 1, \frac{\pi_2^m}{\pi_2^p} = 1, \frac{\pi_3^m}{\pi_3^p} = 1 \tag{3.4}$$

where, $\pi^m$and π^p refer to the dimensionless parameters in the centrifuge and the prototype models respectively. In geotechnical testing, it is customary for the centrifuge model to produce identical self-weight stresses as the prototype model, i.e. $\sigma^m = \sigma^p$ to achieve the similarity. Moreover, as the properties of the soil used in the centrifuge model are typically similar to those in the prototype, then $\rho^m = \rho^p$. Finally, the gravitational acceleration in the centrifuge is n times that of the prototype, namely, $g^m = n \times g^p$(where $n = 60$ in this case). Using equation (3.4),

the scaling factors between the centrifuge and the prototype models are then established and summarised as shown in Table 3.1.

Table 3.1 Scaling Factors for the Centrifuge Model

Parameter	Stress (σ)	Density (ρ)	Gravity (g)	Time (t)	Dimension, (x)	Strain (ε)	Cycles (frequency), (f)
Scaling factor	1	1	n	$1/n$	$1/n$	1	n

As shown in Table 3.1, the dimensions of the centrifuge model are scaled downwards from the dimensions of the prototype model by the gravity scaling factor while importantly maintaining identical self-weight stresses as well as strains of the prototype in the centrifuge model. Figure 3.2 shows the finite element mesh of the prototype abutment and the soil backfill which have been modelled in this chapter using FEM.

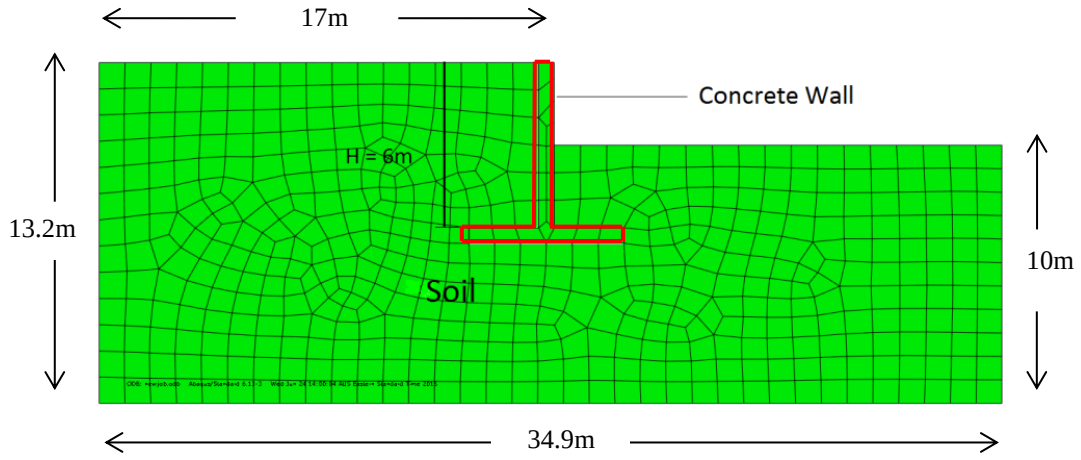

Fig. 3.2 Finite element mesh of the prototype abutment wall and soil backfill

3.2.2 Constitutive Models and Material Properties

Normally, temperature fluctuates at a relatively slow pace, especially the annual fluctuations due to primary seasonal temperature changes. Accordingly, the corresponding changes in the dimensions of the bridge will take place in a slow pattern (i.e. at a very low frequency). Under these circumstances, the analysis can reasonably be modelled using a constitutive model developed for quasi-static

loading/unloading conditions rather than more specifically for cyclic loading. Hence, the Mohr-Coulomb model was adopted to describe the inelastic behaviour of the non-cohesive soil. The Mohr-Coulomb elasto-plastic model in ABAQUS (2013) allows the material to harden and/or soften isotropically and uses a smooth flow potential that has a hyperbolic shape in the meridional stress plane and a smooth elliptic shape in the deviatroic stress plane.

The properties of the soil backfill modelled using the Mohr Coulomb model in the finite element analysis were defined based on the corresponding values described in the centrifuge test. The soil used in the centrifuge test is Leighton Buzzard silica sand. Particle size was between 90 and 150 μm, which offers high model to particle size ratio. Therefore, using the same soil material properties as the prototype model will not have any significant effects on the numerical results (Ng. et al., 1998). Table 3.2 summarizes the soil properties as described by Ng et al. (1998).

Table 3.2 Properties of soil used in the finite element analysis

Material	Density t/m^3	Elasticity modulus (E) kPa	Poisson's ratio (μ)	Friction angle (ϕ) °	Dilation angle (Ψ) °
Non-cohesive soil	1.546	20 x 10^3	0.25	32	2

The concrete wall is modelled as an elastic material with a modulus of elasticity (E) equal to 40×10^6 kPa and a Poisson's ratio of 0.2. A high value for the elasticity modulus of concrete is used to simulate a semi-rigid abutment wall that exhibits extremely small amount of deformation during the cyclic movement.

3.2.3 Interaction Properties and Boundary Conditions

The interface behaviour of the soil-concrete abutment was modelled using a standard surface-to-surface contact with finite sliding. The interaction was activated during the initial step of the analysis. The mechanical frictional behaviour at the interface surfaces was expressed as a tangential friction while the normal behaviour at the interface between the soil and concrete was simulated as a "hard contact" where no separation or penetration is permitted between the two surfaces. In order to avoid any possible separation at the interface between the base of the concrete wall and the soil, tie constraints were provided along the baseline of the abutment wall.

The boundary restraints of the model were defined in the initial step to establish a global equilibrium in the model. The horizontal and vertical movements were restrained along the bottom edge of the model ($u_1 = u_2 = 0$), while the vertical edges on both sides were restrained against the horizontal movement only ($u_1 = 0$).

The initial stresses are taken into account in the analysis and introduced as gravity loads throughout the model, in the initial step of the analysis. A plane strain eight-node quadratic element with reduced integration (CPE8R) was used for concrete and soil in the FE model simulating a central section of a wide abutment wall.

3.3 Discussion of Model Verification and Results

The present chapter involves a series of modelling cases to satisfy the verification of the FE modelling and to investigate the influence of different parameters on the behaviour of the approach soil in response to the abutment movements.

3.3.1 Lateral Earth Pressures

In order to perform a validation of the FE model, identical loading conditions to those prescribed in the centrifuge test, in terms of the applied displacements and the number of cycles, have been simulated. Ng. et al. (1998) presented selected measured and calculated results for the lateral earth pressure coefficient *K* at depths of 2m and 4m (measured from top of the wall) as a result of 10 cycles of ±6mm and ±12mm perturbations. *K* is defined as the ratio of horizontal pressure acting at a certain point on the wall to the vertical effective stress at the same point. Table 3 shows typical results presented by Ng et al. (1998) and the finite element modelling results from Ng et al. (1998) own FE model and the present ABAQUS FE model. The results in Table 3.3 show a good agreement between the finite element modelling from this study and the centrifuge test results.

The dependency of the measured lateral earth pressure with the number of perturbation cycles at different perturbation amplitudes, from the same centrifuge model were also reported by Ng. et al. (1998). The centrifuge results showed an increase in the value of lateral earth pressure coefficient (*K*) during the first 15 to 20 cycles then asymptotes or increases at a decreasing rate during the successive cycles.

Table 3.3 Comparison of lateral pressure coefficient (*K*)

10 cycles, ±6mm perturbation			
Depth from soil surface	*K* measured (Ng et al., 1998)	*K*, FE model (Ng et al., 1998)	*K*, FE model (this study)
2m	0.9	1.3	0.8
4m	0.7	1	0.51
10 cycles, ±12mm perturbation			
2m	1.1	1.8	1.2
4m	0.8	1.3	0.736

Using the ABAQUS (2013) finite element model, the lateral earth pressure responses were computed under the same loading conditions. The modelling results show a reasonably similar behaviour at different perturbation magnitudes. A rapid increase in the values of lateral pressure coefficient *K* is observed within the first few cycles followed by a plateau region within which *K* increases slightly. However such behaviour is dependent on the displacement amplitude, where the increase in *K* value is more apparent in large amplitudes (±30mm) compared to smaller ones (±6mm). The behaviour of lateral pressures has also been compared to selected theoretical models to assess the efficiency of the present FE model. Figure 3.3 illustrates the relationship between the number of cycles and the coefficient of lateral pressure *K* as given by the experimental results, the ABAQUS modelling and other theoretical models (Broms and Ingelson, 1971; England and Tsang, 2001; UK BA42/96, 2003) at different perturbations and number of cycles.

It can be noticed, from Figure 3.3, that the modelling results are generally close to the centrifuge test results at different perturbation (displacement) amplitudes. In contrast with the classical earth pressure models, the ABAQUS FE model accounts for the number of movement cycles of the wall and the subsequent increase in lateral pressures. On the other hand the earth pressure models varied widely in describing the lateral pressures. Rankine and Broms and Ingelson (1971) are apparently so conservative specially at small displacement amplitudes (6 to 12 mm). The UK BA42/96 (2003) and England and Tsang (2001) are found to better predict the lateral pressures at small movements, however, they underestimate the pressures at large wall movements (30mm).

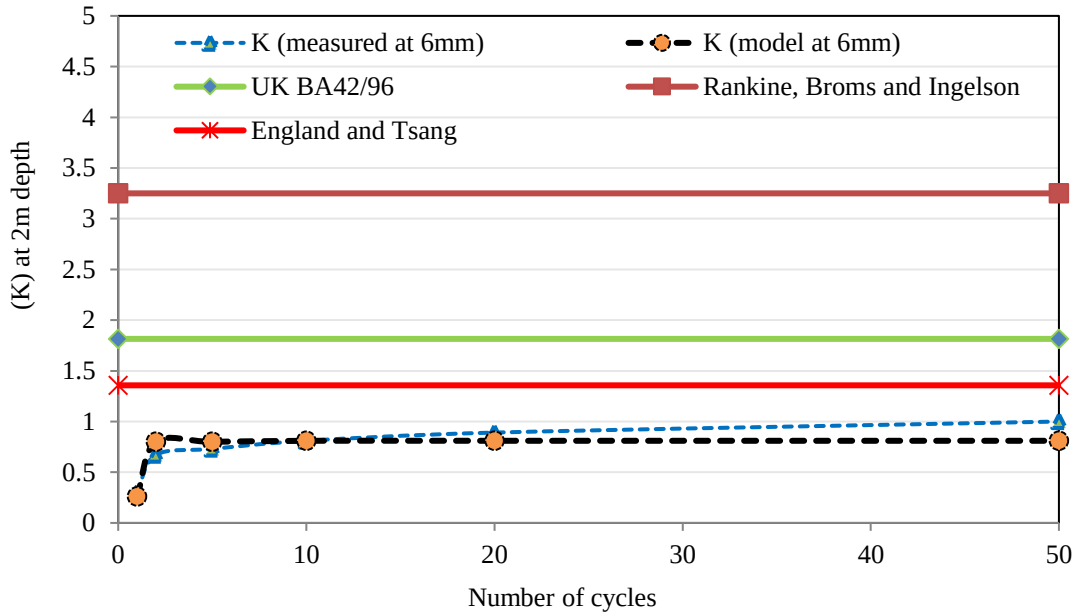

Figure 3.3(a)

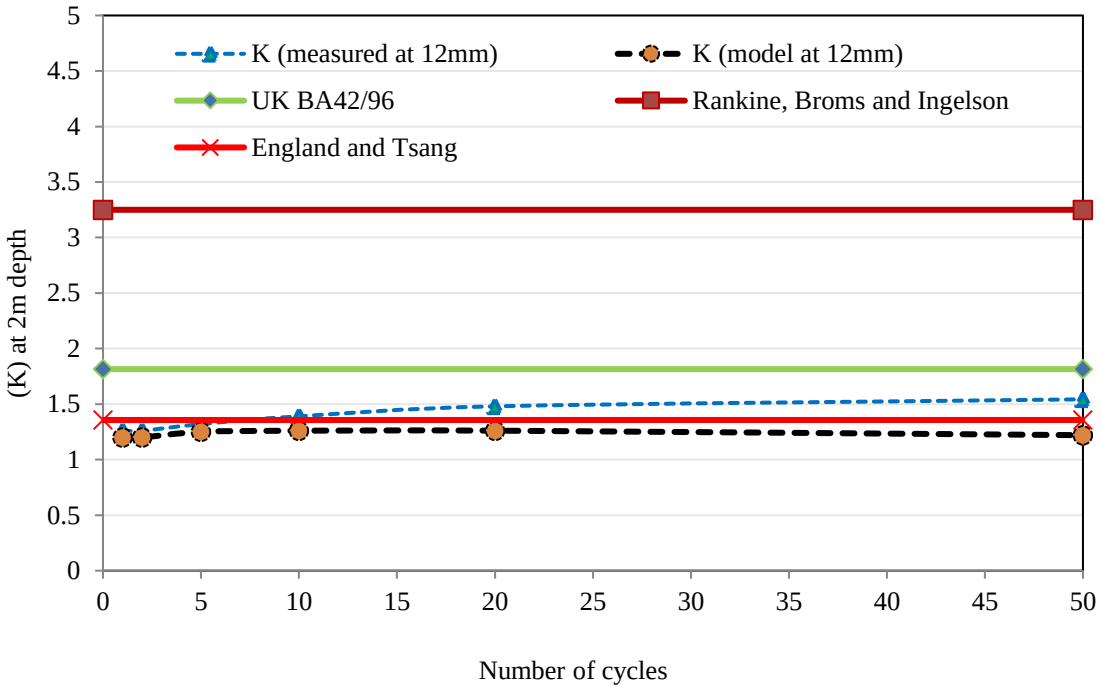

Figure 3.3 (b)

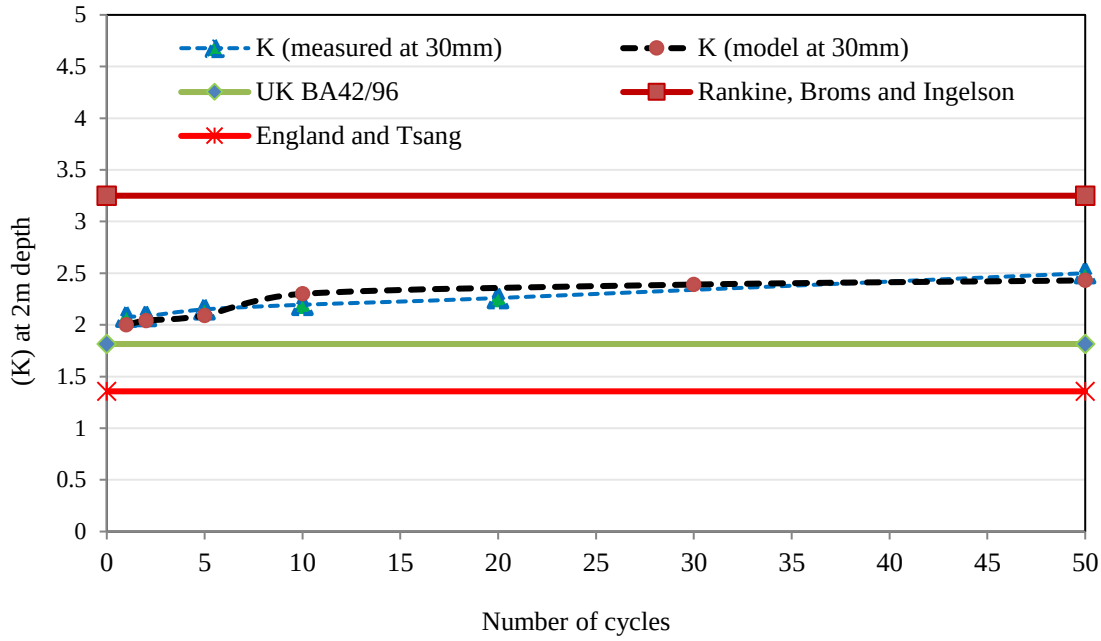

Figure 3.3 (c)

Figure 3.3 FEM results (this study) test results of Ng. et al (1998) and other theoretical models for the lateral pressure coefficient *K* at (a) ±6mm perturbation, (b) ±12mm perturbation and (c) ±30mm perturbation

The distribution of lateral pressures acting along the height of the wall has been computed by the ABAQUS FE model. Figure 3.4 illustrates the lateral pressure distributions at different displacement amplitudes. It is evident that lateral pressures at 2m depth from the soil surface increases significantly with the displacement amplitude to record maximum pressure at ±30mm. This behaviour agrees with the findings of other researchers, where maximum lateral pressures are usually recorded at the upper half or in particular at *H*/3 from top of the wall (Ng. et al.,1998; Lehane, 2003), whereas *H* refers to the wall height.

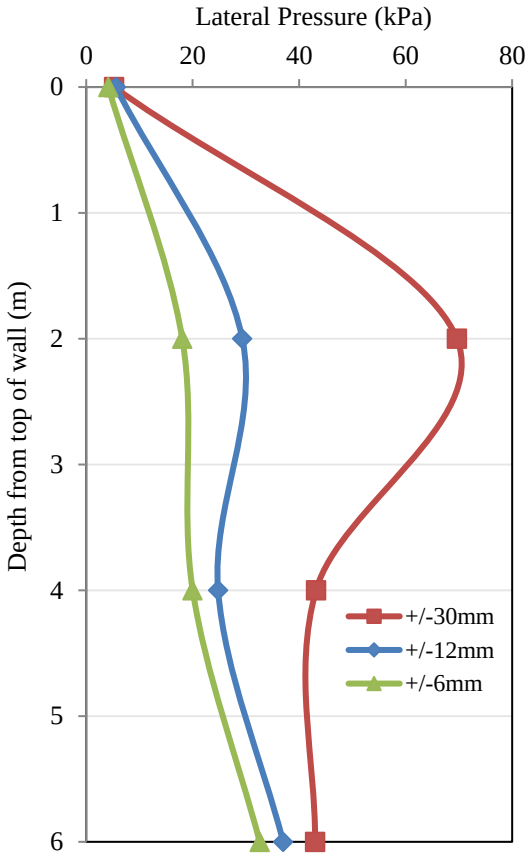

Figure 3.4 Modelling results for the lateral pressure distribution after 10 cycles

3.3.2 Soil Settlement

Modelling results for the settlement of the approach soil due to the cyclic movements of the abutment were also produced by the FE model. As the quantitative settlement results reported by Ng. et al (1998) were limited, the FE results have been qualitatively verified against the corresponding centrifuge data. According to Ng. et al. (1998), the soil deformation in loose fill is a gradual settlement starting with maximum value at the interface between the soil and the abutment, and decreasing gradually away from the wall. Similar settlement profile was observed in the FE modelling results after applying 10 cycles of ±30 mm perturbation (the ±30 mm was described by Ng et al. (1998) as the annual perturbation). Figure 3.5 below illustrates the deformed model with the soil settlement contours.

The profile of the settlement trough after 10 cycles of ±30mm is shown in Figure 3.6. It indicates that the soil surface settlement starts from a distance of 2m to 3m from

the wall and increases until it reaches its maximum value of almost 0.05m at the wall-soil interface.

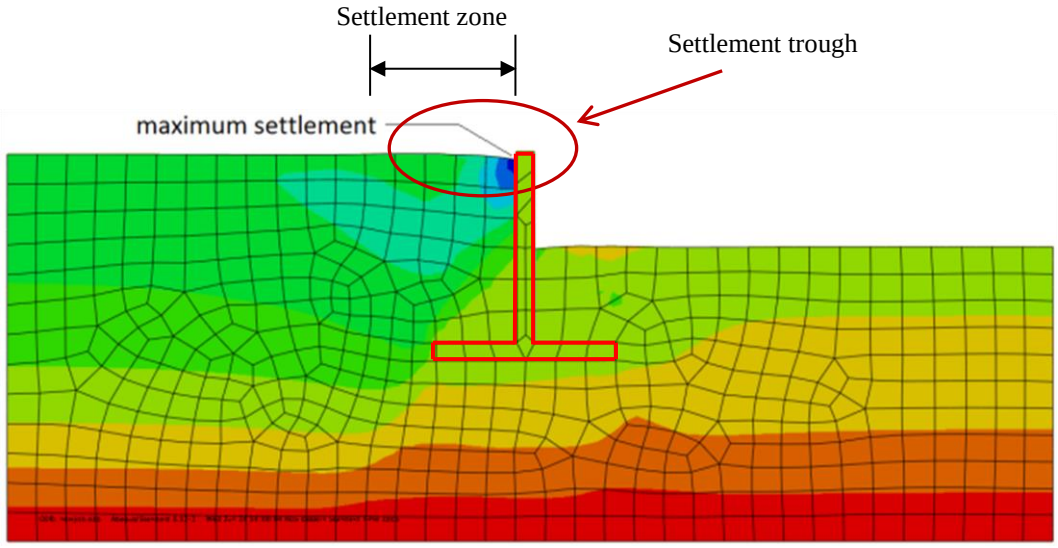

Figure 3.5 The deformed FE model

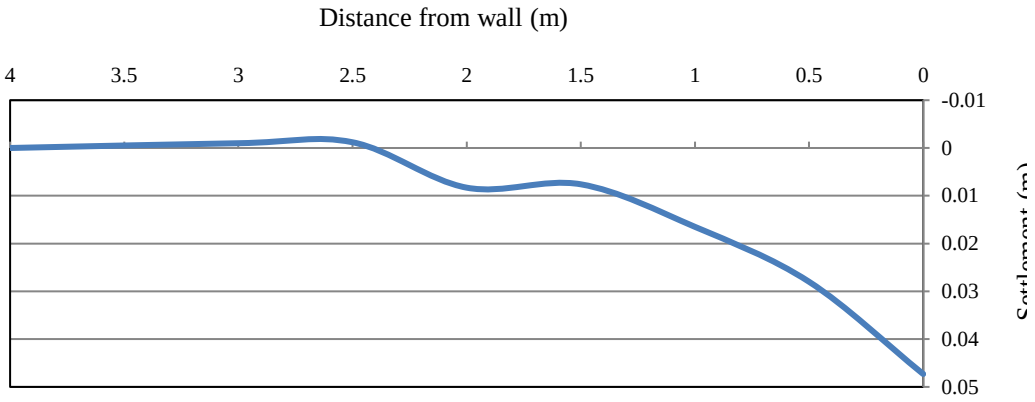

Figure 3.6 Soil surface profile after 10 cycles of ±30mm perturbations

Ng et al. (1998) described the magnitude of settlement in the backfill due to temperature variation as a function of the wall displacement (perturbation amplitude) and the number of cycles. Settlement increases as the number of cycles and amplitude of the perturbation increase. Similar settlement behaviour was also observed in the finite element results for different wall perturbations and number of cycles

The relationship between the magnitude of maximum vertical settlement (u_2) and the number of cycles at different perturbations is summarized in Figure 3.7. The results

indicate that the settlement asymptotes to a small final value (below 10mm) within 50 cycles at small perturbation magnitude (less than 20mm). However, settlement becomes more sensitive to the number of cycles at larger perturbations. It can be noticed that at perturbation equal to ±50mm, the magnitude of maximum settlement increases nonlinearly and sharply to more than 0.6m after 40 cycles. This magnitude of settlement is three times greater than the corresponding settlement induced by ±30mm perturbation. This trend suggests that integral abutment bridges undergo greater than proportional settlement effects the longer the span, in response to the variation in ambient temperatures. This and the increase in lateral earth pressure are a principal reason to limit the overall length of integral abutment bridges. However, there is no universal limit for the maximum allowable overall length of an integral bridge. In fact it varies between countries and depends on the experiences deduced from formerly constructed bridges. In Victoria, Australia, the maximum length of integral bridges is limited by the Victoria Roads Authority to 70m (VicRoads, 2012). This limit is enforced to control the lateral earth pressure acting on the abutment wall, especially during the passive phase of the wall movement.

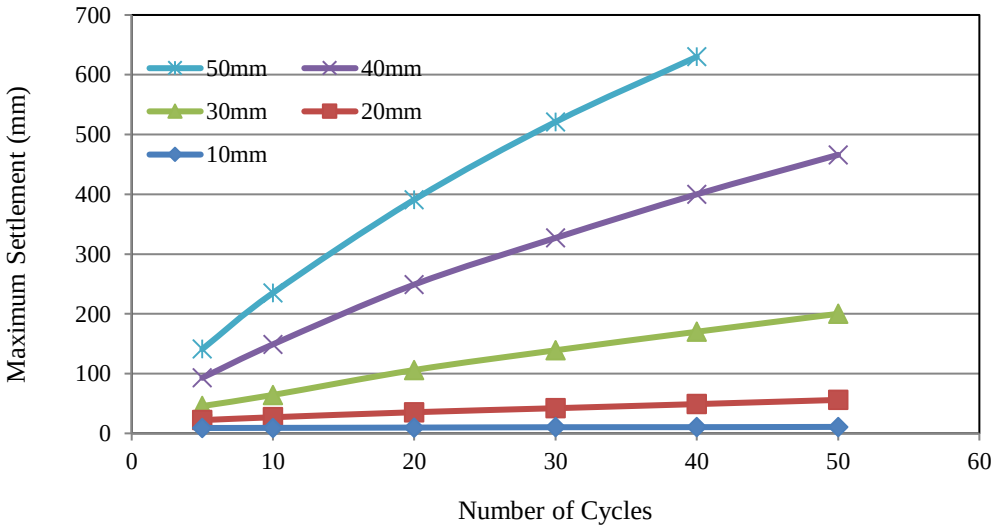

Figure 3.7 Maximum settlements vs. Number of cycles and Perturbations

3.3.3 Influence of Soil Properties on the Settlement and Lateral Pressures

The rotational movement of the abutment wall exerts a loading condition on the retained soil similar to that when it is sheared in a large shear box (Ng. et al., 1998). Soil behaviour under shearing is normally a function of its properties, in particular its density. Therefore, in this section the influence of the relative density on the soil response to the wall cyclic movement is investigated. Finite element modelling is

carried out on loose (Soil 1) and dense (Soil 2) soils, subjected to identical number of cycles and amplitude of perturbation (10 cycles of ±30mm). A summary of the soil properties is given in Table 3.4. It is worthwhile noting that the cited properties of soil, in this section, have been chosen as a reasonable set of parameters for the purpose of the FE modelling and are not determined by physical testing or by backward analysis.

Table 3.4 Properties of Soil used in the Finite Element Analysis

Soil	Description	Unit weight (kN/m^3)	Friction angle (Ø)	Dilation angle (ψ)	Poisson's ratio (μ)
1	Loose	14	32°	0	0.2
2	Dense	18	40°	4°	0.4

The modelling results show a considerable variation in the soil response in terms of both the surface settlements and the lateral earth pressures. The settlements, as given in Figure 3.8a, indicate that the dense soil exhibits a lesser amount of settlement compared to the loose soil. Maximum settlement observed in dense soil was 0.0233m which is 60% less than that observed in loose soil at 0.0593m. The dense backfill also experienced a small amount of heave, at a distance between 2.5m to 5m from the wall. Such behaviour is expected in a dense soil as a result of its dilatancy characteristics. Therefore, the compaction of the approach backfill may play an important role in determining the extent and pattern of the soil surface deformation. Figure 3.8b illustrates the displacement vectors of the soil particles due to the abutment cyclic movements in both soils. Different patterns of settlements can be observed between the loose and dense soils based on the desplacement vectors.

The lateral earth pressure acting on the wall was also found to vary between the loose and dense soils. The data given in Figure 3.9 illustrate the lateral pressure coefficient *K* measured at 2m from the top of the wall at different numbers of cycles. It is observed from the modelling results that the magnitude of *K* is relatively sensitive to the density of the soil. According to Figure 3.9, *K* values for dense soil are noticeably less than those in loose soil. The dense soil has more resistance to the active movement and thus experiences less slippage when the wall moves away from the

backfill during the active phase of the cycle. On the other hand, loose soil, which possesses less shear resistance, slumps more easily during wall active movement. This creates a soil wedge and, after successive cycles of movement, leads to a progressive increase in lateral earth pressure.

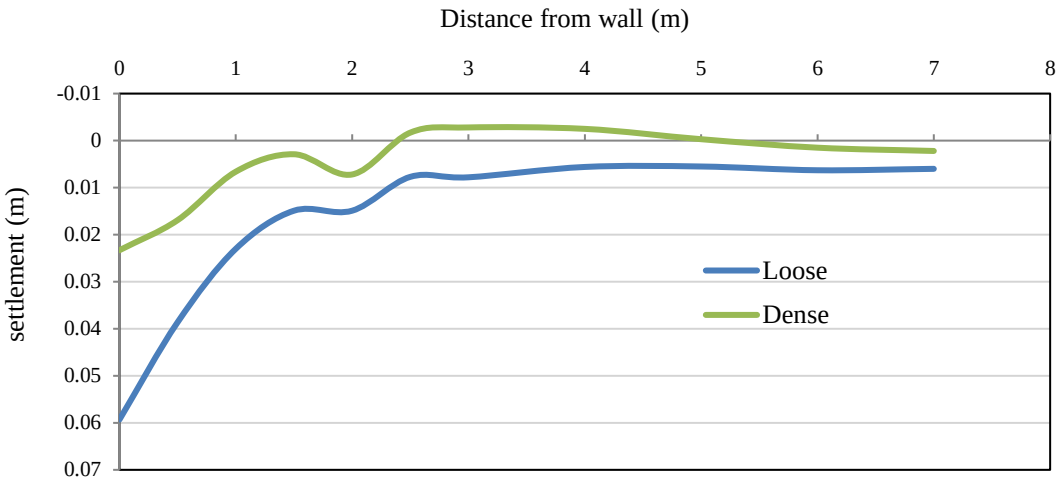

Figure 3.8a Soils 1&2 Surface Profile after 10 cycles of ±30mm wall displacement

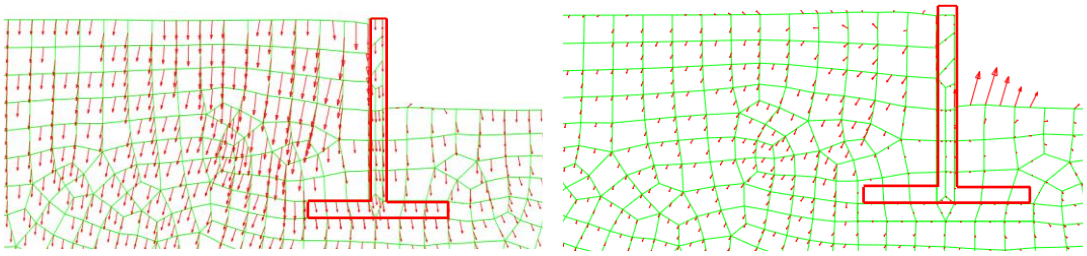

Loose soil Dense soil

Figure 3.8b Displacement vectors of soils particles

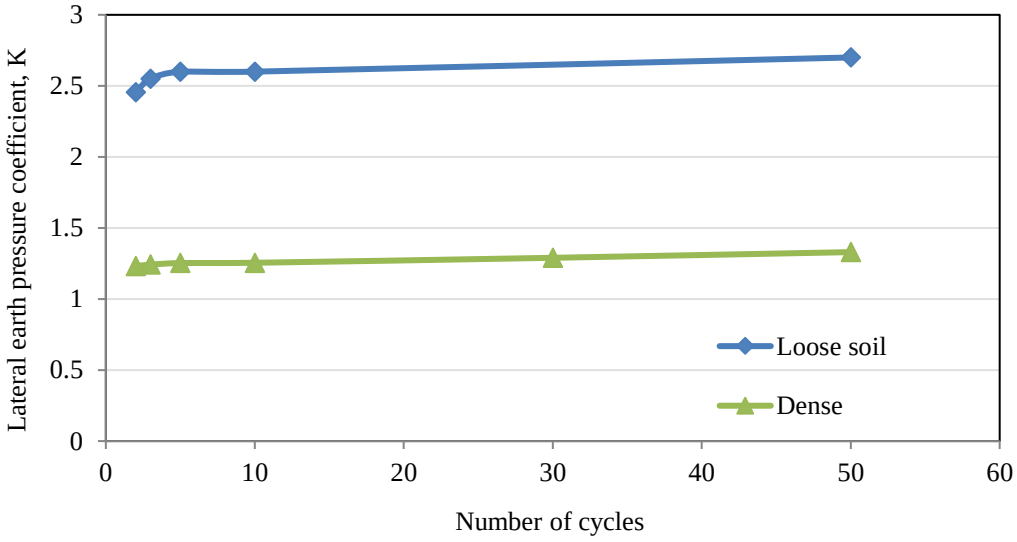

Figure 3.9 Lateral Earth Pressure Coefficient *K*, for Dense and Loose Soils

3.3.4 Influence of Daily and Annual Temperature Variation

The expansion and contraction cycles of bridge deck due to diurnal and seasonal temperature fluctuations normally occur concurrently. In order to capture the effects of both temperature variations on the IABs, a cyclic perturbation pattern was developed to represent the combined daily and annual temperature fluctuations as shown in Figure 3.10. This pattern is used in the finite element model to define the wall movement amplitude. Two separate scenarios were examined using the same model of the loose soil in Table 3.4 above to evaluate the combined effects of daily/annual temperature fluctuations. In the first scenario, only a single cycle of ±40mm perturbations (reflecting annual temperature fluctuations) was applied, while in the second scenario, 365 cycles of ±6mm (daily temperature fluctuations) were applied within one complete cycle of ±40mm (annual temperature fluctuations).

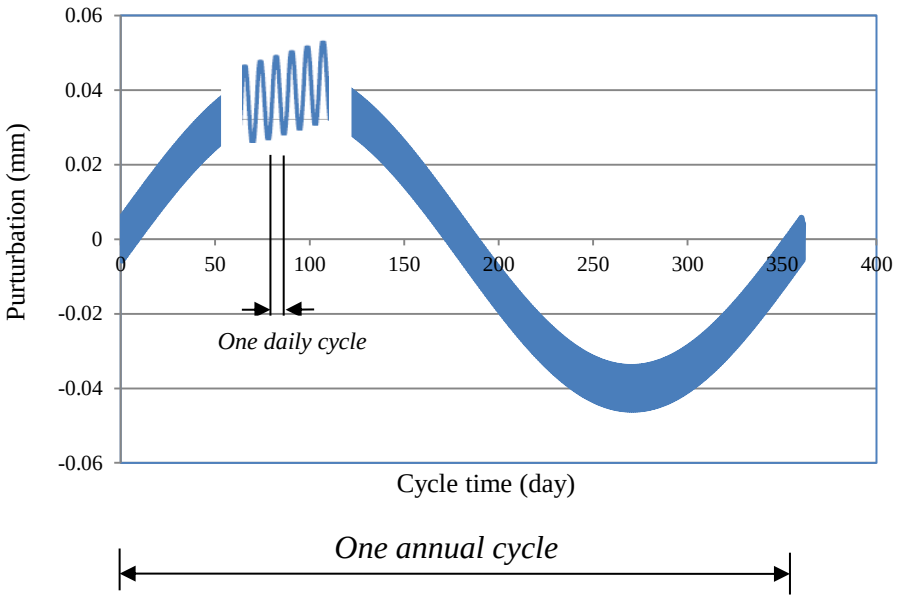

Figure 3.10 Superimposed temperature fluctuation pattern

The modelling results obtained from the two scenarios showed only a slight difference in the soil settlement, but a more significant impact on the lateral earth pressure coefficient (*K*) was observed as illustrated in Table 3.5.

Table 3.5 Maximum settlement and lateral pressure coefficient for (A) Annual temperature only and (B) combined annual and diurnal temperature fluctuations

Amplitude	Maximum settlement [m]	Lateral pressure coefficient (K) at 0.3H*
Single cycle of ±40mm	0.085	2.85
365 cycles of ±6mm superimposed with a single cycle of ±40mm	0.093	3.53

*H refers to the total height of the concrete abutment

The data given in Table 3.5 indicate that the value of lateral pressure coefficient (K) increased by approximately 24% when daily/annual temperature variations are combined, relative to the single cycle with only annual temperature variations. These effects increase with respect to the range of daily temperature variations. For instance, during summer seasons the temperature varies widely in Australia between day and night, which results in greater daily perturbation and consequently larger impact on lateral earth pressure. Hence, considering only the cyclic movements of IAB abutments under a single effect of either daily or annual temperature fluctuations may underestimate the value of lateral earth pressure and consequently may result in improper designs. It is suggested that the combined "daily–annual" temperature variation effects should be taken into account during the investigation of abutment movements.

3.4 Summary

A finite element model has been developed using the ABAQUS/Standard to simulate a centrifuge test in which an abutment wall is experiencing cyclic movements. The modelling results including the lateral earth pressures acting on the wall and the settlements in the soil adjacent to the wall have been compared with centrifuge test results and found to agree well with the measured data. The modelling results indicate the presence of stress ratcheting effects after applying number of movement cycles of relatively large displacement. Excessive settlement has also been observed by the modelling results in response to the wall movement.

The FE model was used to perform a parametric study in which the effects of soil properties and the type of cyclic movements have been investigated. It has been

found that dense soils tend to exhibit less settlements and racheting effects compared to loose soil. On the other hand, estimating the effects of wall movements based on only the annual temperature changes largely underestimates the values of lateral earth pressures. Therefore, the superimposed daily-annual temperature changes should be taken into account when the cyclic movement in IABs is studied.

Chapter Four

Small Wall Physical Model

4.1 Introduction

Physical models of abutment walls under the influence of normal gravity have been used in the past to investigate the soil–structure interaction mechanism in integral abutment bridges (England, 2000; Cosgrove and Lehane, 2003; Tatsuoka et al., 2009). Important data have been obtained with regard to various issues in IABs using physical modelling. In this chapter, the results and findings of an experimental program undertaken in this thesis for a small retaining wall will be discussed in detail. These experiments are intended to fulfil two primary objectives as outlined below:

- Provide an insight into the soil-wall interaction behaviour under different modes of wall movements. This will particularly involve the development of lateral earth pressures exerted on the wall and the settlement in the soil surface.
- Investigate the effectiveness of using the expanded polystyrene geofoam (EPS), as a compressible inclusion, in attenuating the wall movement effects on the adjacent retained soil.

The physical test setup involves a small wall retaining loose sand at one side and subjected to cyclic movements as would be expected to occur in an abutment of an integral bridge. However, it is worthwhile noting that the physical model discussed in this chapter is not intended to represent a down-scaled model of a large prototype. Also the stress levels in this model are not expected to replicate those developed in a wall with prototype dimensions. However, the current physical model is intended to investigate the overall trend of the wall-soil interaction behaviour under certain conditions, which is likely independent of the dimensions of the physical model.

4.2 The Test Program

The experimental program involves five tests varying two principal parameters as follows:

4.2.1 The Mode of Wall Movement

According to Ng. et al. (1998), the movement occurring in the abutment in an integral bridge, as a result of the temperature changes, is a combination of two different modes of movements, *rotation* and *translation*. This means the abutment will translate and rotate at the same time as a result of deck expansion and/or contraction. The reported field data showed that the rotation and translation movements are usually unequal and the domination of either mode is dependent on various factors including the type and height of the abutment and the properties of backfill (Huntly and Valsangkar, 2009). Generally, short abutments tend to translate more compared to deep embedded abutment walls where the dominant movement mode is rotation.

The mode of movement, translation or rotation, has a considerable impact on the magnitude and distribution of the lateral earth pressures acting on the abutment. (Huntly and Valsangkar, 2013). It also affects the extent and depth of the potential soil settlement in the approach soil which consequently influence the relevant design criterion of the run-on slab. Therefore, investigating the variations imposed by the mode of abutment movement will broaden the existing knowledge about the approach issues in IABs and their possible remedies.

However a rigorous analysis that quantifies such effects in IABs is unavailable; therefore, in the present experimental program two modes of wall movements will be examined as follows,

- Translation: in this test, the small wall experiences an absolute translational movement toward and away from the soil as shown in Figure 4.1.a. The moving force is applied at the centre of the wall.
- Rotation: in this test, the wall is hinged at its bottom end so that it can only rotate without any translation. The moving force in this case is applied at the top end of the wall as shown in Figure 4.1.b.

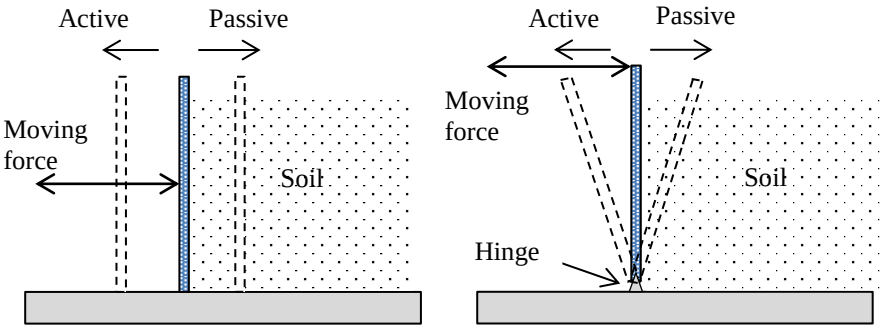

Figure 4.1(a) Figure 4.1(b)

Figure 4.1 Modes of wall movement investigated in the test

4.2.2 The Use of Expanded Polystyrene Geofoam (EPS) inclusion

The testing program also involves the use of EPS inclusion in order to produce comparative results for the lateral pressures and soil settlements for the cases with and without the presence of EPS inclusion. Such results will provide an actual data on the potential performance of the EPS in alleviating the approach problems in IABs. Accordingly two types of tests have been carried out as follows,

- Physical modelling of the wall and the retained soil without EPS geofoam
- Physical modelling of the wall and the retained soil with the presence of EPS inclusion.

In consequence, the experimental program involves a total of five tests, depending on the aforementioned factors. For the simplicity of citing the tests, they will be referred by their corresponding symbols, T1, T2, T3, T4a and T4b as illustrated in Figure 4.2.

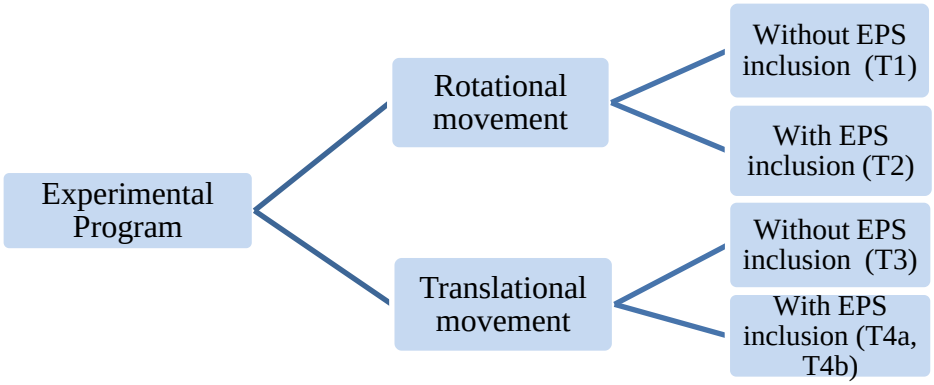

Figure 4.2 Experimental program flowchart

4.3 The Experimental Setup

The tests have been conducted in the Geotechnical Laboratory in Western Sydney University. The testing chamber and the frame, shown in Figure 4.3, were formerly constructed by the university to be used in geotechnical tests of retaining structures. The chamber is 0.7m long, 0.3 height and 0.25m wide with 50mm thick clear acrylic panel forming its face. The wall is represented by 300mm height, 248mm wide and 13mm thick steel plate placed inside the chamber. Two ways of fixation for the wall were used depending on the mode of movement.

During the horizontal translation tests, two movable supporting bars were horizontally attached to the rear side of the wall at 50mm and 250mm from the bottom. The bars were intended to hold the wall and prevent any rotational movement during wall translation. The wall was freely sitting on the bottom panel of the chamber.

In the other tests, where the wall movement is rotational, the wall was fixed with a hinge at its bottom so that it rotates freely without any possible translation. No supporting bars are used in this mode of movement.

In each test, the wall sides were properly lubricated to minimize the friction between the wall and the chamber. “L shaped” clear plastic sheets were placed at the corners around the wall to prevent any soil leakage during wall movement which may affect the settlements.

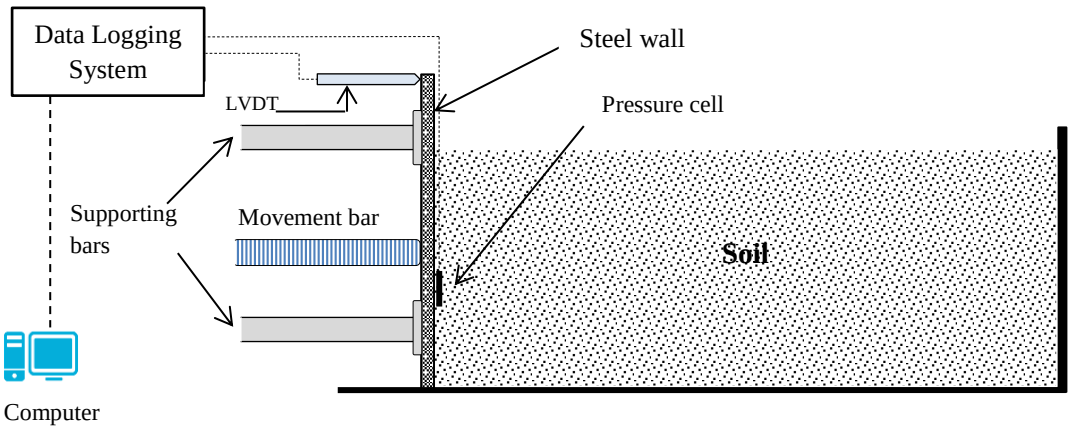

Figure 4.3 The experimental setup (for horizontally-displaced wall)

A, BestTech, pressure cell of 50mm diameter and 11.3mm thickness was used to measure the lateral pressures during the tests. The cell was initially calibrated at low pressures using a 1m high column of water. The cell has a precision of 0.367kPa. It was mounted at the front face of the wall at a height equal to *2H*/3 from the top of the soil surface (*H* refers to the retained height of the soil). Taking into account the dimensions of the model, this location was selected to achieve some lateral pressure as the latter can be very small at the upper part of the wall.

A linear variable differential transformer, LVDT, fixed to the chamber frame is used to measure the horizontal movement of the wall. The readings of the pressure cell and the LVDT were recorded throughout the tests using a data logger. An in-house customized software was developed to store and analyse the data on a desktop computer connected to the data logger.

The moving force was applied during the test through a rotating shaft at the rear side of the wall. The shaft has fine (1mm) threads to allow for a smooth and slow horizontal movement. Equal horizontal displacement of 2mm (at the soil surface level) has been utilized in all tests. This magnitude represents a comparative value to a typical annual displacement amplitude in the actual bridge dimensions (±30mm). The cycle of movement utilized in all tests begins with passive displacement of 2mm against the soil followed by 4mm reversed displacement so that the wall experience 2mm active movement. Eventually the wall is moved passively 2mm to return to its initial position. The combination of wall movements, toward passive, active and back to its original position is interpreted as one single cycle.

4.4 Properties of Materials

4.4.1 Soil

The soil used in the tests is dry siliceous sand supplied from a local dealer in Sydney-Australia. A standard sieve analysis was conducted to identify the particle size distrbution of the sand. The sieving results showed that the sand is quite unifrom with a particle size ranging between 150-300μm. The test was aimed to utilize a loose soil in order to provide an upper-bound figures of the settlements for given loading cycles. Therefore the sand has been placed loosely in the testing chamber without compaction. The height of the soil, in all tests, was 240mm.

After placing the soil, the top surface was gently levelled to achieve the required height of soil. The unit weight of soil has been calculated at each test based on the total weight of soil used and the occupied volume. Soil unit weight was ranging between 14.33kN/m^3 and 14.9kN/m^3.

4.4.2 EPS Geofoam

The EPS geofoam utilized in the test has been cut using a hot wire from a large block of EPS supplied by a local manufacturer with a density of EPS 20kg/m^3. A wedge-shaped EPS inclusion was used in test T2 in which the angle θ between the horizontal surface and the interface planar between the EPS and the soil was approximately 50°. The inclusion, as shown in Figure 4.4, is formed of three pieces of EPS with dimensions of 50mmx80mmx248mm, 100mmx80mm, 248mm and 150mmx80mmx248mm

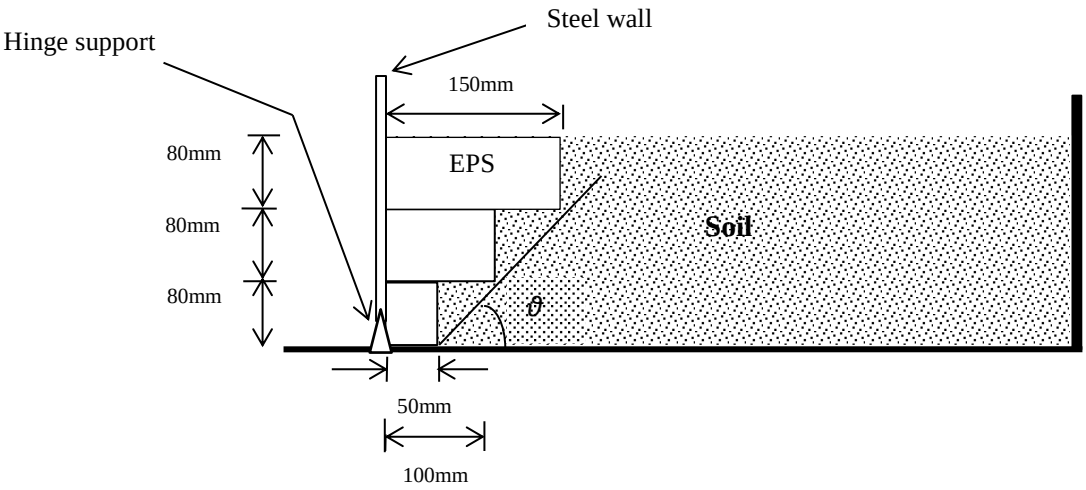

Figure 4.4 Test setup with the EPS inclusion (for hinged wall)

In test T4, two arrangements of EPS were used including single-block and wedge-shaped inclusions.

4.5 Tests Results and Discussion

4.5.1 Hinged Wall Tests

The hinged wall tests are meant to investigate the effects of wall movement on the adjacent soil when the mode of movement is an absolute rotation. This test involves two variations, as discussed below,

4.5.1.1 Test of Hinged Wall without EPS Inclusion (T1)

In this test the soil was tested without the presence of EPS inclusion. After setting up the wall at the initial position, the soil was placed and levelled to the required height of 0.24m. The total weight of soil, *W*, was measured and found equal to 59.632kg. The total occupied volume, *V* was 0.0408m^3. Accordingly the unit weight of soil was determined as,

$$\gamma = \frac{W}{V} \times g \quad (g \text{ refers to the gravity, } 9.81 m.s^{-2}) \tag{4.1}$$

$$\gamma = 14.33 \text{ kN/m}^3$$

The initial lateral soil pressure measured by the pressure cell after placing the soil (at-rest pressure) was 1.07kPa. It follows that the initial coefficient of lateral pressure, K_o was determined as,

$$K_o = \frac{\sigma_h}{\sigma_v} = \frac{1.07}{14.33 \times 0.16} = 0.466 \quad (\text{where } \sigma_v \text{ is expressed as } \gamma * z) \tag{4.2}$$

During the test, the movement shaft rotates at a displacement rate of approximately 4mm/minute, so that each cycle is completed in two minutes. This speed is reasonably slow to simulate quasi-static loading conditions and to avoid sudden soil slumping due to rapid wall movement. The settlement at the soil surface was measured manually using a vernier at the interface with the wall in addition to eight more points located within a horizontal distance of 250mm from the wall.

Soon after starting the test, the measured lateral pressure started to increase and signs of settlement in the soil surface became apparent. After 30 cycles of wall passive and active movements, a clear soil trough became visible as shown in Figure 4.5. The lateral pressures increased noticeably from 1.07Kpa before the test to 4.88kPa at the end of last cycle (30th cycle). The maximum pressure recorded when the wall was at the passive position was 7.82kPa.

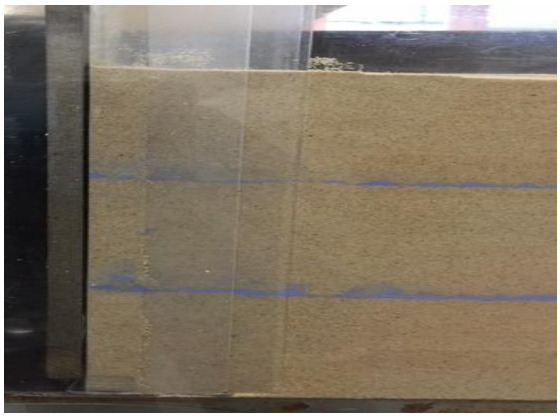

Figure 4.5 (a)

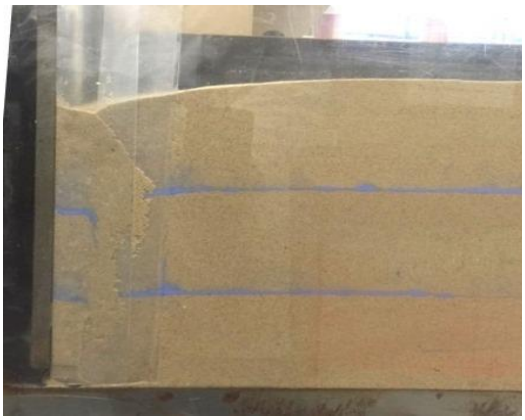

Figure 4.5 (b)

Figure 4.5 The soil surface (a) before and (b) after Test T1.

Figure 4.6 illustrates the change in the lateral pressures with the number of cycles. It is evident that the lateral pressure increases rapidly during the first five cycles and then asymptotes in the following cycles. This behaviour is similar to that observed by England et al. (2000) and Cosgrove and Lehane (2003) in their small scale models tested at normal gravity. This ensues from the large slumping of active soil wedge during the first few cycles which results in rapid densification in the soil located in the vicinity of the wall.

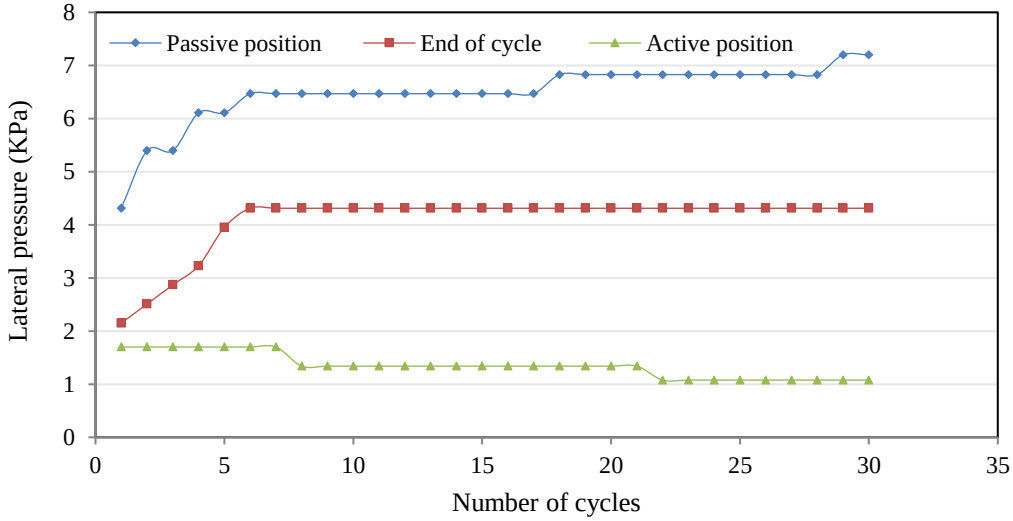

Figure 4.6 Lateral earth pressures at different wall positions - Test T1

The lateral pressures recorded when the wall is at the passive position are approximately 50% greater than those recorded at the end of each cycle, (when the wall is at the initial position). Moreover, the increment rate in the passive lateral pressure is slightly greater than that in the “end of cycle” pressure. The lateral

pressures during wall active movement are seemed to be constant and insensitive to the number of cycles.

The lateral pressure envelope is presented in Figure 4.7 (a), where the pressures are plotted against the lateral displacement. It can be noticed that the pressure varies rapidly when the wall travels between the active and passive positions, which indicates the loading and unloading cycles in the adjacent soil.

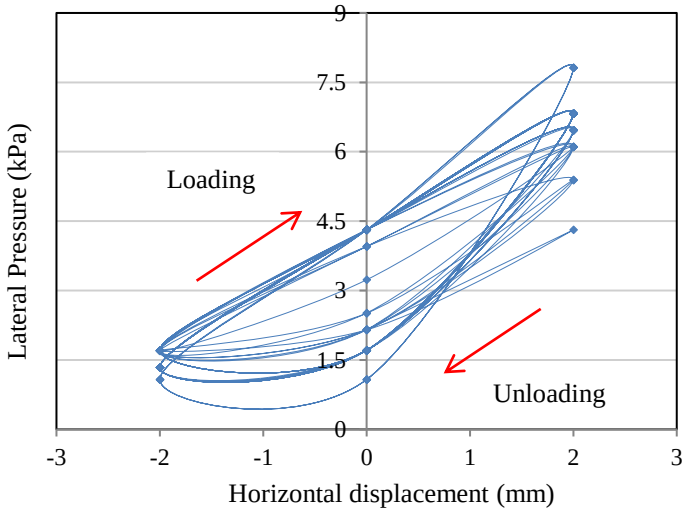

Figure 4.7 (a)

Similar behaviour is also observed for the change in lateral pressure coefficient *K* during the test. Figure 4.7 (b) illustrates the relationship between the measured values of *K* at different wall positions with the number of cycles.

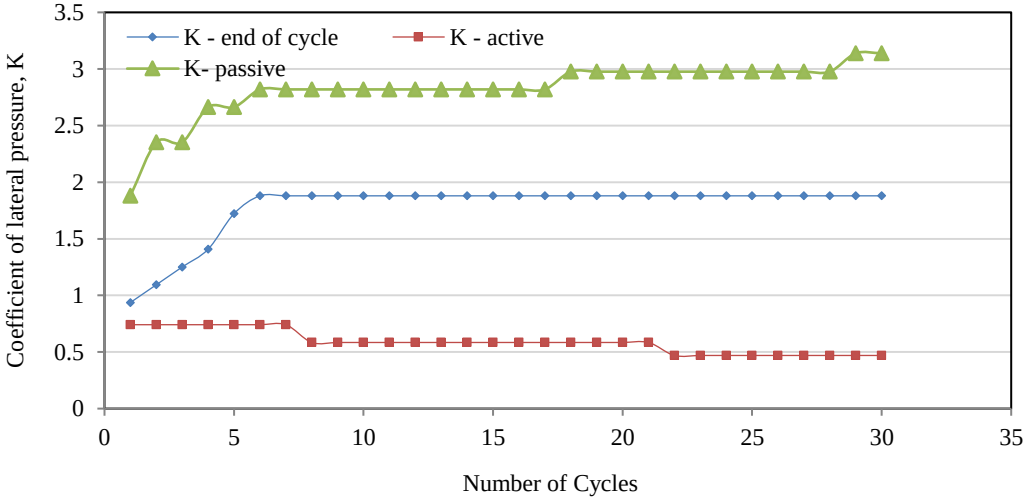

.

Figure 4.7 (b)

Figure 4.7 (a) Lateral pressure envelope during wall movements - Test T1

& Figure 4.7 (b) relationship between *K* and number of movement cycles - Test T1

The settlement results show that the maximum soil settlement occurs at the interface between the wall and the soil. The value of maximum settlement increased non-linearly with number of cycles. Figure 4.8 summarizes the relationship between the maximum settlement and the number of cycles at different wall positions. Unlike the lateral pressures, maximum settlement results were not showing a limiting value after 30 cycles. Also the settlements exhibit limited dependency to the wall position (active or passive). However, the highest settlement values were always recorded when the wall was at its active position.

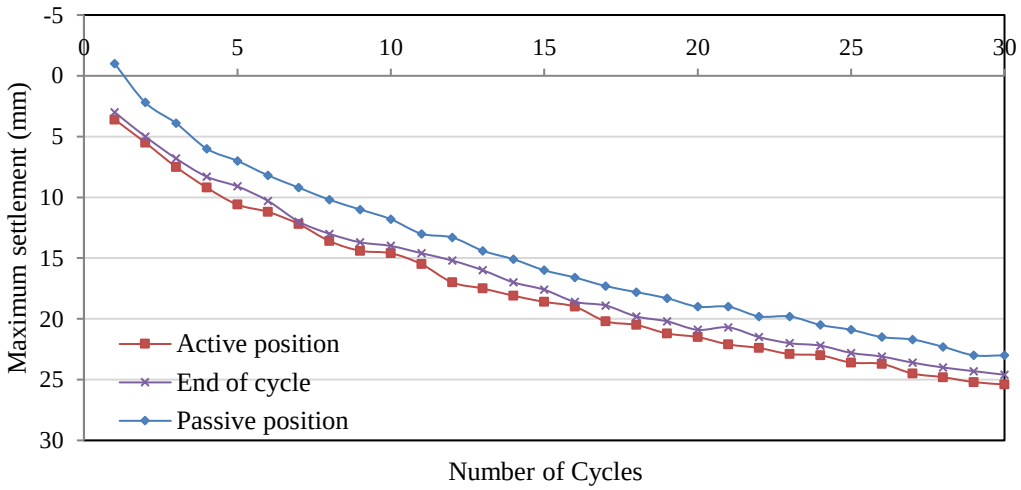

Figure 4.8 Maximum settlements at different wall positions - Test T1

At the end of the test, the maximum measured settlement was equal to approximately 0.1*H*. The extent of the soil trough was equal to approximately 250mm from the wall which slightly exceeds the retained height of the soil, *H*. These results are qualitatively close to those obtained by Cosgrove and Lehane (2003) after testing loose sand undergoing a cyclic displacement by the retaining wall.

In order to represent the extent of settlement effects at the soil surface, the settlements at different distances from the wall were plotted against the number of cycles as shown in Figure 4.9. As would be expected, maximum settlement is observed at the wall-soil interface, and then decreased to an asymptote at approximately 250mm from the wall.

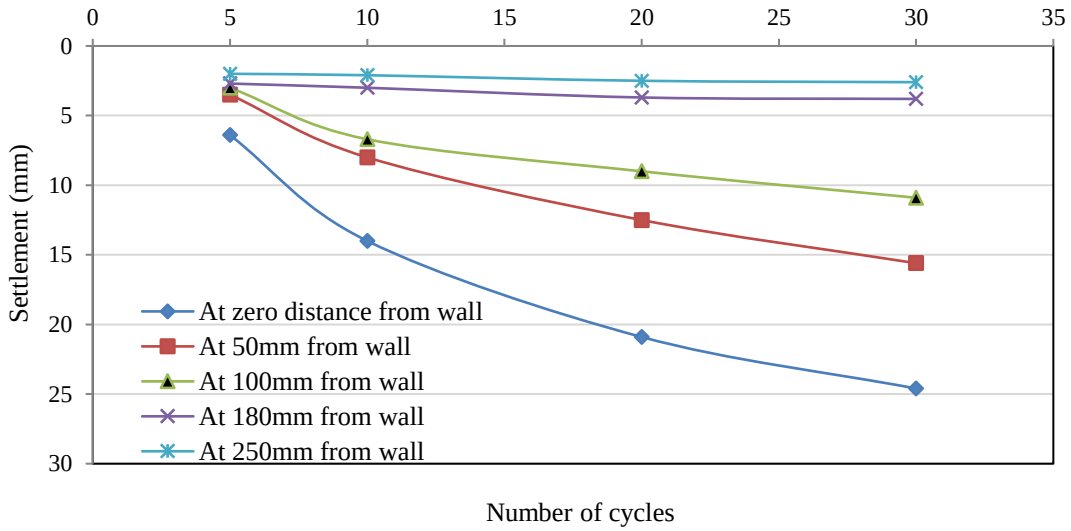

Figure 4.9 Settlement results at different distances from the wall - Test T1

The profile of the soil has been represented to show the stages of settlement during the test, as shown in Figure 4.10. The deformed soil shows a steady settlement increase gradually towards the wall. This pattern represents typical settlement behaviour in a loose soil (Ng. et al., 1998).

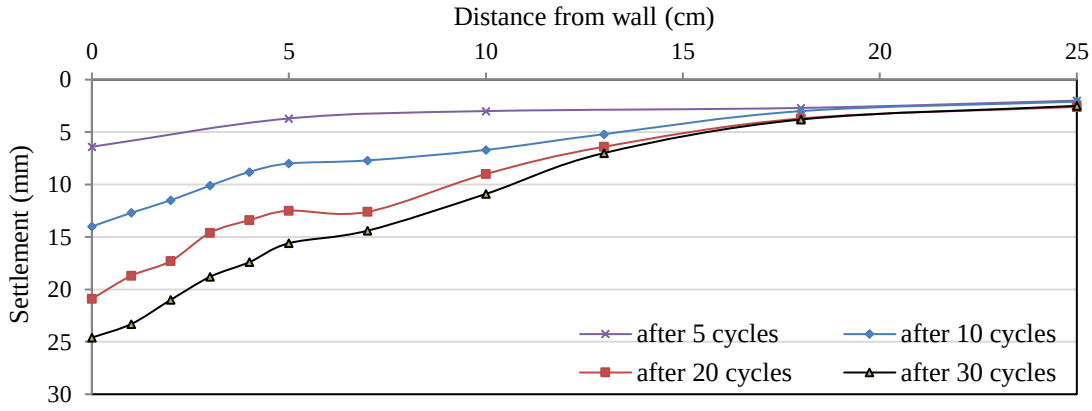

Figure 4.10 The settled soil profile at different cycles - Test T1

4.5.1.2 Test of Hinged Wall with EPS Inclusion (T2)

In this test an EPS inclusion has been placed at the interface between the soil and the wall. The soil was placed and levelled to a nominal height of 240mm. The unit weight of soil was determined based on the total weight and the occupied volume as in T1. The unit weight of soil in this test was 14.27kN/m^3

This test involved the application of 30 (passive / active) cycles of 2mm horizontal displacement at the level of soil surface. Lateral pressure and the settlement results

were measured throughout the test. After 30 cycles of loading, the deformation in the soil surface became apparent as shown in Figure 4.11.

(a) (b)

Figure 4.11 The soil surface (a) before and (b) after Test T2

The results collected from this test (T2) show significant reductions in the lateral soil pressures compared to those observed in test T1. The maximum passive pressure was attenuated to only a fraction of the corresponding value recorded in T1 (from 7.2kPa to 2.874kPa). Figure 4.12 illustrates the lateral pressures at different wall positions as observed in T2.

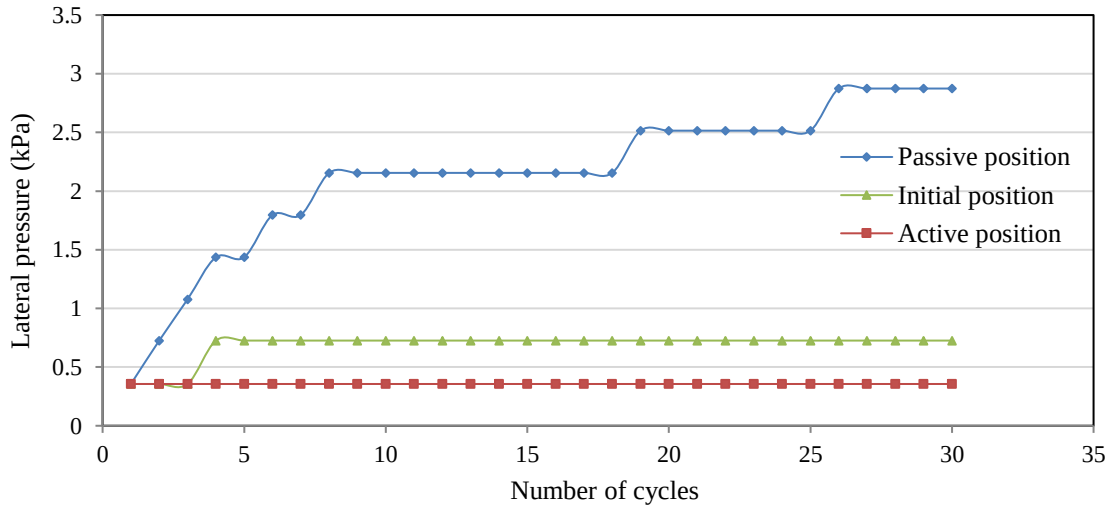

Figure 4.12 Lateral earth pressures at different wall positions - Test T2

The settlement has also been significantly minimized with the presence of the EPS inclusion. The maximum settlement recorded after 30 cycles was 14.7mm and that is approximately 40% less than the corresponding value measured in test T1.

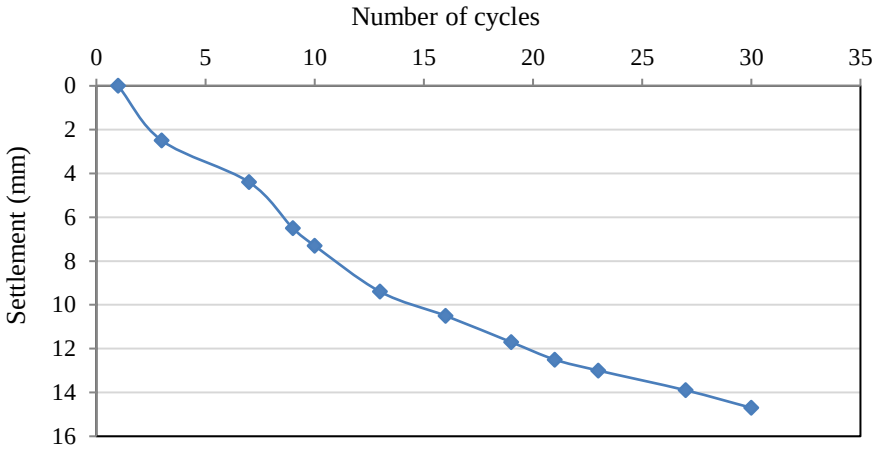

Figure 4.13 Maximum settlement at initial position - Test T2

The pattern of settlement is slightly different for the two tests. The settlement profile for T2 has less extent and depth than for T1. It is evident that the influence zone of wall movement has been minimized due to the existence of the EPS inclusion. This behaviour is manifested in large decrease of settlement rate with the distance from the wall as illustrated in Figure 4.14.

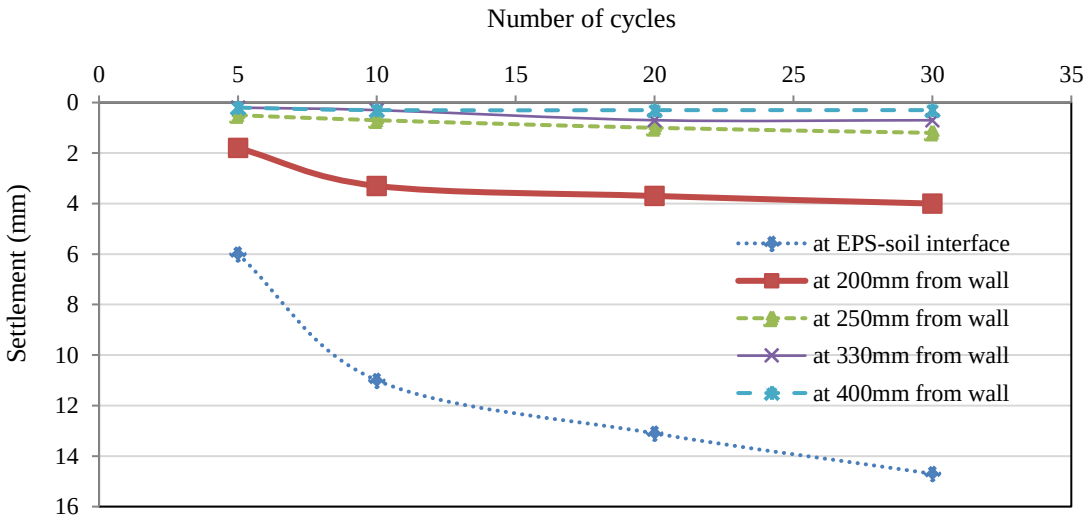

Figure 4.14 Settlement at different distances from the wall – Test T2

4.5.2 Tests of Horizontally-displaced Wall (Translational Movement)

These tests are intended to investigate the soil settlement and the lateral pressures acting on the wall when the movement is an absolute translation without any rotation. In these tests, the wall stands vertically on its base and is supported with two horizontal bars as illustrated earlier in Figure 4.3. This type of test also involves two variations, with (T4) and without the presence of EPS inclusion (T3).

4.5.2.1 Translation Wall Movement without EPS Inclusion (T3)

Similar to the test setup in T1, the soil was loosely placed inside the test chamber without using an EPS inclusion. Thirty cycles of two way, 2mm, translational displacement were applied at the centre of the wall at the same rate adopted in earlier tests T1 and T2. The lateral pressures and the settlements were measured throughout the test.

The results collected from test T3 showed considerable quantitative and qualitative variations to those observed in T1. The lateral earth pressures in test T3 are generally higher than the corresponding values in test T1. The passive pressure increases nonlinearly with the number of cycles to reach a maximum value of 30.19 kPa after 30 cycles. This value is approximately four times higher than the corresponding value in T1. Moreover, passive pressure in T3 was constantly increasing throughout the test without a sign or tendency to asymptote after 30 cycles.

The end-of-cycles pressure experiences a rapid increase during the first ten cycles of the test then stabilized or increased at smaller rate after 15 cycles of wall movements. The maximum value of at-rest pressure recorded in T3 was 17.25. Figure 4.15 shows the lateral pressures measured during test T3 at different wall positions.

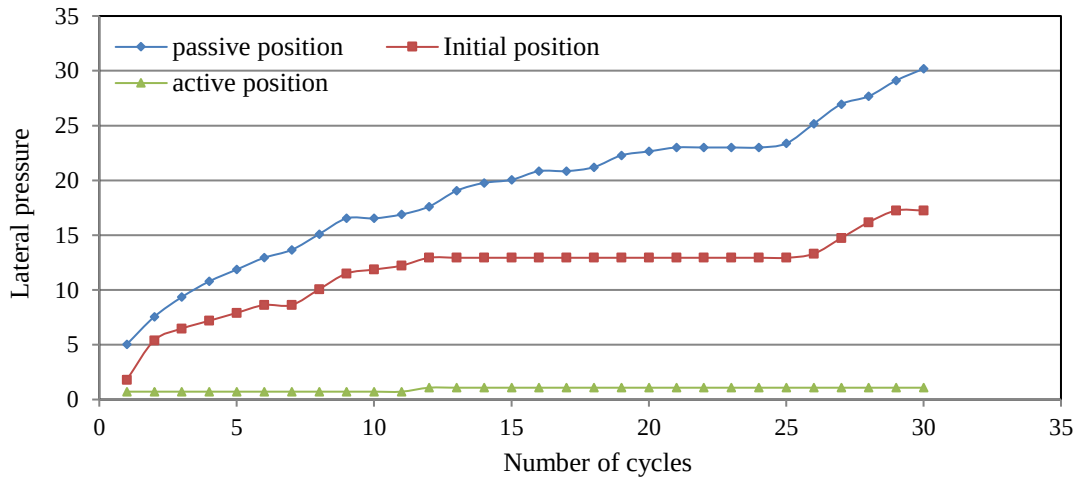

Figure 4.15 Measured lateral pressures at different wall positions -Test T3

The settlement results also showed some differences compared to the test results of T1. The maximum settlement, measured at the interface between the soil and the wall increased significantly with the number of cycles to reach 74.3mm at the end of the test. This value exceeds 30% of the total retained height of the soil and is three times greater than that in Test T1. The results also show an amount of heave at the soil

surface between 15cm and 20cm from the wall. This behaviour was not observed in test T1 whereas the soil did not exhibit any heave during the test. The model before and after the test are shown in Figure 4.16.

(a) (b)

Figure 4.16 The soil surface (a) before and (b) after the Test T3

4.5.2.2 Translation Wall Movement with EPS Inclusion (T4a, T4b)

This experiment involves testing the soil under two-way translational wall movements with an EPS inclusion provided between the soil and the steel wall. The inclusion is represented by 80mm thick EPS board with a density of 20kg/m^3 (Test T4a). According to the selected thickness of the EPS board, the total strain incurred by the wall movement may exceed the elastic strain of the EPS inclusion (0.1%) and some plastic deformations could be accumulated during the test. This will allow for investigating the effects of any possible plastic deformations in the EPS on the soil settlements and the lateral pressures.

The soil was loosely placed in the test chamber and the test was carried out under the same displacement amplitude and loading rate used in previous tests. At the end of the test, a small trough was apparent in the soil adjacent to the EPS geofoam as shown in Figure 4.17.

The lateral pressures measured during the test were considerably less than those in test T3. Maximum lateral pressure recorded in this test was 9.705kPa and that is approximately 65% less than the corresponding value in the test T3. Although the magnitude of pressure increased rapidly during the first few cycles, it showed a clear sign of reduction in its increment rate and asymptote between 22 and 30 cycles.

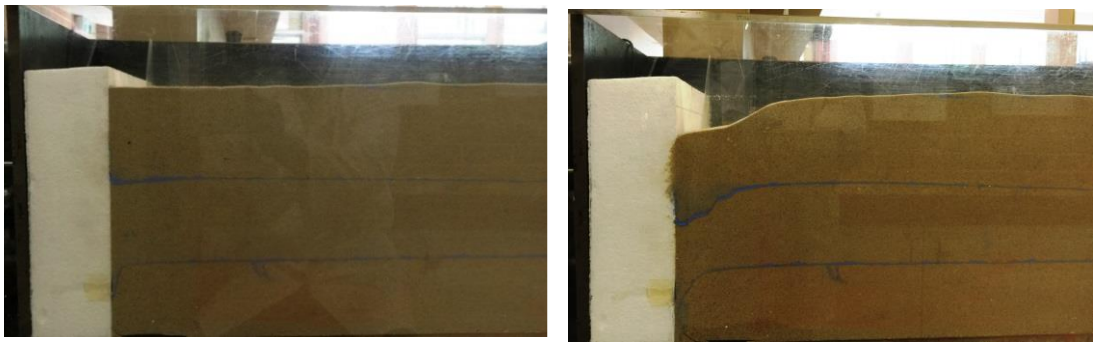

(a) (b)

Figure 4.17 Experimental setup of Test T4a (a) before the test and (b) after the test

On the other hand, the measured values of lateral pressures at the initial and active wall positions were very small and remained almost constant throughout the test.

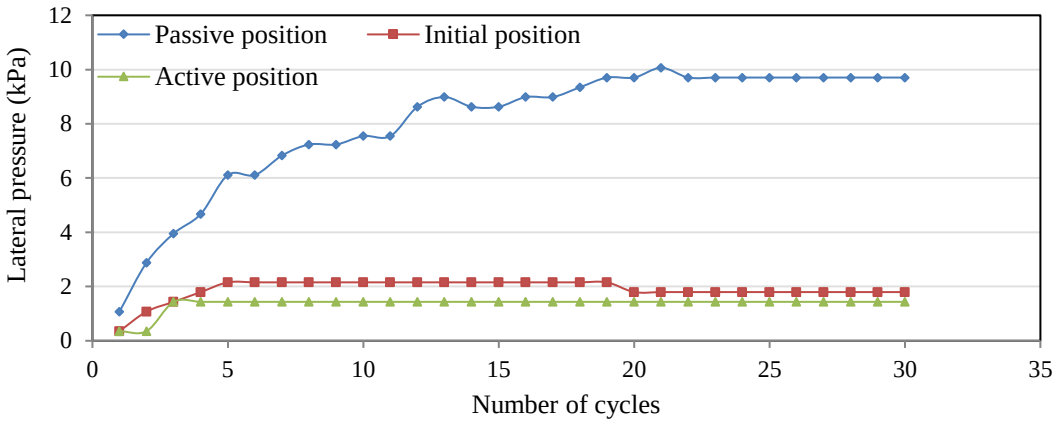

Figure 4.18 Lateral pressures results - Test T4a

The settlement results collected from test T4a were also less than those measured in test T3. According to Figure 4.19, the maximum settlement after 30 cycles was 31.3 mm, which is equivalent to 50% of the corresponding value in test T3.

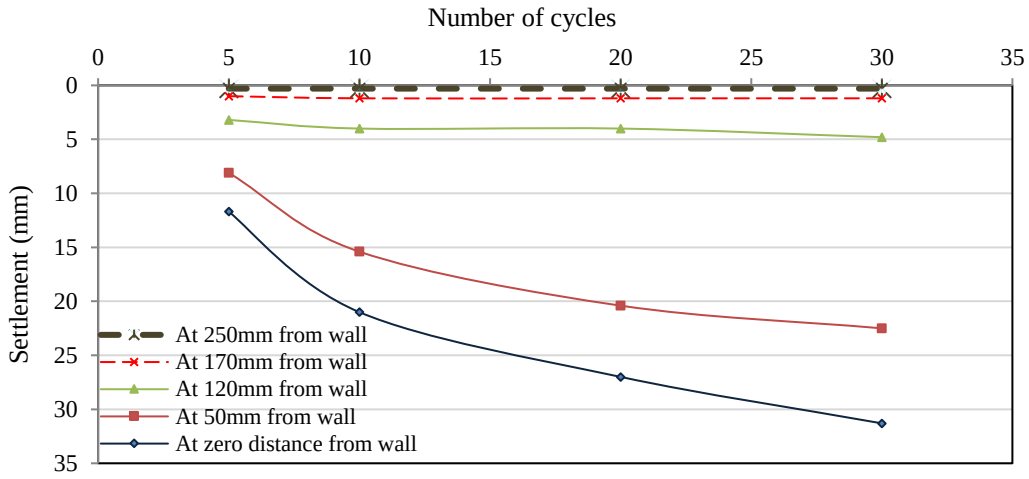

Figure 4.19 Soil surface settlements at different distances from the wall – Test T4a

In order to verify the potential effectiveness of EPS inclusion in different arrangements, test T4b was carried out using EPS arrangement similar to that used in Test T2 (wedge-shaped inclusion). The results of the second version of test T4, T4b, revealed a considerable variation in the soil settlement. This fact indicates that the wedge shaped inclusion is more effective in attenuating the soil settlement than the single-block inclusion irrespective of the mode of wall movement. Figure 4.20 summarized a comparison between the settlement results using single-block and wedge-shaped EPS inclusions as observed in tests T4a and T4b respectively.

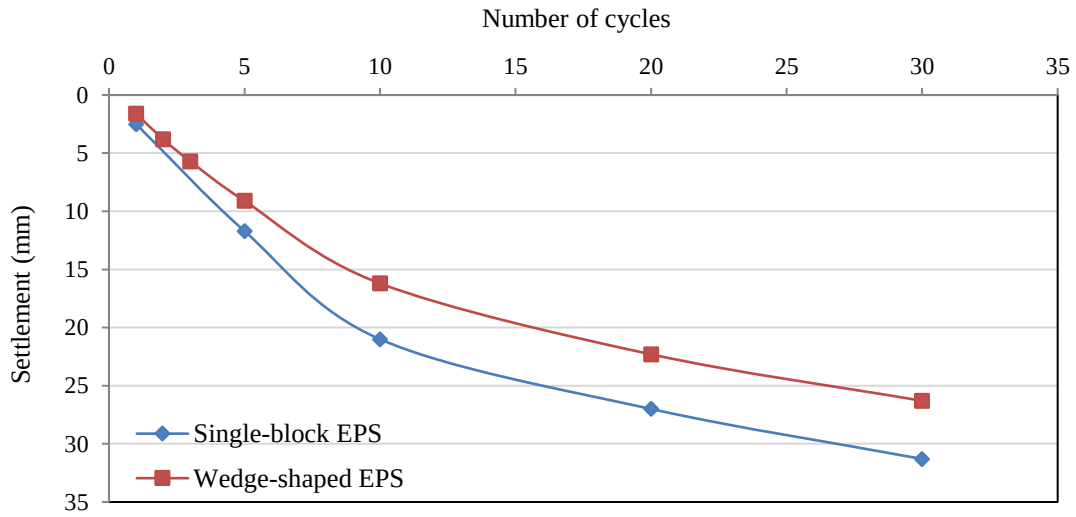

Figure 4.20 Maximum settlement in tests T4a and T4b using different arrangements for the EPS inclusion

4.5.3 Discussion of Results

The experimental results reported in this chapter showed various behaviours for the retained soil in response to the different modes of wall movements and the presence of an EPS inclusion. In this section, results collected from tests T1 through T4 will be reviewed and analysed.

4.5.3.1 Influence of Mode of Wall Movement

In order to analyse the influence of different wall movements on the retained soil, it is worthwhile first to discuss the soil-wall interaction mechanism under cyclic displacement. Generally, the movement of the wall in both modes (rotation and translation) involves cycles of passive and active displacements. During the passive phase, the wall compresses the adjacent soil, which results in a densified passive wedge of soil. When the wall moves back towards the active position, an active soil

wedge will slide down and slightly translate towards the gap behind the wall. In the following passive movement, the wall will encounter additional pressure to overcome the resistance, from the "formerly moved" active wedge, until it reached the passive position. This additional pressure, imposed by the active wedge resistance, will result in additional densification in the passive wedge. The repetition of such scenario over successive cycles will lead to,

- Highly densified soil in the passive soil wedge which eventually dilates and heaves under shearing,
- Escalation in the lateral pressure acting on the wall and
- More settlements in the loosened soil in the active wedge.

Although the aforementioned mechanism and the subsequent effects on the soil are the same irrespective of the mode of movement, the latter yet, imposes significant variations in the measured lateral pressures and soil settlements. Evidently the translation movement has greater effects on the retained soil than the wall rotation as illustrated in Figures 4.21 & 4.22. This is basically because the volume of soil affected or displaced during the translational movement is larger (theoretically two times) than that for the case of rotation. Consequently, the volumetric strain in test T3 is greater than that in T1.

$$\varepsilon_{v3} > \varepsilon_{v1} \tag{4.3}$$

$$\Delta x_3 \,.\, \Delta y_3 \,.\, \Delta z_3 > \Delta x_1 . \Delta y_1 . \Delta z_1 \tag{4.4}$$

As a plane strain case, the deformation in y direction Δy is constant.

Accordingly,

$$\Delta x_3 \,.\, \Delta z > \Delta x_1 . \Delta z_1 \tag{4.5}$$

Therefore, the larger volumetric strain in test T3 was reflected as greater amounts of settlement (Δz) and soil densification (Δx). The heave in the soil surface observed in test T3 indicates the increase in the density of the passive wedge of the soil, which normally dilates during shearing. This behaviour was not observed in test T1 because

the applied amplitude together with the mode of movement were not sufficient to densify the passive soil wedge.

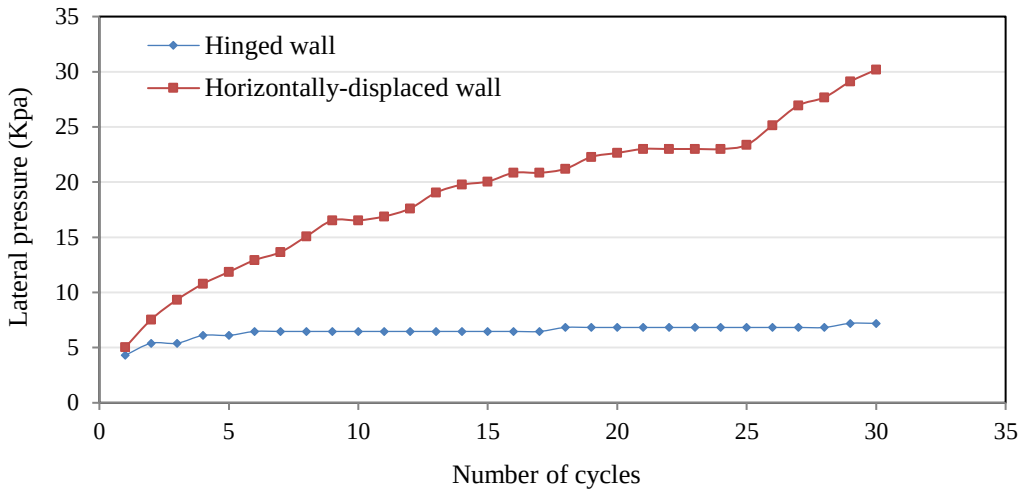

Figure 4. 21 Lateral pressures (passive position) of Tests T1 and T3

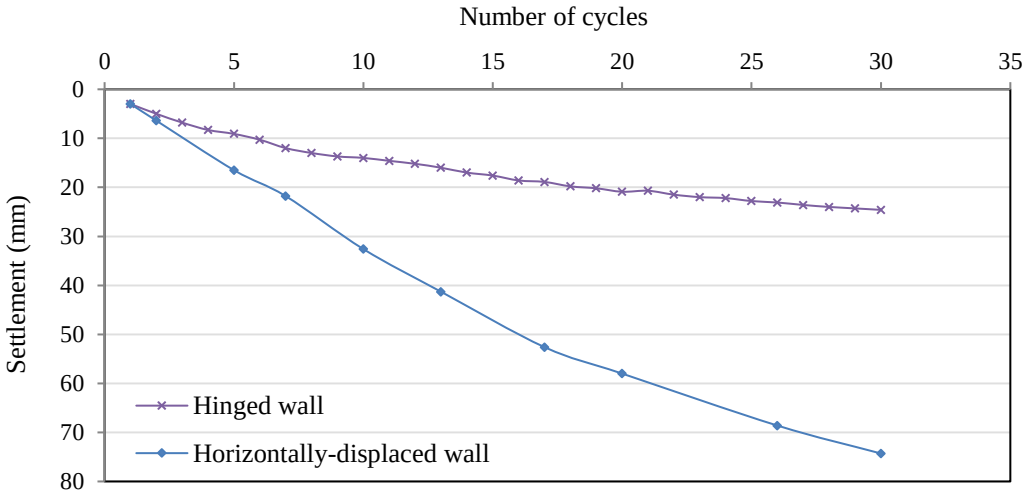

Figure 4.22 Maximum settlements measured in tests T1 and T3

4.5.3.2 Influence of the EPS Inclusion

In both modes of wall movements, rotation and translation, the EPS inclusion has functioned effectively in alleviating the lateral pressures and the soil settlements as shown in Figure 4.23 and Figure 4.24. For instance, the maximum measured lateral pressure and settlement in test T3 were reduced by 68% and 58% respectively compared to those in T4a. These reductions in the stresses and the settlement have a significant influence on the initial design requirements and the in-service maintenance works necessary for the bridge approaches. Therefore, in addition to its

potential structural and geotechnical advantages, the use of EPS will incur considerable cost savings in the long term.

The function of the highly compressible EPS inclusion is to absorb the wall displacement, without disturbing the adjacent soil, and subsequently dissipating the lateral pressures associated with the movement. However, in the results collected from test T2, T4a and T4b, this function seemed to be only partially achieved. A degree of lateral pressure, due to wall displacement, is evidently being transferred to the soil and consequently the settlement and lateral earth pressure were attenuated but not substantially vanished.

Based on the general equilibrium expression,

$$\sigma_{EPS} = \sigma_{soil} \tag{4.4}$$

$$\sigma_{EPS} = \varepsilon_{soil} . E_{soil} \tag{4.5}$$

$$\varepsilon_{soil} = \left(\frac{\sigma_{EPS}}{E_{soil}}\right) \tag{4.6}$$

According to Equation 4.6, the "most important" strain in the retained soil is a function of the compressive strength of the EPS and the stiffness of soil. In other words, to maximise the advantage of the EPS inclusion in rectifying the wall movement effects, an EPS with lower compressive strength and denser backfill need to be used. However, this criterion need to be employed with due attention to the other intended functions of the EPS inclusion such as bearing the vertical loads and the lateral soil pressure.

The arrangement of the EPS as a single-block or a wedge-shaped inclusion, also has a clear influence on the performance of the EPS inclusion. The wedge-shaped inclusion seems to be more effective than a single-block of EPS. However, the wedge-shaped inclusion requires a larger volume of EPS and consequently increase the overall project cost. Therefore, the selection of the proper design for the EPS inclusion would need to compromise between the properties of EPS, the incurred cost and the extent to which the settlement and the lateral pressures need to be minimized.

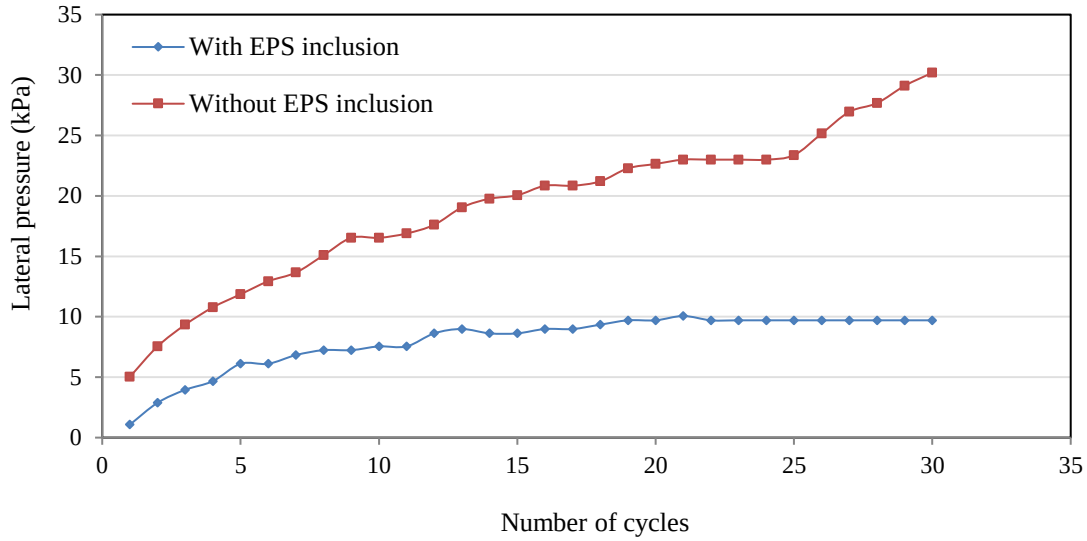

Figure 4.23 Lateral pressure with and without EPS inclusion (translation movement)

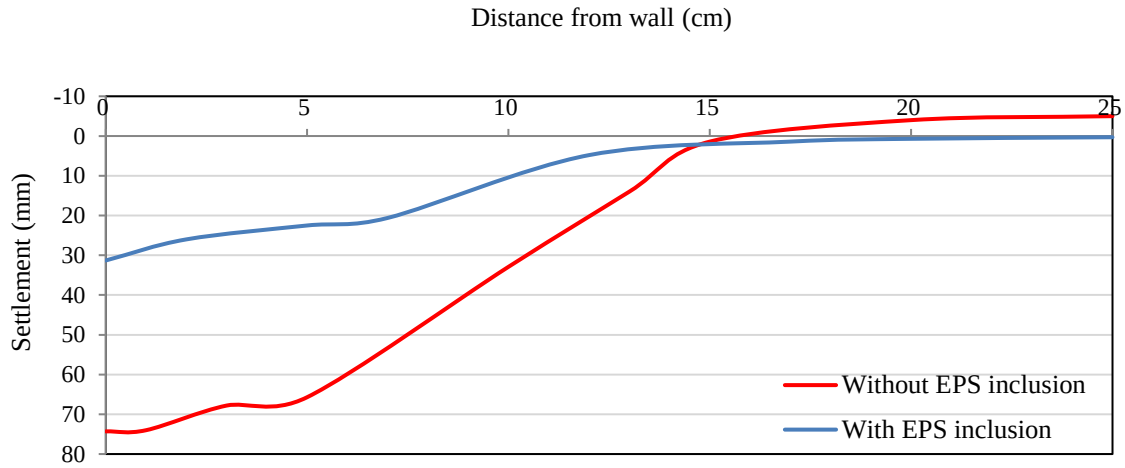

Figure 4.24 Settled soil profile of tests T3 and T4b

4.6 Summary

Five physical model tests were carried out on a small wall retaining loose sand to investigate the influence of the mode of wall movement and the use of an expanded polystyrene geofoam inclusion on the settlement problems at the approach of IABs. The data collected from the tests are summarized in Table 4.1. Based on the experimental test results, the following conclusions have been drawn:

Table 4.1 Summary of the test results

Test	Description	Max. Measured Pressure (kPa)	Maximum Settlement (mm)
T1	Rotational movement no EPS inclusion	7.817	24.6
T2	Rotational movement with wedge-shaped EPS inclusion	2.874	14.7
T3	Translational Movement no EPS inclusion	30.19	74
T4-a	Translational movement with single-block of EPS inclusion	9.705	31.3
T4-b	Translational movement with wedge-shaped EPS inclusion	-	26.3

- An abutment in an integral bridge will move cyclically in response to the ambient temperature changes. Such movement is a combination of two different modes, rotation and translation. These movements are usually unequal and the dominant mode is dependent on the type and height of the abutment in addition to the backfill properties.
- The dominant mode of abutment movement has a significant effect on the soil-structure interaction behaviour in IABs. Abutments with mainly translational movement experience higher approach settlements and lateral earth pressures than those with principally rotational movement.
- The use of EPS inclusion is effective in minimizing the soil settlement and lateral pressures irrespective of the type of wall movement.
- The design of the EPS inclusion, in particular its arrangements, compressive strength and thickness, plays an important role in its potential performance. However, the initial cost incurred will have to be compromised with the objectives or the intended functions of the EPS inclusion.

- In addition to its potential in rectifying the approach problems in IABs, the EPS possesses compressive strength that is sufficient to support the overburden loads specially in locations where weak or compressible underlying soil exists. Therefore, the EPS provides a unique design alternative that can be utilized as a light weight embankment and compressible inclusion at the same time.

Chapter Five

Finite Element Modelling of Integral Abutment Bridges with EPS Inclusion

5.1 Introduction

Computer simulations utilising reliable numerical models have been applied extensively in many engineering applications of practical interest. It provides an effective tool to produce results at minimal time, cost and effort. In its application to IABs, computer modelling has been used to investigate the soil-structure interaction behaviour under the temperature induced loads (Dicleli, 2000; Horvath, 2000; Kim and Laman, 2010; Bloodworth et al., 2012). However, to develop an efficient and reliable computer model, sufficient calibration and validation with physical data need to be undertaken.

In this chapter, a finite element model is developed using the ABAQUS/Standard finite element modelling software and validated against the experimental test data reported earlier in Chapter 4. As part of the work presented in this chapter, the ability of the model to simulate the constitutive behaviour of the expanded polystyrene geofoam (EPS) is verified. This verification is important to model the soil-wall interaction when an EPS inclusion is used. The finite element model is also to be validated against the adequacy in replicating the physical test results of the different modes of wall movements.

Upon validating the numerical model using the small wall test results, it is utilized to investigate the potential application of the EPS in rectifying the approach problems in IABs considering prototype dimensions. The model will provide an effective and flexible tool to study the effects of the EPS inclusion in different settings and arrangements on the lateral earth pressures and soil settlements in IABs approaches.

5.2 Model Description

5.2.1 Model Dimensions

The ABAQUS/standard (ABAQUS, 2013) finite element modelling software is used to develop the two-dimensional plane strain finite element (FE) model. The model is applied to study the IAB wall at prototype scale, with and without EPS inclusion.

The meshed ABAQUS model of the prototype wall is illustrated in Figure 3.2 in Chapter 3.

5.2.2 Constitutive Model and Material Properties of the Soil

The movements of the wall, forward and backward, utilized in the physical test were quite slow and can reasonably be modelled as a quasi-static loading condition. Therefore, as discussed earlier in chapter three, the Mohr-Coulomb model will be adopted to describe the constitutive behaviour of soil. The Mohr-Coulomb elasto-plastic model in ABAQUS (2013) allows the material to harden and/or soften which is likely to occur in the soil during the test. In order to accurately simulate the behaviour of materials as exhibited during the experimental test, the properties of the materials utilized in the test need to be determined.

The soil used in the test was dry fine sand in a loose state. It was necessary to determine the internal friction angle ($\emptyset$) and the cohesion (C) of the soil as they would be required as input data for the FE model. Therefore, four strain-controlled direct shear tests were carried out to determine the soil friction angle and cohesion. The samples were taken from the same soil used in the experiments and were tested via a GeoCon digital shear –box testing machine. The shear box test results are shown in Figures 5.1 and 5.2.

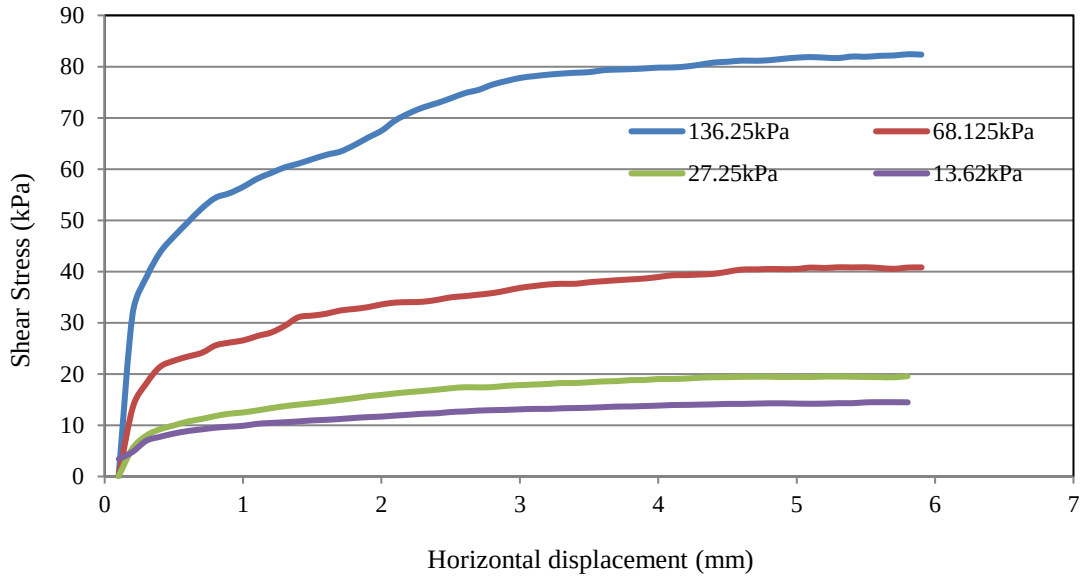

Figure 5.1 Horizontal displacement vs Shear stress at different normal stress

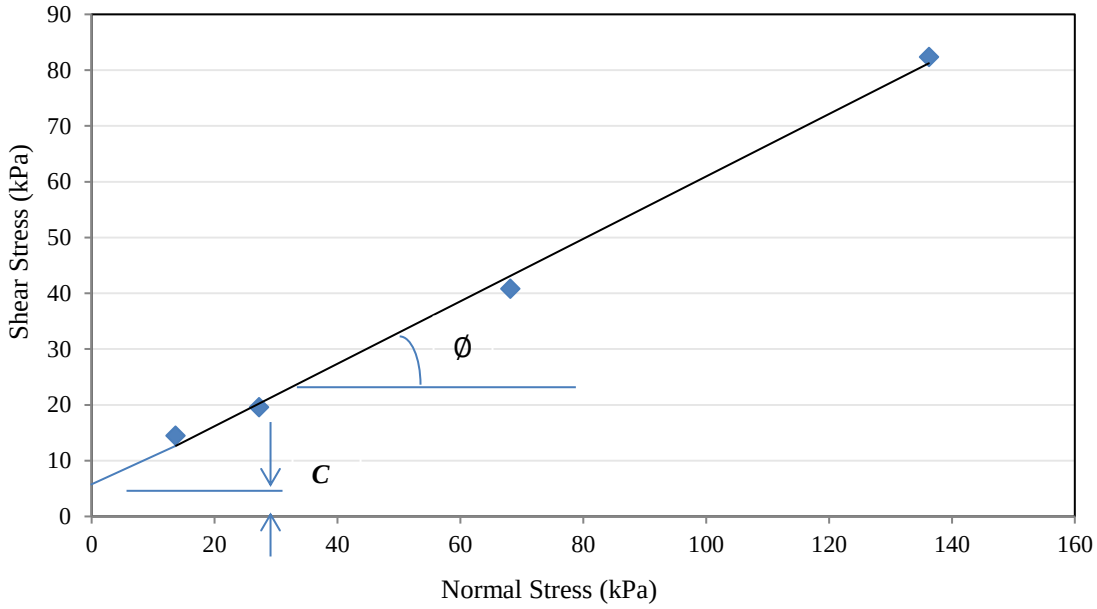

Figure 5.2 Coulomb Failure envelope of the soil

According to Mohr-Coulomb theory, the shear stress at the shear plane can be represented in a linear relationship with the normal stress. Therefore, the shear stress of the soil is given by,

$$\tau = c + \sigma . tan\emptyset \tag{5.1}$$

$$\emptyset = tan^{-1}\left\{\frac{\tau - c}{\sigma}\right\} \tag{5.2}$$

Consequently, the internal shear angle and the cohesion of the soil, which is the intercept of the axis representing shear stress, were determined as 29.2° and 4kPa respectively.

5.2.3 Constitutive Model and Material Properties of the EPS

As a lightweight and highly compressible material, the Expanded Polystyrene geofoam (EPS) was modelled using an isotropic Hyper-foam constitutive model. The hyper-foam model is suitable for cellular materials that permit large volumetric changes and allow for energy dissipation. The mechanical behaviour considered by the hyper-foam model, during compression, involves three distinguished stages. At small strains (less than 5%) the material deforms elastically due to the bending of cell walls and that shows as a little straight line at the beginning of the stress–strain curve as shown in Figure 5.3. The next stage involves a plateau of strain under approximately constant stress. Finally densification occurs in the material due to the

collapse of cell walls resulting in a rapid increase in the compressive stress (ABAQUS, 2013). The behaviour prescribed by the hyper-foam model is, therefore, closely identical to the constitutive behaviour of EPS geofoam.

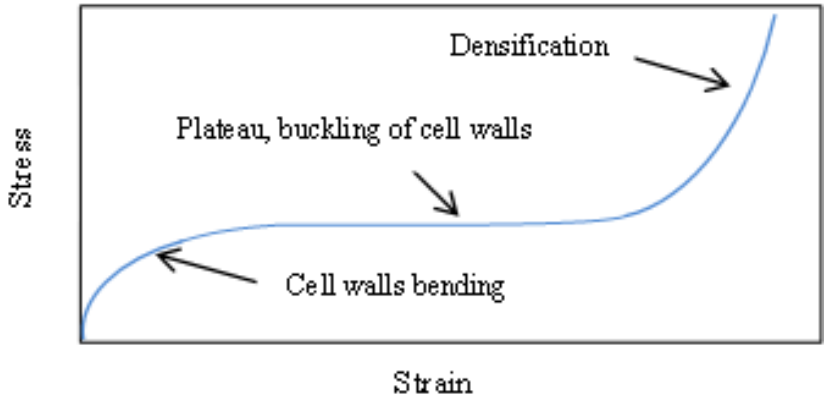

Figure 5.3 Compressive Stress–Strain curve for Hyper-foam

The Hyper-foam model in ABAQUS (2013) needs to be calibrated with experimental data to define the properties of material as input data for the model. Accordingly three different laboratory tests have been carried out on EPS samples including,

- Confined uniaxial compression test: In this test, three (50mm diameter and 50mm height) EPS samples were tested using a 50kn Wykeham Farrance electro-mechanical loading frame. The load was applied through a load cell mounted at the top of the specimen. An LVDT was used to measure the vertical deformation in the specimen. Specimen's height to diameter ratio (H/D) is chosen to be 1:1 to avoid any possible buckling effects. On the other hand, the contact ends of specimens have been properly smoothed with a sand paper to eliminate the end restraining effects. Each specimen was loaded to a total strain of 30% at a loading rate equal to 2%/minute. Test results for the three samples are presented in Figure 5.4.

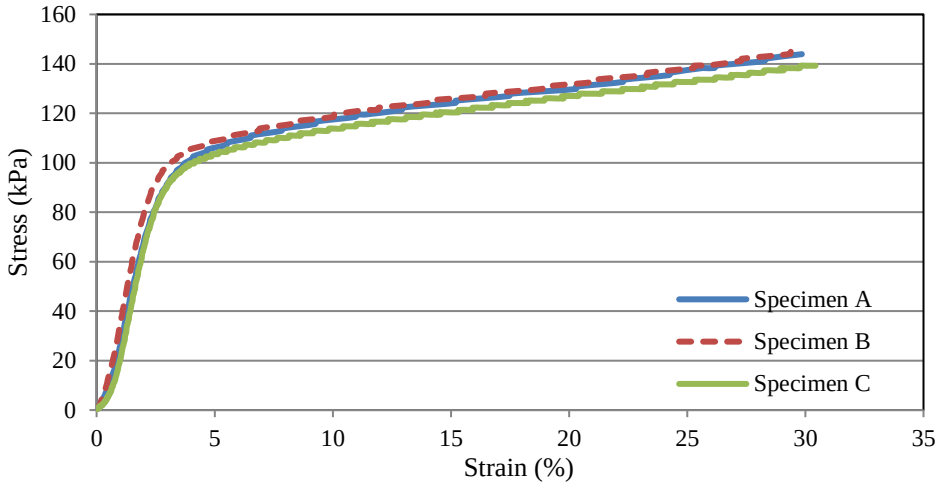

Figure 5.4 Strain-Stress relationship of EPS samples in uniaxial compression test

- Three-dimensional drained hydrostatic test: This test was conducted using a Wykeham Farrance pressure cell where the specimens were subjected to a uniform hydrostatic confining pressure. A GDS controller was used to control the pressure inside the cell and to measure the volumetric strain in the specimen. Samples tested have the same dimensions as in the uniaxial test. The hydrostatic test results are presented in Figure 5.5.

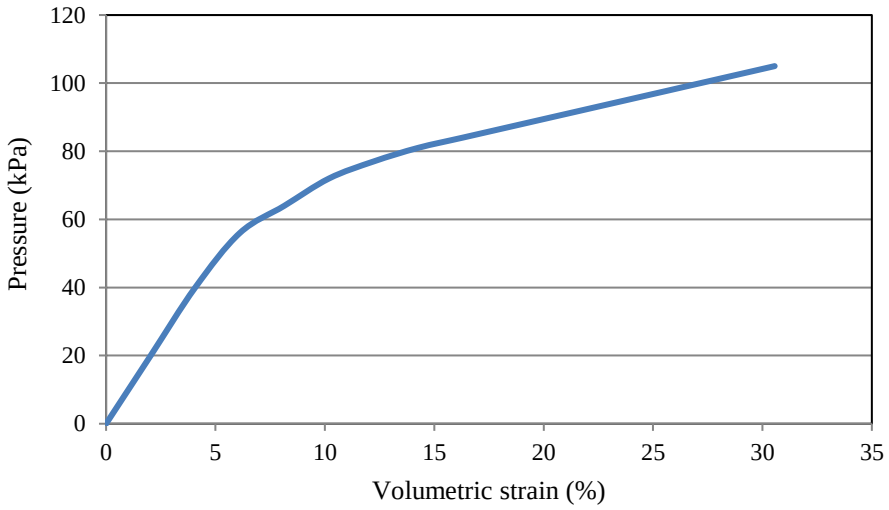

Figure 5.5 Hydrostatic test results

- Simple shear test: A 60mm x 60mm EPS specimen with a height of 55mm was tested under a simple shear load to determine the shear resistance of the EPS. In the test, the bottom surface of the sample was pasted to the base with a strong adhesive while the top surface was tightly inserted into a movable rigid steel frame. A monotonic shearing load was applied at a strain rate of

2%/minute. The applied load and the horizontal displacement of the specimen were measured throughout the test. The shear strain γ is calculated as the ratio between the horizontal displacement Δx to the effective height of the sample *H*. The shear test results are shown in Figure 5.6 (b). The EPS samples used in all tests were taken from the same EPS block supplied by a local firm in Sydney-Australia. The EPS density was 20kg/m^3.

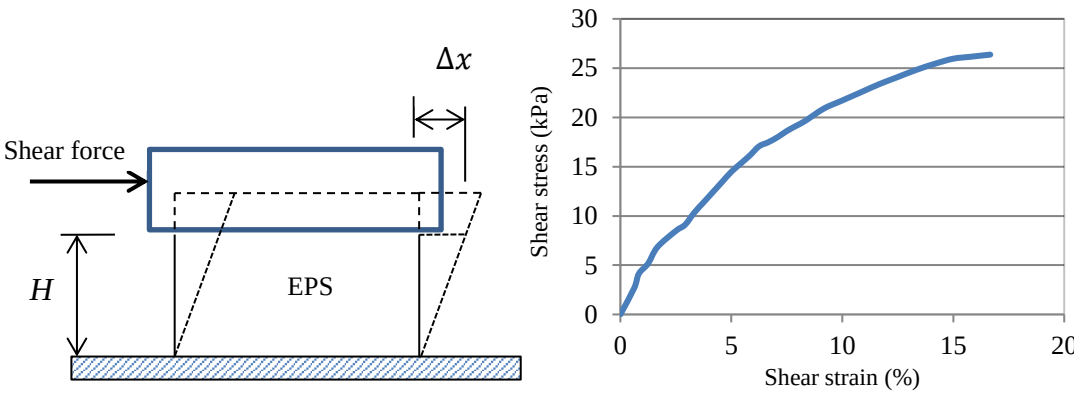

(a) (b)

Figure 5.6 Shear test on EPS sample

5.2.4 Interaction Properties and Boundary Conditions

Similar to the case described earlier in Chapter 3, the interaction behaviour at the soil-wall and soil-EPS interfaces was modelled as a standard surface-to-surface contact with finite sliding. The interaction was activated during the initial step of the analysis. The mechanical frictional behaviour at the surfaces of interface was expressed as a tangential friction, while the normal behaviour at the interface between the soil, concrete and the EPS was simulated as a "hard contact" where no separation or penetration is permitted between any two surfaces.

Direct shear tests were also carried out to determine the coefficient of friction between the soil and the EPS geofoam. The soil, in loose state, was sheared against a block of EPS geofoam at normal stresses of 13.6 kPa, 27.3 kPa and 68.1 kPa. Based on the test results the soil-EPS friction coefficient was determined as 0.42.

5.3 Model Verification

In order to verify the efficiency of the model in simulating the wall – soil interaction behaviour when an EPS geofoam inclusion is involved, the same setup used in the

physical small wall tests has been simulated using the FE model. Taking into account that the physical model was carried out under normal gravity, $g = 1$, the geometry of the FE model applied in the verification including the dimensions of the wall and the soil are made equal to those in the physical model. The Mohr-Coulomb parameters (C &Ø) of the soil used in the model are identical to those determined by the laboratory tests. The density of soil prescribed in the model has also been determined based on the actual unit weight of sand used in the physical model. The elasticity modulus of the soil was assumed as 30,000 kPa in reference to the typical value of the elasticity modulus of uniform loose sand. Also the Hyper-foam model was calibrated using the tests results of the EPS geofoam.

The meshed ABAQUS model for the small wall is shown in Fig 5.7. The materials properties, displacement amplitude and mode of wall movements were all identical to those utilized in Tests T2 and T4.

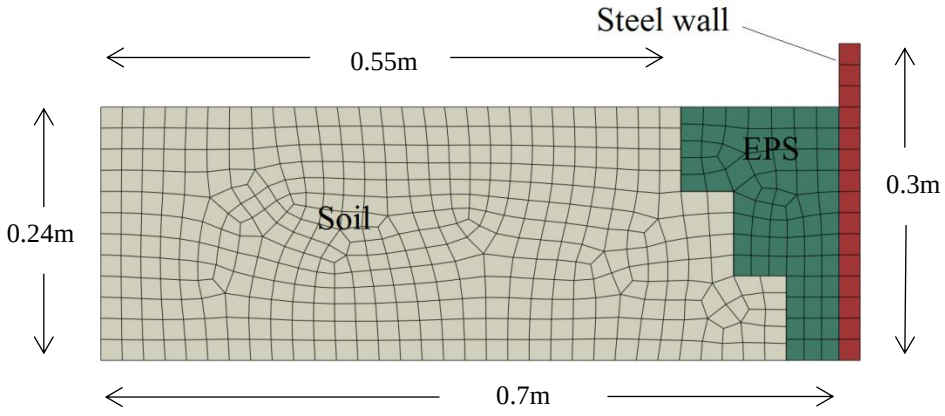

Figure 5.7 The meshed ABAQUS model for small wall

The FE modelling results for the maximum settlement of soil surface as well as the lateral earth pressures have been plotted together with the corresponding experimental results for comparison as appear in Figures 5.8 and 5.9. Taking into account the complexity of soil-structure interactions and the soil densification effects, the modelling and experimental results agree well with each other and the discrepancies between them are generally insignificant.

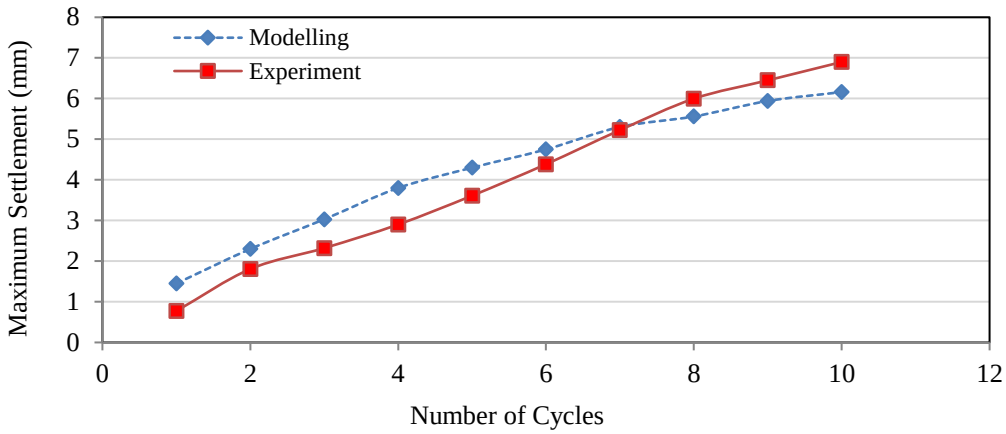

Figure 5.8 Finite element and experimental (test T2) results for the soil settlement

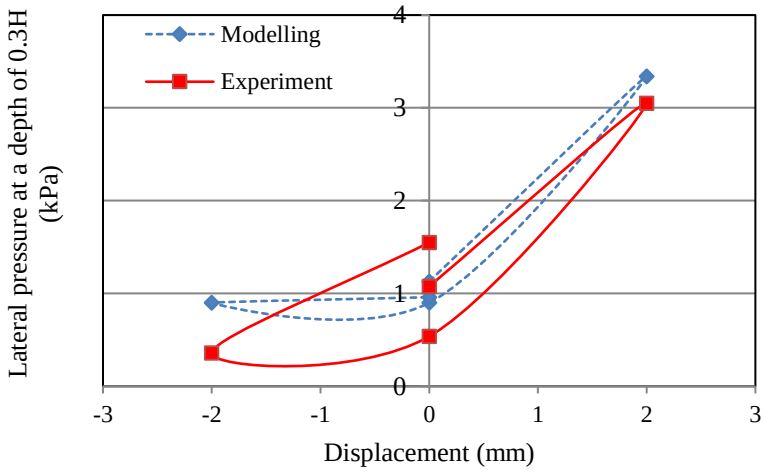

Figure 5.9 (a)

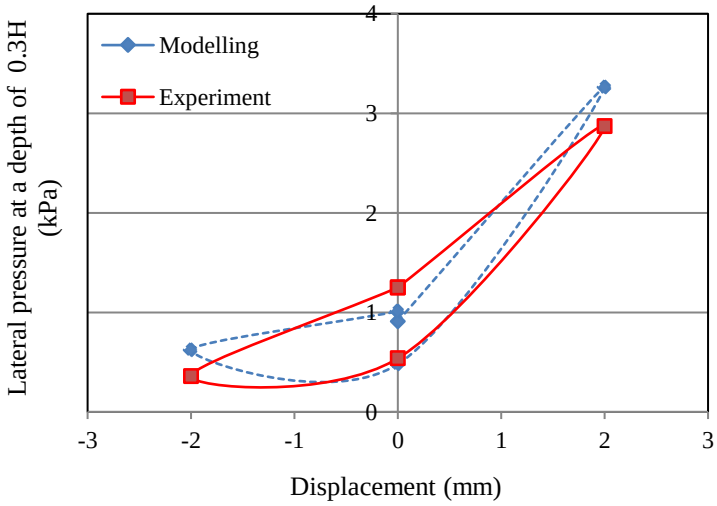

Figure 5.9 (b)

Figure 5.9 Lateral pressures acting on the wall during (a) Cycle 10 & (b) Cycle 5 of test T2

In order to maximize the validation range for the FE model, the test T4 has also been simulated in which the wall translated horizontally which induced greater settlements and lateral soil pressures compared to test T2. A comparison between the modelling and the experimental results of test T4 is given in Figures 5.10.

According to Figure 5.10, the modelling results of the maximum soil settlement are exhibited as an almost straight line which slightly deviate from the actual non-linear experimental results. This behaviour could be justified by the influence of two factors. First, any plastic deformation or the hardening effects taking place in the EPS geofoam may not have been substantially captured by the Hyper-foam model. In such a circumstance, the elasto-plastic model developed by Wong and Leo (2006) can be utilized to better replicate the actual behaviour of the EPS geofoam and consequently improve the modelling results of soil settlements.

The second influencing factor is the constitutive model of the soil which has not been able to replicate the densification and the associated changes in the soil properties due to the successive passive-active cycles of movements. The soil normally densifies under the continuous loading and un-loading cycles which results in an increase in the density, stiffness and also the shear strength of the soil.

An examination of the stresses in the EPS geofoam reveal that they are generally rather small in magnitude in the small wall model, thus the plastic zones in the geofoam are quite insignificant. In consequence, the plasticity or lack of it in the geofoam is not a primary reason why the small physical model and the FE settlement results in Figure 5.10 do not match sufficiently well (compare experimental results versus modelling results with constant cohesion, *C*). It was later confirmed in the FE modelling of the typical prototype wall (see later section) that the regions where the yield stress have been exceeded in the geofoam inclusions are quite small.

Unlike the geofoam, however, the loose sand was yielding and densifying with every cycle of wall movements hence the specification of the shear strength in the Mohr-Coulomb model and the effects of densification are likely to be consequential. In an attempt to investigate the potential effects of yielding and soil densification on the FE modelling results, the FE ABAQUS model has been utilized to back analyse the soil density, stiffness, shear angle and cohesion. Based on the backward analyses it was found that the settlement results are sensitive to the magnitude of soil cohesion.

Other parameters had very small or negligible effects. A modified analysis was undertaken, by slightly adjusting for soil cohesion in every five cycles of the wall movement in the ABAQUS model. The results showed that the settlement results of the physical model could be matched accurately by the FE model if the cohesion was adjusted (see Figure 5.10, variable cohesion c case). The adjusted cohesion values are shown in Figure 5.11.

The observations that can be drawn from the validation effort using the small wall are: (1) the calibration of the Mohr-Coulomb constitutive model for stress ranges suitable for the prototype wall was not appropriate for the stress ranges of the small wall. In this instance, the calibrated cohesion initially used in the small wall modelling (4 kPa) was higher than it should be as shown by the back analysis; (2) the cohesion part of the shear strength dominates over the internal friction angle part in the small wall case because of the small stresses. Hence the modelling was very sensitive to the specified cohesion value of the soil. This would not be the case in the prototype wall where internal friction will be more dominant and stresses are higher. As shown in the verification effort in Chapter 3 using data from the centrifuge tests which share stress similarity with the prototype, the Mohr-Coulomb constitutive model had performed very adequately.

In light of the above observations, the Mohr-Coulomb model for the loose sand and the Hyper-foam model were deemed adequate to be used for the modelling study of IABs of prototype dimensions, with and without EPS inclusions.

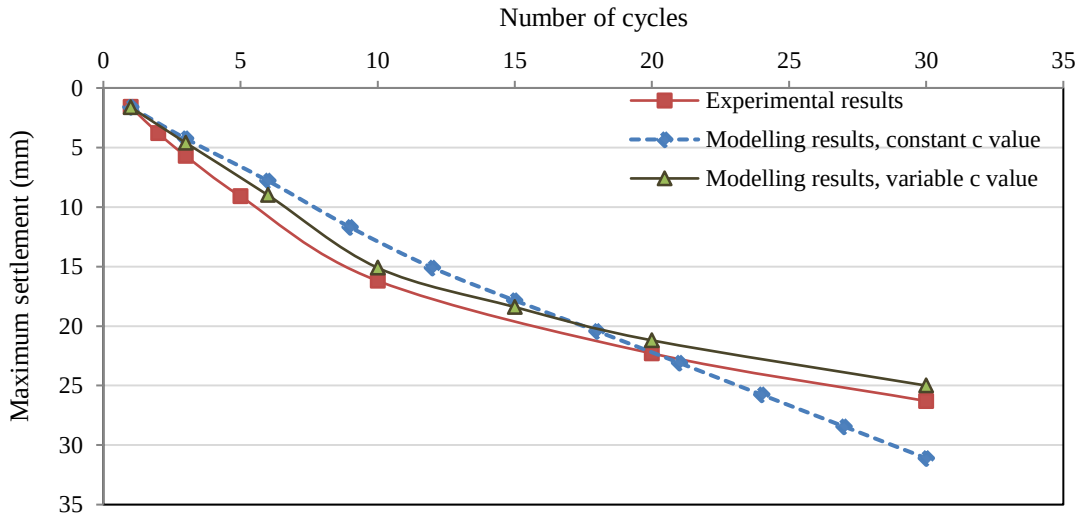

Figure 5.10 FE modelling and the experimental results for test T4

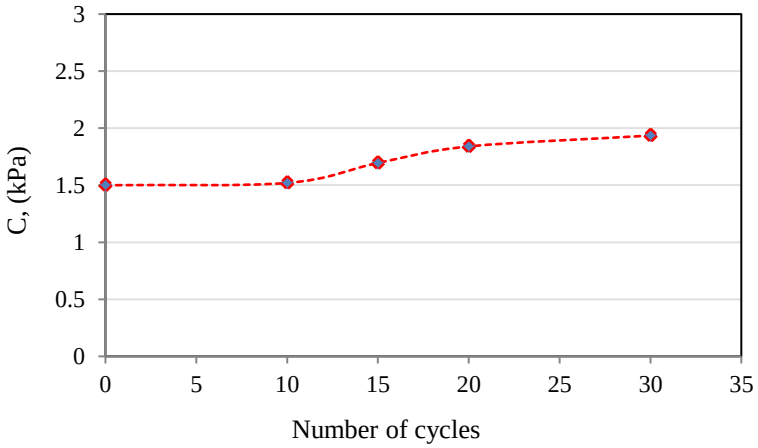

Figure 5.11 The variance of the cohesion of soil during the analysis

5.4 Application of the ABAQUS Model on Prototype Dimensions

Based on the outcomes of the numerical validation discussed in section 2.3 above, it can be concluded that the current FE model is sufficiently reliable to replicate the wall-soil interaction when an EPS inclusion is utilized. Consequently, it is possible to apply the model now for cases with prototype dimensions that involve the use of EPS geofoam.

In order to produce results to quantitatively assess the efficiency of the EPS inclusion in prototype dimensions, the same model discussed earlier in Chapter 3 will be simulated but with the use of EPS geofoam as a remedial measure for the soil settlement and lateral pressure problems. The FE ABAQUS model described in Chapter 3 has been modified so that a wedge-shaped EPS inclusion is provided at the interface between the soil and the wall. The density and other properties of the EPS geofoam have been set equal to those utilized in calibrating the Hyper-foam model. Hence, the effectiveness of incorporating the EPS geofoam can be investigated by comparing the results with the corresponding ones in Chapter 3 (the model without EPS inclusion). For an easy reference, the model described earlier in Chapter 3 will be cited as Model-1 and the modified model discussed in this section (with EPS inclusion) will be cited as Model-2

The EPS blocks in Model-2 were arranged in a wedge shape behind the abutment wall as illustrated in Figure 5.12. The slope angle θ of the assumed planar interface between the EPS wedge and the soil is a primary design variable that may affect the settlement and lateral pressure results (Horvath, 2000). Therefore, two variations of

Model-2 were simulated based on two different values for the angle θ. In Model-2a, the magnitude of angle θ was assumed as $45 + \emptyset/2$, where $\emptyset$ is the internal friction angle of the soil. The case of Model-2a represents the soil on the verge of active failure state. The angle θ was assumed equal to the internal friction angle of soil ($\emptyset = \theta$) in Model-2b.

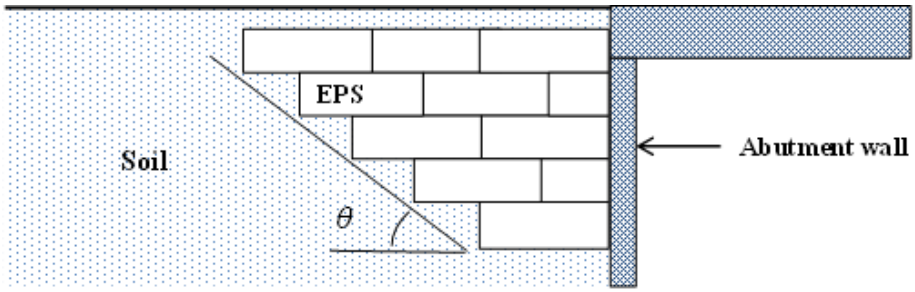

Figure 5.12 EPS arrangement behind the wall

The modelling results show that the EPS inclusion generally performs well in reducing both the lateral earth pressure and settlement effects compared to Model-1 (where no EPS inclusion is used). Also, unlike the settlement results in Model-1, the critical settlement spot in Model-2a was observed at the interface between the EPS geofoam and the soil as illustrated in Figure 5.13. Surface settlements at the interface between the EPS and the wall were very small and insensitive to the increase in number of cycles. Instead, the settlement of interest is now at the soil–EPS interface.

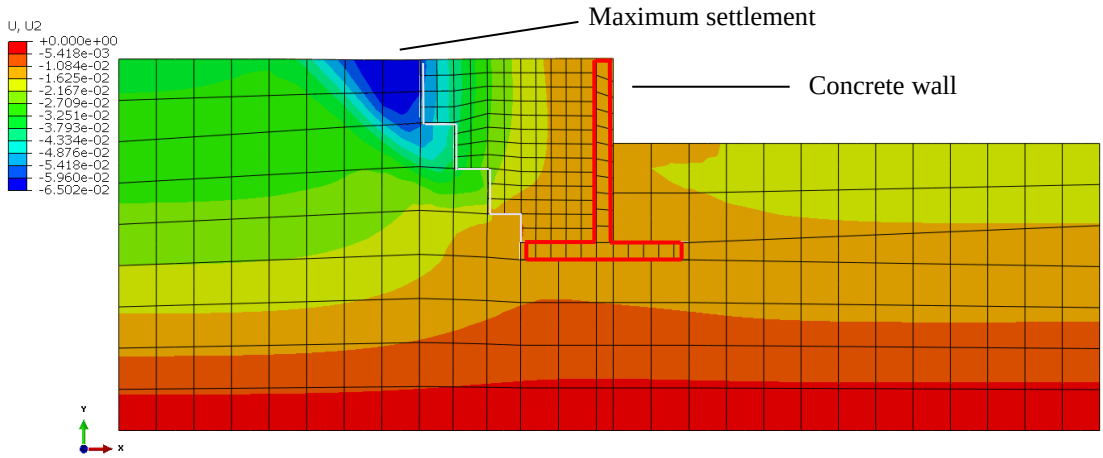

Figure 5.13 The deformed FE Model-2a

Significant differences were observed in lateral earth pressure and the maximum soil settlement results in Model-2a and Model-2b due to the difference in the value of the

angle θ. The results obtained from Model-2b show that the lateral stress acting at 2m from the top of the wall was decreased by 75% compared to the corresponding value of Model-2a and by 97% compared to Model-1, as shown in Figure 5.14.

A similar result was also observed in the magnitude of maximum soil settlement, where the values of soil settlements in Case 2b are far less than those observed in Case 2a and in Case 1 (without EPS) as shown in Figure 5.15.

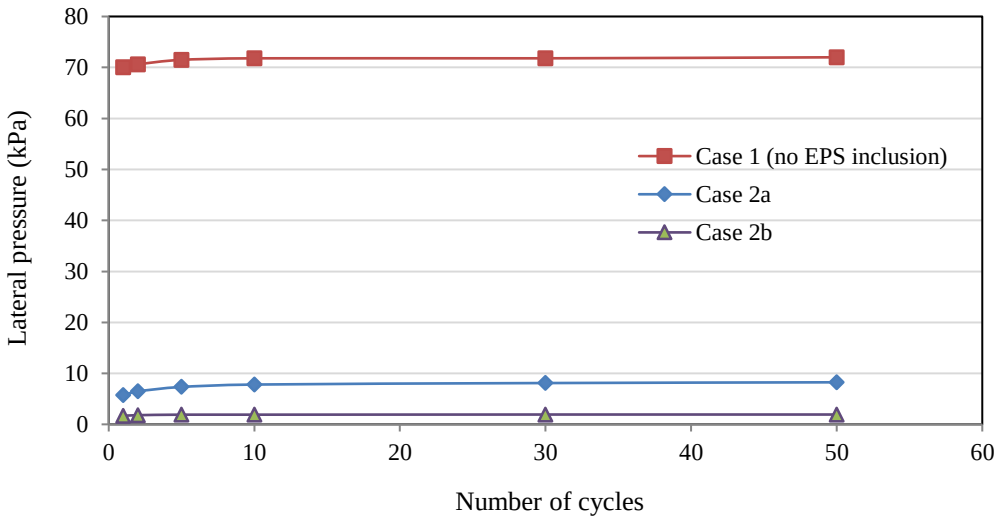

Figure 5.14 Lateral pressure vs Number of cycles

The reason for the significant reduction in the lateral earth pressures and the settlement when the slope of the EPS wedge, θ, was set to the soil internal friction angle $\emptyset$ (Case 2b) is due to increased stability of the soil behind the EPS blocks. As a result, the soil behind the EPS blocks applies extremely small lateral stresses, if any, on the EPS inclusion. Therefore, the amount of lateral stress transferred from the soil to the wall through the EPS wedge will be very small. The greater extent of the EPS wedge further dissipates the effects of wall movements on the adjoining soil. This effect consequently minimizes the volumetric strain and the associated settlement in the soil surface.

However, although the Case 2b is likely to diminish the lateral stress and settlement problems in the IAB approaches, such an option will require the replacement of a larger volume of soil and substituting it with EPS geofoam. This option is more costly and may not be a cost-effective solution. An optimum value for the angle θ may need to be selected by giving due consideration to both the overall construction cost and technical efficiency.

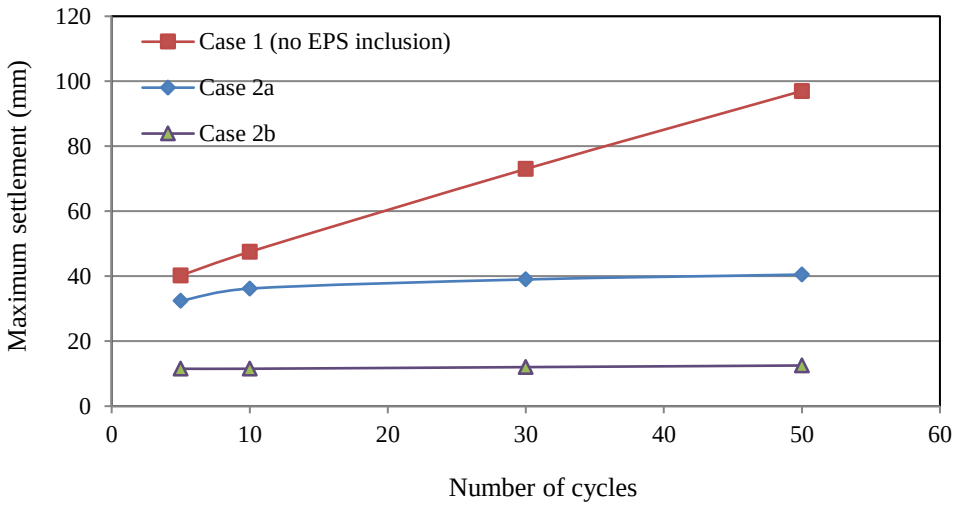

Figure 5.15 Maximum settlement vs Number of cycles

5.5 Summary

A plane strain finite element model has been developed using the ABAQUS/Standard and validated using experimental results obtained from a small wall retaining loose sand and subjected to active and passive displacements, as described earlier in Chapter 4. The purpose is to validate the FE model in simulating the abutment-soil interaction behaviour at the approach when an EPS geofoam inclusion is provided. Then this model was applied in simulating prototype-scale cases. The FE modelling is used to assess the effectiveness of the EPS geofoam in rectifying the approach problems in the IABs. Based on the modelling results, the following conclusions have been obtained,

- The Hyper-foam constitutive model available in the ABAQUS/Standard has reasonably replicated the behaviour of EPS geofoam used in typical IABs.
- An elasto-plastic constitutive model such as one developed by Wong and Leo (2006) can be utilized in the FE element model to better describe the behaviour of the EPS geofoam inclusion especially in applications where the presence of plasticity is substantial (such as for IABs with much longer spans than the typical case).
- The Mohr-Coulomb constitutive model can be used to model the impact of movement cycles on the backfill of IABs effectively provided the shear strength and, in some cases the densification effects, are properly included.
- The EPS geofoam inclusion provides an effective remedial measure to alleviate the soil settlements and lateral pressure at the IABs approaches.

Also, it is worthwhile noting that differential settlement directly due to the different compressibility between the approach embankment soil and the EPS geofoam is insignificant compared to that due to the abutment cyclic movement. Nevertheless, engineers will need to design for different self-weight of the different parts of the embankment if it is built on soft foundation soil. This type of design is routinely done by geotechnical engineers and should not detract from the advantanges and effectiveness of using EPS geofoam.

- The angle θ of the interface planar between the soil and the EPS wedge plays an important role in the overall performance of the inclusion. However, the incurred cost of using EPS geofoam is related to the interface angle θ and the volume of the geofoam material used. Hence an optimised design for using EPS geofoam need to be found between satisfying required lateral and settlement criteria and the incurred costs.

Chapter Six

Summary and Conclusions

6.1 Summary

Integral abutment bridges (IABs) are receiving growing interest as a favourable construction practice in many countries due to the significant savings in their construction and maintenance costs. In addition, IABs have been shown to demonstrate improved structural performance in various aspects of design, such as the resistance to seismic loading. However, the absence of the expansion joints in the IABs results in temperature induced movements in the bridge abutments, which consequently lead to a settlement in the approach soil and a rapid increase in the lateral earth pressure acting on the abutment. Using a compressible material as an inclusion between the soil and abutment wall may reduce the aforementioned effects to allowable values. Expanded polystyrene geofoam (EPS) is an excellent choice for such applications due to its numerous merits. Besides being a highly compressible material, EPS geofoam is extremely light weight and has a high compressive strength. Therefore, it largely reduces the loads on the subsoil and at the same time carries the vertical loads adequately.

This thesis consists of numerical and experimental studies of the soil-structure interaction behaviour in IABs and the effectiveness of the EPS geofoam to mitigate the approach problems in the IABs. First, a finite element model has been developed using the ABAQUS/Standard software for a normal IAB system. The model was validated using centrifuge experimental data and then applied to perform a simple parametric study by varying the parameters contributing to the soil settlement and lateral pressure development at the approach of IABs. A physical model, involving a small wall retaining loose sand was then used to investigate the influence of an EPS inclusion on the settlements and soil lateral pressures in response to different modes of wall movements. Laboratory tests and numerical analyses have also been conducted as necessary to calibrate and verify the Hyper-foam constitutive model in simulating the EPS geofoam behaviour. Finally, a two-dimensional finite element model was developed to investigate, in prototype dimensions, the effectiveness of EPS in attenuating the approach issues in IABs. Different arrangements of EPS inclusions, including single-block and wedge shaped inclusions, have been studied.

6.2 Conclusions

The outcomes of the numerical and experimental studies conducted in this research are summarized as follow,

- The classical theories for lateral earth pressures such as Coulomb and Rankine do not capture well the lateral soil pressures in the IABs due to the ratcheting effects developed under cyclic abutment movements.
- The lateral pressures acting on the abutment in IABs is a function of the amplitude and the mode of wall displacement as well as the number of the movement cycles. Lateral pressures are higher at the upper part of the abutment and less at the bottom part. Maximum pressure is usually recorded at a height equal to H/3 from the soil surface, where H is the total height of the retained soil.
- The existing Australian standards (AS 5100) do not include guidelines for the integral bridges. The British standards BA42/96 (2003) and the recommendations of the PCI committee in the United States are generally adopted in the design and construction of the IABs in Australia. However, the existing guidelines dealing with the approach issues in the IABs are highly empirical and do not account for the number of abutment movement cycles. Therefore, in some cases, the value of lateral soil pressures acting on the abutment such as in the UK standard BA42/96 (2003) is underestimated.
- The two-dimensional finite element model, that utilizes Mohr-Coulomb constitutive model for the soil, replicates the soil-wall interaction behaviour reasonably well under cyclic movements. However, further improvements can be made to the model by taking into consideration the soil densification due to the cyclic movements of the abutment wall.
- The temperature induced abutment movement is a combination of translation and rotation. The dominant mode of movement, translation or rotation, has a significant impact on the developed lateral pressures and soil settlements. Abutments with mainly translational movement experience more severe effects compared to that with principally rotational movement. In practice it will be necessary and important to distinguish between dominantly

translational (short walls) or dominantly rotational wall (tall walls). Guidelines for what constitutes a short or a long wall, however, are lacking.

- Studying the effects of cyclic displacements in IABs considering only the major temperature changes (the annual variation) rather than the superimposed daily-annual variation will largely underestimate the lateral earth pressures acting on the abutment.
- The Hyper-foam constitutive model replicates the EPS geofoam behaviour well at relatively small strains (below elastic limits). However, at larger strains, the EPS may exhibit an amount of plastic deformation, which could not be captured by the Hyper-foam model accurately.
- The use of the EPS geofoam, as a fill material between the abutment and the soil, significantly reduces the lateral pressure and the soil settlement in the IAB approaches. The stiffness of the EPS and the retained soil influence the effectiveness of the EPS inclusion. EPS of a relatively low stiffness is advised to be used with a heavily retained soil to obtain the best results from a purely inclusion perspective. However, this must be weighed against the need for the EPS to support the vertical overburden.
- The wedge-shaped EPS inclusion generally performs better than the single-block inclusion in terms of alleviating the lateral soil pressure and settlements. The angle of the inclined interface between the soil and the EPS wedge also has a considerable impact on the inclusion performance. Selecting an interface angle equal to the internal shear angle of the soil improves the efficiency of the EPS inclusion. However, the additional incurred cost due to the additional volume of EPS required in such an alternative need to be considered.

6.3 Recommendation for Future Studies

- This research has shown that EPS geofoam perform effectively in reducing the approach problems in IABs, namely in terms of a significant reduction in the lateral pressures and alleviation of the approach settlement. The EPS utilized in the experimental and numerical analyses is of medium grade with a density of 20kg/m^3. Further studies are advised to consider EPS geofoam of different densities and also different arrangements, such as providing a resilient EPS thin board between the wall and the full EPS wedge, to further

reduce the temperature effects on IAB approaches especially the soil settlement.

- The hyper-foam model provided by the ABAQUS (2013) is able to replicate the EPS behaviour reasonably well. However, in order to simulate the EPS behaviour when plastic deformations and hardening effects are expected, an elasto-plastic constitutive model such as the one developed by Wong and Leo (2006) need to be employed in the FE modelling.
- It is recommended that a constitutive model that incorporates soil densification should be considered for future modelling to more accurately take into account the effects of densification due to the cyclic movements.
- The temperature induced movements of the abutment takes place in a slow pattern corresponding to the annual temperature fluctuation. Therefore, time dependent creep deformation is likely to occur in the EPS geofoam due to its rheological behaviour. Further studies are recommended to involve the creep strain component in the analysis of EPS when used in IAB approaches.
- Guidelines for what constitute a translational-dominant, a rotational-dominant wall or a mixed wall need to be investigated and established.
- The physical model adopted in this research produced important data on the influences of the mode of wall movements and the use of EPS inclusion on the soil settlement and lateral pressures developed under the wall displacement. However, a future study using a prototype-scale physical model or centrifuge tests is recommended in the interest of producing similar stress conditions as in the field for quantifying the actual effects of the EPS inclusion on the approach problems in IABs.
- Future studies are recommended to use three-dimensional computer model in modelling the soil-structure interaction in IABs to simulate the realistic situation of the approach including the slopes on both approach sides.
- The computer model developed in this study deals with the EPS geofoam inclusion as a continuum material. However, in future studies it is recommended to simulate the EPS inclusion as stacked blocks of EPS geofoam, as would be expected in the actual practice, to capture the effects of friction and any possible movements between the blocks.

References

ABAQUS Inc. (2013). ABAQUS Version 6.13 user's manual, Providence, Rohde Island, USA.

Arellano, D. and T. D. Stark (2009). Load bearing analysis of EPS-block geofoam embankments. *8th International Conference on the Bearing Capacity of Roads, Railways and Airfields*.

Arsoy, S., Barker, R. M., & Duncan, J. M. (1999). The behaviour of integral abutment bridges (Vol. 3, p. 13). Charlottesville, VA: Virginia Transportation Research Council.

Bayoglu F., (2004). Soil – structure interaction for integral bridges and culverts. Licentiate Thesis, KTH.

BA42/96 (2003). Design manual for roads and bridges, Vol. 1, Section 3, Part 12: The design of integral bridges: Amendment 1. UK Highways Agency.

Barr, P. J., Halling, M. W., Huffaker, C., & Boyle, H. (2013). Behaviour and analysis of an integral abutment bridge. *Bridges Transportation Research Board*.

BASF Aktlengesellschaft (2006). Rigid styropor foam as a lightweight construction material for highway foundations: GEOFOAM. Technical Information. Ludwigshafen- Germany 510/1 - 510/10

Bloodworth, A. G., Xu, M., Banks, J. R., & Clayton, C. R. (2011). Predicting the earth pressure on integral bridge abutments. *Journal of Bridge Engineering*, *17*(2), 371-381.

Broms, B. B., & Ingelson, I. (1971). Earth pressure against the abutments of a rigid frame bridge. *Geotechnique*, *21*(1), 15-28.

Burke Jr, M. P. (2009). Integral and semi-integral bridges. John Wiley & Sons.

Butterfield, R. (1999). Dimensional analysis for geotechnical engineers. *Geotechnique*, *49*(3), 357-366.

Civjan, S. A., Bonczar, C., Brena, S. F., DeJong, J., & Crovo, D. (2007). Integral abutment bridge behaviour: Parametric analysis of a Massachusetts bridge. *Journal of Bridge Engineering*, *12*(1), 64-71.

Cosgrove, E., & Lehane, B. M. (2003). Cyclic loading of loose backfill placed adjacent to integral bridge abutments. *International Journal of Physical Modelling in Geotechnics*, *3*(3), 9-16.

Chun, B. S., H.-S. Lim, M. Sagong and K. Kim (2004). "Development of a hyperbolic constitutive model for expanded polystyrene (EPS) geofoam under triaxial compression tests. *Geotextiles and Geomembranes 22*(4): 223-237.

Dicleli, M. (2000). Simplified model for computer-aided analysis of integral bridges. *Journal of Bridge engineering*, *5*(3), 240-248.

Elragi, A. F. (2000). Selected engineering properties and applications of EPS geofoam.

England, G. L., Bush, D. I., & Tsang, N. C. (2000). Integral bridges: a fundamental approach to the time-temperature loading problem. Thomas Telford.

England, G. L., & Tsang, N. C. M. (2001). Towards the design of soil loading for integral bridges—Experimental evaluation. *Department of Civil and Environmental Engineering, Imperial College, London*.

Gibbens, B., & McManus, A. (2011, October). Design of Peninsula Link Integral Bridges. *Austroads Bridge Conference, 8th, 2011, Sydney*, New South Wales, Australia (No. AP-G90/11).

Hassiotis, S., & Roman, E. K. (2005). A survey of current issues on the use of integral abutment bridges. *Bridge Structures*, *1*(2), 81-101.

Hoppe, E. J. (2005). Field study of integral back wall with elastic inclusion (No. FHWA/VTRC 05-R28).

Hoppe, E. J., & Gomez, J. P. (1996). *Field study of an integral back wall bridge* (No. FHWA/VA-97-R7).

Horvath, J. S. (1994). "Expanded Polystyrene (EPS) geofoam: An introduction to material behaviour. *Geotextiles and Geomembranes*, *13*(4): 263-280.

Horvath, J. S. (2000). Integral-abutment bridges: problems and innovative solutions using EPS geofoam and other geosynthetics. Res. Rpt. No. CE/GE-00, 2.

Horvath, J. S. (1997). The compressible inclusion function of EPS geofoam. *Geotextiles and Geomembranes*, *15*(1), 77-120.

Huntley, S. A., & Valsangkar, A. J. (2013). Field monitoring of earth pressures on integral bridge abutments. *Canadian Geotechnical Journal*, *50*(8), 841-857.

Khodair, Y. A. (2009). Lateral earth pressure behind an integral abutment. *Structure and Infrastructure Engineering*, *5*(2), 123-136.

Lehane, B. M. (2011). Lateral soil stiffness adjacent to deep integral bridge abutments. *Géotechnique*, *61*(7), 593-603.

Lock, R. J. (2002). Integral bridge abutments. MEng Project Report. CUED/DSOILS/STR320, 2002 (Cambridge, UK: Schofield Centre).

Mistry, V. C. (2005). Integral abutment and joint-less bridges. *The FHWA Conference* (IAJB 2005).

Nam, M. S., & Park, Y. H. (2013). Relationship between Earth Pressure and Thermally Induced Movement of Integral Abutments. *Journal of Performance of Constructed Facilities*, *29*(4), 04014093.

Ng, C. W., Springman, S. M., & Norrish, A. R. (1998). Centrifuge modelling of spread-base integral bridge abutments. *Journal of geotechnical and geoenvironmental engineering*, *124*(5), 376-388.

Ossa, A. and M. P. Romo (2009). "Micro- and macro-mechanical study of compressive behaviour of expanded polystyrene geofoam. *Geosynthetics International*, *16*(5): 327-338.

Tan, D., Reid, C., Rajeev, P., Piratheepan, J., & Sivakugan, N. (2014). Earth pressure development in integral abutment bridge subjected to thermal loadings. *8th Australasian Congress on Applied Mechanics* (ACAM), PP 408-415.

Tatsuoka, F., Hirakawa, D., Nojiri, M., Aizawa, H., Nishikiori, H., Soma, R., Tateyama, M. & Watanabe, K. (2009). A new type of integral bridge comprising geosynthetic-reinforced soil walls. *Geosynthetics International*, *16*(4), 301-326.

Thevaneyan, K.D., John, P.F., & Jianqiao Y. (2014). Superstructure behaviour of a stub-type integral abutment bridge. *Journal of Bridge Engineering, 19* (6) (2014), pp. 04014012-1–04014012-12

Sandford, T. C., & Elgaaly, M. (1993). Skew effects on backfill pressures at frame bridge abutments. *Transportation research record*, (1415).

Vicroads, 2012. Design of Integral and Semi-Integral Bridges. Bridge Technical Note BTN 2012/003 Version 1.0. Victoria. Australia

White, D. J., Mekkawy, M. M., Sritharan, S., & Suleiman, M. T. (2007). "Underlying" Causes for Settlement of Bridge Approach Pavement Systems. *Journal of performance of constructed facilities*, *21*(4), 273-282.

Wolde-Tinsae, A. M., Klinger, J. E., & White, E. J. (1988). Performance of jointless bridges. *Journal of performance of constructed facilities*, *2*(2), 111-125.

Wong, H., & Leo, C. J. (2006). A simple elastoplastic hardening constitutive model for EPS geofoam. *Geotextiles and Geomembranes*, *24*(5), 299-310.